

THE THERMAL DIFFUSIVITY OF URANIUM DIOXIDE

by

Leslie David Montgomery

A Thesis Submitted to the
Graduate Faculty in Partial Fulfillment of
The Requirements for the Degree of
MASTER OF SCIENCE

Major Subject: Nuclear Engineering

Approved:

Signatures have been redacted for privacy

Iowa State University
Of Science and Technology
Ames, Iowa

1963

TABLE OF CONTENTS

	Page
I. INTRODUCTION	1
II. LITERATURE SEARCH	3
III. FORMULATION	11
A. Derivation of Experimental Equations	11
B. Feasibility of Experiment	14
IV. EXPERIMENTAL ERRORS	20
A. Description of Experimental Oscillograph Trace	20
B. Errors to be Investigated	20
C. Derivation of Error Relationships	20
D. Determination of the Influence of Errors upon Thermal Conductivity	26
E. Times of Minimum Error Influence	26
F. Results and Conclusions	35
V. DESCRIPTION OF EXPERIMENTAL APPARATUS	39
VI. EXPERIMENTAL PROGRAM	45
A. Sample Analysis	45
1. Thermocouple position	45
a. Longitudinal position	45
b. Radial position	48
2. Length of Sample	52
3. Enrichments	58
4. Temperature distributions	61
B. Stress Analysis	75
1. Axial maximum temperature differences	75

	Page
2. Radial stress	78
VII. PREPARATION OF DATA FOR ANALYSIS	89
A. Graphing Experimental Data from Oscillograph Chart	89
B. Determination of Thermal Diffusivity	89
VIII. RESULTS AND CONCLUSIONS	91
IX. SUGGESTIONS FOR FURTHER EXPERIMENTATION	114
X. BIBLIOGRAPHY	115
XI. ACKNOWLEDGMENTS	116
XII. APPENDIX A	119
XIII. APPENDIX B	121

TABLE OF ILLUSTRATIONS

	Page
Fig. 1 Reported thermal conductivity values of uranium dioxide	10
Fig. 2 Sample oscillograph chart	21
Fig. 3 Influence of $\frac{d\Delta T}{\Delta T}$, $\frac{dt}{t}$, $\frac{dA}{A}$ upon $\frac{dD}{D}$ vs time (in units of $\frac{KL^2}{D}$) where $0 \leq K < 1.8$	27
Fig. 4 Error in the temperature difference, $\frac{d\Delta T}{\Delta T}$, vs time (in units of $\frac{KL^2}{D}$) where $0 \leq K < 1.8$	32
Fig. 5 Error in the slope, $\frac{dA}{A}$, vs time (in units of $\frac{KL^2}{D}$) where $0 \leq K < 1.8$	33
Fig. 6 Error in the time, $\frac{dt}{t}$, vs time (in units of $\frac{KL^2}{D}$) where $0 \leq K < 1.8$	34
Fig. 7 Combined error in slope and time, $\frac{dA}{A} + \frac{dt}{t} + \frac{dA}{A} \cdot \frac{dt}{t}$, vs time (in units of $\frac{KL^2}{D}$) where $0 \leq K < 1.8$	36
Fig. 8 Combined error in temperature difference and time, $\frac{d\Delta T}{\Delta T} + \frac{dt}{t} + \frac{d\Delta T}{\Delta T} \cdot \frac{dt}{t}$ vs time (in units of $\frac{KL^2}{D}$) where $0 \leq K < 1.8$	37
Fig. 9 Schematic diagram of sample	39
Fig. 10 Experimental "L" frame support to be inserted in the transparent slot liner within TREAT	41
Fig. 11 Transparent meltdown facility	42
Fig. 12 Inner and outer capsule subassemblies	43
Fig. 13 Cutaway isometric of TREAT	44
Fig. 14 Temperature difference (%) vs time of UO_2 , $L=0.25$ cm	53
Fig. 15 Temperature difference (%) vs time of UO_2 , $L=0.35$ cm	54
Fig. 16 Temperature difference (%) vs time of UO_2 , $L=0.50$ cm	55

	Page
Fig. 17 Radial temperature distribution within UO_2 rod	56
Fig. 18 Transient No. 141 series SVII - shot 3 - pin No. 4	63
Fig. 19 Sample power as a function of time. Taken from transient No. 141 series SVII - shot 3 - pin No. 4	64
Fig. 20 Relative flux <u>vs</u> normalized radius of one half inch diameter UO_2 samples of designated enrichments	68
Fig. 21 Temperature of UO_2 sample as a function of radius at various times, $k = 0.015$, 5% enrichment	71
Fig. 22 Temperature of UO_2 sample as a function of radius at various times, $k = 0.015$, 10% enrichment	72
Fig. 23 Temperature of UO_2 sample as a function of radius at various times, $k = 0.025$, 5% enrichment	73
Fig. 24 Temperature of UO_2 sample as a function of radius at various times, $k = 0.025$, 10% enrichment	74
Fig. 25 Polar stress of UO_2 sample as a function of radius at various times, $k = 0.015$, 5% enrichment	80
Fig. 26 Radial stress of UO_2 sample as a function of radius at various times, $k = 0.015$, 5% enrichment	81
Fig. 27 Polar stress of UO_2 sample as a function of radius at various times, $k = 0.015$, 10% enrichment	82
Fig. 28 Radial stress of UO_2 sample as a function of radius at various times, $k = 0.015$, 10% enrichment	83
Fig. 29 Polar stress of UO_2 sample as a function of radius at various times, $k = 0.025$, 5% enrichment	84
Fig. 30 Radial stress of UO_2 sample as a function of radius at various times, $k = 0.025$, 5% enrichment	85
Fig. 31 Polar stress of UO_2 sample as a function of radius at various times, $k = 0.025$, 10% enrichment	86
Fig. 32 Radial stress of UO_2 sample as a function of radius at various times, $k = 0.025$, 10% enrichment	87
Fig. 33 Experimental temperature and power <u>vs</u> time, transient No. 539	92

	Page
Fig. 34 Experimental temperature and power <u>vs</u> time, transient No. 535	93
Fig. 35 Experimental temperature and power <u>vs</u> time, transient No. 536	94
Fig. 36 Experimental temperature and power <u>vs</u> time, transient No. 537	95
Fig. 37 Experimental temperature <u>vs</u> time, transient No. 539, time zero = time of peak reactor power	97
Fig. 38 Experimental temperature <u>vs</u> time, transient No. 535, time zero = time of peak reactor power	98
Fig. 39 Experimental temperature <u>vs</u> time, transient No. 536, time zero = time of peak reactor power	99
Fig. 40 Experimental temperature <u>vs</u> time, transient No. 537, time zero = time of peak reactor power	100
Fig. 41 Experimental temperature difference <u>vs</u> time, transient No. 539	101
Fig. 42 Experimental temperature difference <u>vs</u> time, transient No. 535	102
Fig. 43 Experimental temperature difference <u>vs</u> time, transient No. 536	103
Fig. 44 Experimental temperature difference <u>vs</u> time, transient No. 537	104
Fig. 45 Comparison of normalized experimental to normalized theoretical temperature difference <u>vs</u> time for various values of diffusivity, D, transient No. 539	106
Fig. 46 Comparison of normalized experimental to normalized theoretical temperature difference <u>vs</u> time for various values of diffusivity, D, transient No. 535	107
Fig. 47 Comparison of normalized experimental to normalized theoretical temperature difference <u>vs</u> time for various values of diffusivity, D, transients No. 536, No. 537	108
Fig. 48 Reported and experimental thermal conductivity values of uranium dioxide	110

	Page
Fig. 49 Initial cracking of sample at the end of transient No. 535	112
Fig. 50 Extensive cracking as occurred during transient No. 536	113

I. INTRODUCTION

Recent advancements in the field of nuclear reactor technology has placed increased emphasis upon the development of fuels that can be operated at high temperatures. Since uranium and its lower alloys exhibit low melting points and structural instability at elevated temperatures due to the accumulation of fission gases, solid fuels in reactors of the future may consist of alloys of uranium with non-fissionable materials or consist of uranium compounds.

Work is now in progress to study various refractory uranium compounds as potential high-temperature fuels. The materials being studied include uranium oxides, carbides, silicides, nitride, sulfide, and others. Perhaps the most important trait of a desirable fuel compound would be good stability in irradiation at high temperatures. Other desirable characteristics are a high melting point, low neutron absorption cross section, chemical and metallurgical inertness, high thermal conductivity, high uranium density, and good mechanical strength with resistance to thermal shock.

It is unlikely that one compound will possess all of the aforementioned characteristics. The compound, uranium dioxide, fulfills many of these requirements, but it lacks structural strength, has a low uranium atom density, and has poor thermal conductivity. Nevertheless more experimental work has been performed on the investigation of the physical properties of uranium dioxide than upon any other uranium fuel compound. At the present time it appears to be the most promising of the ceramic fuels.

The amount of data available on the thermal conductivity of sintered

uranium dioxide, at high temperatures and under irradiated conditions, is quite limited. The apparent reason for the lack of such data appears to be twofold: (1) the difficulty of conducting experiments at high temperatures by which to measure the thermal conductivity of uranium dioxide, (2) the effect of cracking produced by thermal stresses upon the thermal conductivity is difficult to take into account.

There are a number of existing transient and steady state methods for measuring thermal conductivity; however, there is some dissatisfaction with the length of time required to make reliable measurements. If the time required to measure the thermal conductivity is relatively long, errors due to the cooling of the sample may be introduced in the values obtained. A need exists for a rapid and reliable method for measuring the thermal diffusivity of uranium dioxide over wide ranges of temperature and under reactor operating conditions.

The object of this study is to test the feasibility of an entirely new method of measuring the thermal diffusivity of ceramic reactor fuel materials with a specific application to that of uranium dioxide at temperatures in excess of 1000°C.

It is hoped that an accurate measurement of the thermal diffusivity of UO_2 at high temperatures will be obtained and that this method will prove applicable to other ceramic fuels.

II. LITERATURE SEARCH

Some of the uranium compounds that are under investigation as potential high-temperature reactor fuel materials are uranium oxides, carbides, silicides, nitride, and sulfide. Although the bulk of the high-temperature fuel development is being carried on with UO_2 it may be of interest to briefly survey its competitors.

Eperman (10) states that under exceptional conditions the uranium borides might be utilized as a high-temperature fuel. Uranium forms the borides, UB_2 and UB_4 . Both compounds have melting points above 1500°C , but neither compound has good chemical stability with air or steam. Since boron has a high neutron absorption cross section the use of a boride would require the separated B^{11} isotope.

The carbides of uranium, UC and UC_2 , have high melting points, higher uranium density than UO_2 , and at elevated temperatures possess thermal conductivities five to six times greater than UO_2 . The thermal conductivity of uranium carbides remains fairly constant as temperatures increase, while that of UO_2 decreases appreciably with increasing temperatures. Uranium carbide UC and UC_2 are chemically unstable in hot water or air but appear to be useful in gas cooled or in liquid metal cooled reactors.

The nitride of uranium also has a very high melting point and uranium atom density. Its main disadvantages are chemical instability and a high neutron absorption cross section.

Uranium sulfide compares to UO_2 in melting point and uranium atom density and is stable in boiling water but will readily oxidize in high-temperature air.

The uranium compounds of silicon possess favorable properties at

high temperatures and have a better thermal conductivity than that of UO_2 . Under irradiation the uranium-silicon compounds undergo severe distortion, swelling, and decomposition which may limit their use as reactor fuels.

In addition to the compounds already mentioned a variety of alkaline-earth uranites are being studied. These compounds are quite stable and have melting points in excess of 1500°C . Irradiation of such samples at 200°C caused fragmentation and complete release of fission gases. Decomposition occurred when these compounds were heated to 1800°C .

Although an extensive exploratory program is being conducted to develop a satisfactory high-temperature fuel material, more research has been conducted, and more information is available on UO_2 than any other refractory fuel compound. For this reason UO_2 is more widely utilized as a reactor fuel material than any other uranium compound at the present time.

Before a potential fuel material can be practically utilized in a reactor an accurate measurement of its thermal conductivity must be obtained. Thermal conductivity may be measured by either static or dynamic methods. In dynamic methods the temperature is varied suddenly or periodically for one portion of the sample and the temperature change with time is measured to determine the thermal diffusivity, k/CP . In static methods, the sample is allowed to come to a steady state and the temperature distribution is measured to determine the thermal conductivity, k .

A study of the literature, by the author, indicates that there are a large number of methods which have been used to measure the thermal diffusivity and thermal conductivity of materials. A survey of the

methods that may be applied to refractory fuel compounds will illustrate some of the difficulties which may be encountered in an experiment such as the one proposed.

Two experimental groups (26,7) have utilized a xenon flash lamp to determine the thermal diffusivity of various non-fissionable materials over a wide range of temperatures. A high-intensity, short-duration light pulse is absorbed in the front surface of a thermally insulated specimen a few millimeters thick coated with camphor black, and the resulting temperature history of the rear surface is measured by a thermocouple and recorded with an oscilloscope. The oscilloscope pattern is photographed and the thermal diffusivity of the sample is calculated from the time-versus-temperature curve as described by Jenkins and Parker (26).

Dr. Arthur L. Loeb (22) has proposed an idealized experiment for the measurement of the thermal conductivity of ceramic materials at high temperatures. The experimental method consists of surrounding a long, uniformly heated cylindrical core by a hollow cylinder of the ceramic, and using the cylindrical form of the heat flow equation in determining the conductivity from the average temperature gradient across a certain distance in the ceramic.

Upon further investigation Dr. Loeb found that heat loss due to end effects of the sample produced appreciable errors in the obtained thermal conductivity values. Experiments to alleviate this problem were reported to be in progress.

Preliminary experiments have been performed by Firman, Johnson, and Findley (11) to develop a method for measuring thermal conductivity

suitable for in-pile use. A transient method is employed involving the measurement of sinusoidally varying temperature at two points along a specimen rod which is periodically heated at one end. The thermal diffusivity of the material is calculated from a simple relationship between the amplitude decrement and the velocity of the temperature wave which exists within the sample.

Such an experiment was performed on nickel, Armco iron and C.Y. 9 carbon, from which values were obtained that agree with existing data. Firman, et al. (11) stated that this method would yield accurate values with materials whose thermal diffusivity is above $0.02 \text{ cm}^2/\text{sec}$. This fact would prohibit the use of this method on UO_2 , but it may be applicable to other refractory fuels.

The thermal conductivity of UO_2 has been treated experimentally over a wide range of temperatures. Most of the present experiments described below were conducted under out-of-pile conditions.

Kingery and Vasilos, et al. (20) reported data on UO_2 having 73% theoretical density. The measurement was made utilizing a linear flow comparison method. Samples of known conductivity were placed in series with unknown samples. Kingery has also measured the thermal conductivity of UO_2 having 95% theoretical density by this same method. This is the only conductivity information available on high density uranium dioxide over a wide range of temperatures.

Hedge and Fieldhouse (17) at Armour using a stacked disc method measured the thermal conductivity of uranium dioxide that was 75% of theoretical density to 1670°C . The method used consists of measuring, during steady state, the radial heat flow and radial temperature drop

in a vertical stack of disks composed of the material whose thermal conductivity is to be measured. The disks were in the form of annular rings and the heat which flowed through the disks was supplied by an electric heater centered in the axial hole of the stacked disks. The temperature gradient was measured by means of thermocouples inserted in very small vertical holes, one near the axial hole and the other near the outer edge of the disks. The thermal conductivity of the disk material was calculated from the power input, the distance of the inner and outer thermocouples from the axis of the disk, between the holes.

At approximately 1670°C severe cracking of the sample occurred and prevented further experimentation. The values obtained by Hedge and Fieldhouse were appreciably lower than those measured by Kingery.

An experimental determination of the thermal conductivity of UO_2 of 96% theoretical density, over the range 800°C to 1150°C, has been conducted by R. Scott (31) at Harwell, England. The experimental method was based on the measurement of the radial temperature difference between the center and surface of a cylindrical sample while heat was being generated throughout its volume by the passage of electric current.

The thermal conductivity of 85% theoretical density UO_2 was measured to 2100°C by R. D. Reiswig (28, p. 48-49). A radial heat flow method, similar to that employed by Hedge and Fieldhouse, was used. Instead of thermocouples, as used by Hedge and Fieldhouse, Reiswig used a Pyro Micro-Optical pyrometer, focused down eight holes, to measure the radial temperature difference existing between the center and the outer edge of the sample. The values obtained by Reiswig agree favorably with those of Kingery and Hedge and Fieldhouse.

The chief source of error in Reiswig's experiment was probably due to an error in the measured power input. Cracks, due to thermal stresses, formed in all disks except one, allowing some of the measured power to escape from the heater rod to the radiation shield by direct radiation rather than by conduction through UO_2 .

Englander (9) in France reports an average value of 0.01 $\text{cal-cm}^{-1}\text{-sec}^{-1}$ -per degree C at approximately 70°C for material having a density of 9.2 g/cm³.

The first in-pile determination of the thermal conductivity of uranium dioxide appears to have been made by Flinta (12, p. 519) in Sweden. The UO_2 samples had 91% of theoretical density and were subjected to a neutron flux of $1.8 \times 10^{12} \text{n-cm}^{-2}\text{-sec}^{-1}$ in the research reactor, R1. The method was essentially a stacked disc method. Five annulus shaped discs 15 mm. in diameter and 2 mm. in length were stacked together, with a tungsten rod passing through the central hole and serving as a heat source in addition to that caused by the fissioning. The thermal conductivity was calculated using the temperature gradient which existed between two thermocouples, one located near the center of the sample and the second located near the outside surface of the UO_2 pellets.

The thermal conductivity was found to be erratic with neutron irradiation, and it dropped to $0.007 \text{W-cm}^{-1}\text{-}^{\circ}\text{C}^{-1}$ after three heating cycles.

The latest in-pile measurement of the "effective" thermal conductivity of sintered uranium dioxide was made by J. D. Eichenberg (8) in the Materials Testing Reactor. PWR fuel element pellets 0.3535 inches in diameter were stacked in a stainless steel capsule and subjected to an estimated neutron flux of 0.7×10^{20} nvt thermal. By measuring the

temperature difference between the center on the sample pellets and the exterior, the thermal conductivity was determined up to 480°C and the values were about 50% of those obtained by Hedge and Fieldhouse.

The only determination of the thermal conductivity of UO_2 at temperatures in excess of 2100°C has been carried out by J. Lambert Bates (2) at Hanford Atomic Products Operation. Bates made laboratory investigations of unirradiated UO_2 at temperatures to the melting point and established the characteristic temperatures at which certain physical changes occur. By observing similar physical changes in post-irradiation specimens, Bates deduced the temperature profile of the sample during irradiation and from this obtained an estimate of thermal conductivity. Such estimates lead to values larger than those now commonly assumed at temperatures greater than 1400°C.

A summary of results and comparison of the values given by the various experimental methods used is given in Fig. 1.

Due to the lack of "effective" thermal conductivity data at high temperatures, since out-of-pile values cannot be extrapolated to meet conditions of irradiated material, and to investigate the discrepancy of thermal conductivity values above 1400°C, a direct in-pile method to measure the thermal conductivity of UO_2 has been proposed.

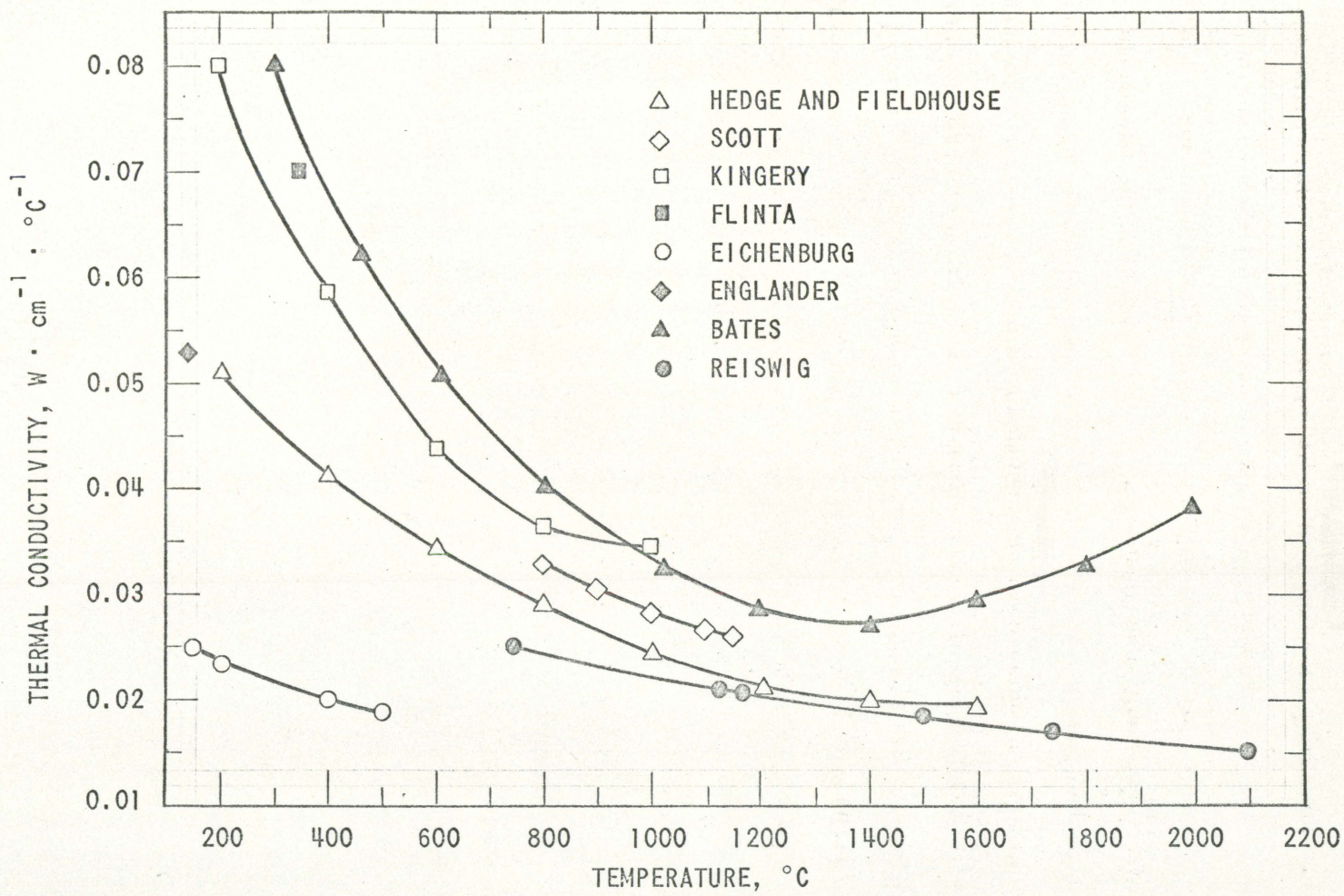


Fig. 1 Reported thermal conductivity values of uranium dioxide

III. FORMULATION

A. Derivation of Experimental Equations

An experiment has been prepared (14) to determine the thermal diffusivity of UO_2 in the Transient Reactor Test Facility, (TREAT). Two rods of different U^{235} enrichment are bonded end to end. The combined rod is then exposed to a uniform, intense burst of neutron radiation within TREAT, causing a temperature rise in each portion which is approximately proportional to its respective enrichment. The heat within the sample is generated internally by the fission process. By means of two thermocouples embedded within the rod, $\pm L$, distance from the interface, the temperature difference, ΔT , existing between the two thermocouple positions can be measured as a function of time. If the value of ΔT at a certain time is known, the thermal diffusivity of the sample may be found, using the formula, (as derived by Golden [14])

$$\Delta T = \left[T_{01} - T_{02} \right] \operatorname{erf} \frac{L}{2\sqrt{Dt}} \quad (1)$$

Another method, from the same experiment, for determining the thermal diffusivity of the sample is by measuring the slope, $(\partial \Delta T / \partial t)_L$, of the photographic data trace, which is a record of ΔT vs time, at a time, t , and using the formula, (also derived by Golden [14])

$$\left(\frac{\partial \Delta T}{\partial t} \right)_L = - \frac{1}{\sqrt{\pi}} \left[\frac{T_{01} - T_{02}}{t} \right] \frac{L}{2\sqrt{Dt}} e^{-\left(\frac{L}{2\sqrt{Dt}}\right)^2} \quad (2)$$

In the two equations, (1) and (2),

$T_{01} - T_{02}$ = maximum temperature difference between the two portions of the sample

ΔT = temperature difference between the two portions

of the sample rod at $t > 0$

t = time, $t=0$ at time of maximum AT

$\pm L$ = distance of each thermocouple from the interface

D = thermal diffusivity of the sample material

The following assumptions are made:

- (1) thermal conductivity varies linearly with temperature;
- (2) temperature as a function of time and position can be described by the one-dimensional rectangular form of the time-dependent heat equation;
- (3) the rod extends to $\pm \infty$;
- (4) the initial temperature (just following the neutron burst) in each of the two regions is uniform;
- (5) radial heat loss by radiation is negligible for the anticipated time scale of the experiment, (a few seconds);
- (6) the product of density and specific heat (the volumetric heat capacity) is constant.

The experiment in question is similar to that discussed by R. H. Stokes (32) dealing with the diffusion of solutions of two concentrations across an initially sharp boundary between two semi-infinite columns of liquid. Stokes gives the basic differential equation for one-dimensional diffusion with a diffusion coefficient, D , which is a function of concentration as:

$$\frac{\partial c}{\partial t} = \frac{\partial}{\partial x} \left(D \frac{\partial c}{\partial x} \right) \quad (3)$$

If temperature is substituted for concentration, the equation becomes:

$$\frac{\partial T}{\partial t} = \frac{\partial}{\partial x} \left(D \frac{\partial T}{\partial x} \right) \quad (4)$$

which is applicable for the case in point. The solution of the above equation, given by Stokes, is presented in Appendix A.

To obtain an accurate determination of thermal diffusivity by application of the above model precise measurements of the temperature distribution, within the sample, as a function of time, must be made. Since it is felt that such measurements cannot readily be made in the TREAT reactor at high temperatures, this model is not considered further.

As a simplification of the above model, it was next assumed that the thermal conductivity is constant for the range of temperature encountered in a given experiment. An analytical solution of the heat equation, under this condition, is given in Appendix B. Using this assumption and the original assumptions, 2-6, it was found that for a rod of infinite length:

$$T_1 = T_{01} - \frac{1}{2} \left(T_{01} - T_{02} \right) \operatorname{erfc} \frac{|x|}{2 \sqrt{Dt}} \quad (5)$$

$$T_2 = T_{02} + \frac{1}{2} \left(T_{01} - T_{02} \right) \operatorname{erfc} \frac{|x|}{2 \sqrt{Dt}} \quad (6)$$

By subtracting the above equations it was found that:

$$\Delta T = T_1 - T_2 = \left(T_{01} - T_{02} \right) - \left(T_{01} - T_{02} \right) \operatorname{erfc} \frac{L}{2 \sqrt{Dt}}$$

or

$$\Delta T = \left(T_{01} - T_{02} \right) \operatorname{erf} \frac{L}{2 \sqrt{Dt}} \quad (7)$$

yielding the basic equation for determining D by measuring ΔT at a given time, t.

Two thermocouples are placed at a distance $\pm L$ from the interface, connected in series, to measure the rate of change of temperature difference with respect to time. If equation (7) is differentiated with

respect to time:

$$\left(\frac{\partial \Delta T}{\partial t}\right)_L = \left(T_{01} - T_{02}\right) \frac{2}{\sqrt{\pi}} \frac{a}{\partial t} \int_0^{\frac{L}{2\sqrt{Dt}}} e^{-\lambda^2} d\lambda$$

or

$$\left(\frac{\partial \Delta T}{\partial t}\right)_L = -\frac{1}{\sqrt{\pi}} \left(\frac{T_{01} - T_{02}}{t}\right) \left(\frac{L}{2\sqrt{Dt}}\right) e^{-\left(\frac{L}{2\sqrt{Dt}}\right)^2} \quad (8)$$

Define

$$a = \frac{L}{2\sqrt{Dt}}$$

Then

$$\left(\frac{\partial \Delta T}{\partial t}\right)_{L,\tau} = -\frac{1}{\sqrt{\pi}} \left(\frac{T_{01} - T_{02}}{\tau}\right) a e^{-a^2} \quad (9)$$

which is the equation used to determine thermal diffusivity by measuring the slope of the photographic data trace at a given time, τ .

B. Feasibility of Experiment

The validity of equations 7 and 9 will be established if the validity of the preceding assumptions can be proven.

Assumptions 2 and 4 are based upon the conclusion that the initial axial neutron distribution within each portion of the sample is constant. Since the internal heat is produced by the fission process which is initiated by neutron absorption the temperature distribution will be uniform if the neutron distribution is uniform. Uniform heat generation will permit temperature as a function of time and (axial) position to be described by the one-dimensional rectangular form of the time-dependent heat equation.

Paine and Taraba (33) have derived the equation:

$$\phi(z,\tau) = A(\tau) e^{-[B(\tau)z]} + C(\tau)$$

from experimental data which gives the longitudinal distribution of thermal neutron flux in a cylindrical fuel specimen during irradiation.

where

$\phi(z,\tau)$ = the average cross sectional flux at distance z ,
from the end of the cylinder

$A(\tau), B(\tau), C(\tau)$ = constants varying with sample radius and enrichment, for further definition see (33)

τ is defined as $= a[0.91 a(\Sigma_{ab} + \Sigma_s)]$

a = radius of the sample.

Normalization of the above equation yields:

$$\frac{\phi}{C} = 1 + 0.278 e^{-BZ}$$

The calculated values of $\frac{\phi}{C}$ for various values of Z in a 10% enriched UO_2 sample for $a=0.64$ cm. for which $B = 1.79 \text{ cm.}^{-1}$ are tabulated in Table 1.

Table 1. Axial flux distribution

Z cm.	normalized z to end of sample	BZ	e^{BZ}	$0.278e^{-BZ}$	$\frac{\phi}{C}$	$\frac{\phi}{C}$ normalized to end of sample
0	0	0	1.00	0.278	1.278	1.00
0.2	0.1	0.358	1.43	0.194	1.194	0.935
0.4	0.2	0.716	2.05	0.136	1.136	0.891
0.8	0.8	1.432	4.18	0.067	1.067	0.836
1.0	0.5	1.790	5.98	0.046	1.046	0.820
1.2	0.6	2.150	8.58	0.032	1.032	0.813
1.4	0.7	2.510	12.30	0.023	1.023	0.804

Table 1 (Continued)

Z cm.	normalized z to end of sample	B2	e^{BZ}	$0.276e^{-BZ}$	$\frac{\phi}{C}$	$\frac{\phi}{C}$ normalized to end of sample
1.6	0.8	2.860	17.46	0.016	1.016	0.796
1.8	0.9	3.220	25.03	0.011	1.011	0.793
2.0	1.0	3.580	35.87	0.008	1.008	0.789

From the normalized values of $\frac{\phi}{C}$ in Table 1 it can be concluded that the axial flux distribution within the UO_2 sample can be considered constant over the thermocouple region thereby validating assumptions 2 and 4.

As a test of the validity of the third original assumption the temperature difference, ΔT , is computed, both for a rod of infinite extent and for one whose total length is 6 cm.

For the numerical calculations the variables involved are given values that are considered to be typical for the experiment involved.

Let

$$T_{01} = 2300^{\circ}\text{K}$$

$$T_{02} = 2100^{\circ}\text{K}$$

$$\rho C_p = .86 \text{ cal/cm}^3\text{-}^{\circ}\text{K}$$

$$k = .015 \text{ cal/sec-cm-}^{\circ}\text{K}$$

$$D = .0174 \text{ cm}^2/\text{sec}$$

take

$$L = 1 \text{ cm}$$

$$\tau = 5 \text{ sec}$$

Then

$$\alpha = \frac{L}{2\sqrt{Dt}} = \frac{1}{2\sqrt{.0174(5)}} = 1.695$$

The temperature difference, ΔT , for a rod of infinite length:

$$\Delta T = (T_{01} - T_{02}) \operatorname{erf} \frac{L}{2\sqrt{Dt}} = 200^\circ\text{K}(0.98347)$$

$$\Delta T = 196.7^\circ\text{K}$$

In the case of the rod whose total length is 6 cm:

$$\begin{aligned} \Delta T = & (T_{01} - T_{02}) \left[\operatorname{erf} \left(\frac{L}{2\sqrt{Dt}} \right) - \operatorname{erfc} \left(\frac{2a-L}{2\sqrt{Dt}} \right) + \operatorname{erf} \left(\frac{2a+L}{2\sqrt{Dt}} \right) \right. \\ & \left. + \operatorname{erfc} \left(\frac{4a-L}{2\sqrt{Dt}} \right) \right] \end{aligned}$$

$$\Delta T = 200^\circ\text{K}[0.98347 - \text{negligible}] = 196.7^\circ\text{K}$$

Thus, the validity of the third assumption is established.

To confirm the fifth assumption, the heat loss due to thermal radiation was calculated using the following model. The following conditions were used to determine the case of greatest heat loss:

- (1) all temperature gradients in the system were neglected,
- (2) the temperature of the sample was assumed to be T_{01} ,
- (3) the emissivity of the surface of the sample was set equal to one,
- (4) the sample radiates to the interior of the TREAT transparent test capsule, which is composed of polished zircaloy, having an emissivity ≈ 0.08 ,
- (5) and the ratio of the sample surface area to the effective enclosure surface area is $\approx .167$.

Then if the sample is a solid cylinder of diameter, d , the instantaneous

heat transfer rate per unit length at time zero is given by Jakob and Hawkins (19) as:

$$\frac{q}{t} \approx \sigma \epsilon d \frac{T_{01}^4}{1 + .167 \left(\frac{1}{0.08} - 1 \right)} = \frac{\pi d^2}{4} \rho C_p \frac{dT_1}{dt}$$

from which

$$\frac{dT_1}{dt} \approx \frac{1.37 \sigma T_{01}^4}{\rho C_p d}$$

If $d = 1$ cm, and $T_{01} = 1900^\circ\text{K}$, which is a typical experimental temperature, then:

$$\frac{dT_1}{dt} \approx 28 \text{ K/sec}$$

Thus at the end of five seconds,

$$\Delta T_1 \approx 140^\circ\text{K}$$

which represents the maximum amount of heat that will be lost from the sample due to radiation under isothermal conditions.

In the actual experiment there exist several conditions that will appreciably lower the above radiation heat loss.

In the above calculations the emissivity of uranium dioxide was given the maximum value of one. Under actual conditions the emissivity will be less than one, which will tend to decrease the amount of heat lost from the sample because of radiation.

The calculated values of ΔT represent the amount of heat lost from the outside of the sample, neglecting all internal temperature gradients.

A series of calculations were made using the RE-147 computer code, as described by Heestand (18), to obtain an accurate internal temperature

distribution under non-isothermal conditions. These calculations are discussed in Section VI - A-4. From these calculations it was concluded that radial radiant heat loss will have negligible effect upon the axial temperature of the sample because of the poor thermal conductivity of UO_2 . This conclusion is substantiated by Fig. 17, which illustrates the percentage temperature decrease within the sample at a given time vs radius. It can be seen from Fig. 17 that under non-isothermal conditions the axial temperature is not affected by radiant heat loss for periods of time as long as six seconds.

Since the thermocouples are located on the axis of the sample and responsive to the axial flow of heat, it is felt that any effect that radiant heat loss will have upon the experimental thermal diffusivity is negligible.

If experience proves the fifth original assumption invalid, it may be necessary to build a thermal radiation shield around the sample. Such a shield might be a thin shell of UO_2 enriched so as to match closely the initial temperature distribution in the sample.

IV. EXPERIMENTAL ERRORS

A. Description of Experimental Oscillograph Trace

The data to be analyzed from the given experiment will return from the National Reactor Testing Station at Idaho Falls, Idaho, in the form of a photographic oscillograph trace similar in shape to Fig. 2. The trace will be a measure of the temperature difference existing between the portions of different enrichments in the sample as a function of time. The given formulae with which to compute the thermal diffusivity of a sample employ either a value of ΔT or of the slope at some point of time, t .

B. Errors to be Investigated

It is the object of this section to determine at what value of t the most accurate measurement of ΔT or slope, A , may be obtained in order to yield the most accurate computed value of D .

The aspects to be investigated are as follows:

- (1) What influence will a given error in the measurement of time, t , have on the value of D .
- (2) What influence will a given error in the measurement of the temperature difference, ΔT , have on the value of D .
- (3) What influence will a given error in the measurement of the slope, A , have on the value of D .
- (4) Which is the most accurate method of computing D , using ΔT or by using A , at some value of time, t .
- (5) What is the time, t , at which the most accurate value of ΔT or A may be obtained.

C. Derivation of Error Relationships

To derive the relationships

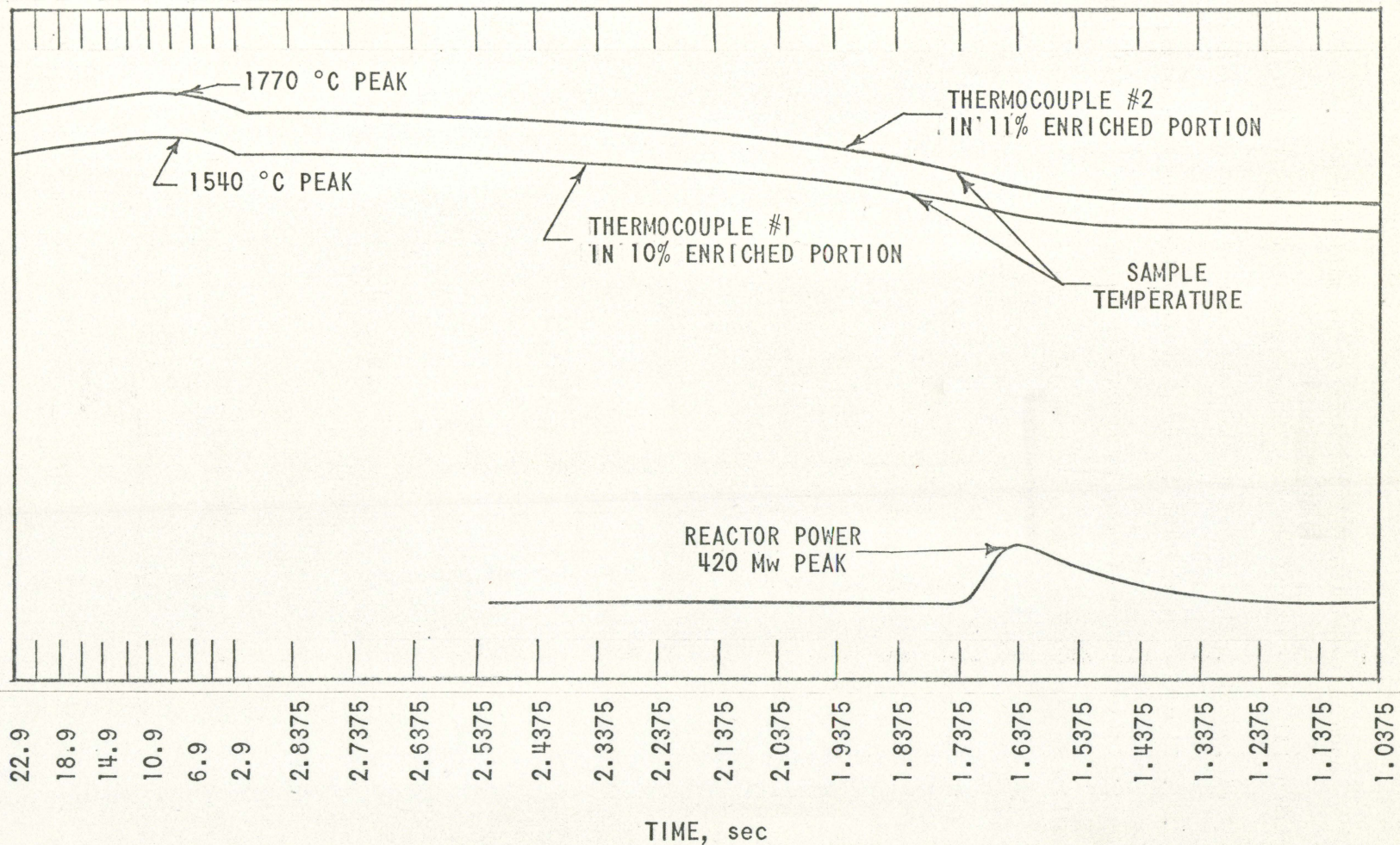


Fig. 2 Sample oscilloscope chart

$$\frac{dD}{D} = f_1 \left(\frac{dt}{t} \right)$$

$$\frac{dD}{D} = f_2 \left(\frac{d\Delta T}{\Delta T} \right)$$

$$\frac{dD}{D} = f_3 \left(\frac{\frac{d\Delta T}{\Delta T}}{\frac{dt}{t}} \right)$$

The basic formulae, as derived by Golden (14), are as follows:

$$\left(\frac{\partial \Delta T}{\partial t} \right)_L = - \frac{1}{\sqrt{\pi}} \left(\frac{T_{01} - T_{02}}{t} \right) \frac{L}{2 \sqrt{Dt}} e^{- \left(\frac{L}{2 \sqrt{Dt}} \right)^2}$$

and

$$\Delta T = \left(T_{01} - T_{02} \right) \operatorname{erf} \frac{L}{2 \sqrt{Dt}}$$

and

$$d\Delta T = - \frac{1}{\sqrt{\pi}} \left(T_{01} - T_{02} \right) \alpha e^{-\alpha^2} \frac{dD}{D}$$

where

$$\alpha = \frac{L}{2 \sqrt{Dt}}$$

1. For the relationship between the error in thermal diffusivity associated with an error in time:

$$\frac{dD}{D} = f_1 \left(\frac{\partial t}{t} \right)$$

Using the basic equation

$$\left(\frac{\partial \Delta T}{\partial t} \right)_L = - \frac{1}{\sqrt{\pi}} \left(\frac{T_{01} - T_{02}}{t} \right) \frac{L}{2 \sqrt{Dt}} e^{- \left(\frac{L}{2 \sqrt{Dt}} \right)^2}$$

Let,

$$A = \left(\frac{\partial \Delta T}{\partial t} \right)_L$$

$$B = -\frac{1}{\sqrt{\pi}} \left(T_{01} - T_{02} \right)$$

Substituting into the original equation,

$$A = \frac{BL}{2t\sqrt{Dt}} e^{-\frac{L^2}{4Dt}}$$

solving for B,

$$B = \frac{2At\sqrt{Dt}}{L} e^{+\frac{L^2}{4Dt}}$$

and differentiating B, once with respect to t, yields,

$$\frac{\partial B}{\partial t} = \frac{A}{2L\sqrt{Dt}} e^{+\frac{L^2}{4Dt}} \left(6Dt - L^2 \right)$$

Also differentiating B once with respect to D, yields,

$$\frac{\partial B}{\partial D} = \frac{A}{L\sqrt{Dt}} e^{+\frac{L^2}{4Dt}} \left[\frac{2D^2t^2 - L^2t}{2D} \right]$$

Since

$$\frac{\partial D}{\partial t} = \frac{\frac{\partial B}{\partial t}}{\frac{\partial B}{\partial D}} = \frac{\partial B}{\partial t} \times \frac{\partial D}{\partial B}$$

Then

$$\begin{aligned} \frac{\partial D}{\partial t} &= \frac{\frac{A}{2L\sqrt{Dt}} e^{+\frac{L^2}{4Dt}} \left(6Dt - L^2 \right)}{\frac{A}{L\sqrt{Dt}} e^{+\frac{L^2}{4Dt}} \left(\frac{2D^2t^2 - L^2t}{2D} \right)} \\ &= \frac{3}{2} \frac{6Dt - L^2}{2D^2t^2 - L^2t} \end{aligned}$$

or,

$$\frac{\partial D}{\partial t} = \frac{D}{t} \left(\frac{6Dt - L^2}{2Dt - L^2} \right)$$

yielding,

$$\frac{dD}{D} = \left(\frac{6Dt - L^2}{2Dt - L^2} \right) \frac{dt}{t}$$

2. For the relationship between the error in thermal diffusivity associated with an error in slope, A:

$$\frac{dD}{D} = f_2 \left(\frac{dA}{A} \right)$$

Using the same basic equation as in part A, let,

$$A = \left(\frac{\partial AT}{\partial t} \right)_L$$

$$B = -\frac{1}{\sqrt{\pi}} (T_{01} - T_{02})$$

Once more,

$$A = \frac{BL}{2t\sqrt{Dt}} e^{-\frac{L^2}{4Dt}}$$

Differentiating A once with respect to D, gives

$$\frac{\partial A}{\partial D} = \frac{BL}{4t^{3/2} D^{3/2}} e^{-\frac{L^2}{4Dt}} \left[\frac{L^2}{2Dt} - 1 \right]$$

Multiplying both sides by ∂D and dividing by A, gives,

$$\frac{\partial A}{A} = \frac{BL}{4t^{3/2} D^{3/2}} \left[\frac{L^2}{2Dt} - 1 \right] e^{-\frac{L^2}{4Dt}} \frac{dD}{A}$$

or

$$\frac{dA}{A} = \frac{BL}{Aht^{3/2}D^{1/2}} \left[\frac{L^2}{2Dt} - 1 \right] e^{-\frac{L^2}{4Dt}} \frac{dD}{D}$$

Substituting into the original equation,

$$A = \frac{BL}{2t\sqrt{Dt}} e^{-\frac{L^2}{4Dt}}$$

yields,

$$\frac{dA}{A} = \frac{1}{2} \left[\frac{L^2}{2Dt} - 1 \right] \frac{dD}{D}$$

or,

$$\frac{dD}{D} = \left[\frac{4tD}{L^2 - 2Dt} \right] \frac{dA}{A}$$

3. The relationship between the error in thermal diffusivity associated with an error in temperature difference,

$$\frac{dD}{D} = f_3 \left(\frac{d\Delta T}{\Delta T} \right) ,$$

is discussed in Golden's personal communication (14).

Given:

$$\begin{aligned} \frac{d\Delta T}{\Delta T} &= -\frac{1}{\sqrt{\pi}} \left(T_{01} - T_{02} \right) \frac{L}{2\sqrt{Dt}} e^{-\frac{L^2}{4Dt}} \frac{dD}{D} \\ \therefore \frac{dD}{D} &= \frac{-\pi\sqrt{\Delta T}}{\left(T_{01} - T_{02} \right) \frac{L}{2\sqrt{Dt}}} \frac{d\Delta T}{\Delta T} \end{aligned}$$

where ΔT at time, t , is given by,

$$\Delta T = \left(T_{01} - T_{02} \right) \operatorname{erf} \frac{L}{2\sqrt{Dt}}$$

Substituting the formula for ΔT into $dD/D = f_3(\Delta AT/\Delta T)$ and simplifying gives,

$$\frac{dD}{D} = -\sqrt{\pi} \left[\frac{2\sqrt{Dt}}{L} \right] e^{-\frac{L^2}{4Dt}} \operatorname{erf} \left[\frac{L}{2\sqrt{Dt}} \right] \frac{d\Delta T}{\Delta T}$$

D. Determination of the Influence of Errors upon Thermal Conductivity

Determining the influence of

$$\frac{dt}{t}, \frac{d\Delta T}{\Delta T}, \text{ and } \frac{dA}{A} \text{ upon } \frac{dD}{D}.$$

Using the derived equations, substitute a constant value in place of dt/t , $d\Delta T/\Delta T$, and dA/A . D was taken to equal $.185 \text{ cm}^2/\text{sec}$, $l=1 \text{ cm}$. Values of t were taken from $t=0$ to $t=15 \text{ sec}$.

To find the position in time where there exists the least influence of the given error upon dD/D ; the ratios $\frac{d\Delta T/\Delta T}{dD/D}$, $\frac{dA/A}{dD/D}$, and $\frac{dt/t}{dD/D}$, were plotted as a function of t .

The point of minimum influence of the various errors in t , ΔT , and A upon D will be at that time where

$$\frac{\frac{d\Delta T}{\Delta T}}{\frac{dD}{D}} + \frac{\frac{dA}{A}}{\frac{dD}{D}} + \frac{\frac{dt}{t}}{\frac{dD}{D}} \rightarrow \infty, \text{ namely}$$

a certain error in $d\Delta T/\Delta T$, dA/A , or dt/t approaches a 0 percent error in dD/D .

Since the ratios of errors are plotted the yielded traces are independent of the value of the constant error used in place of $d\Delta T/\Delta T$, dA/A , or dt/t . Fig. 3 shows the plotted ratios as functions of t , in units of

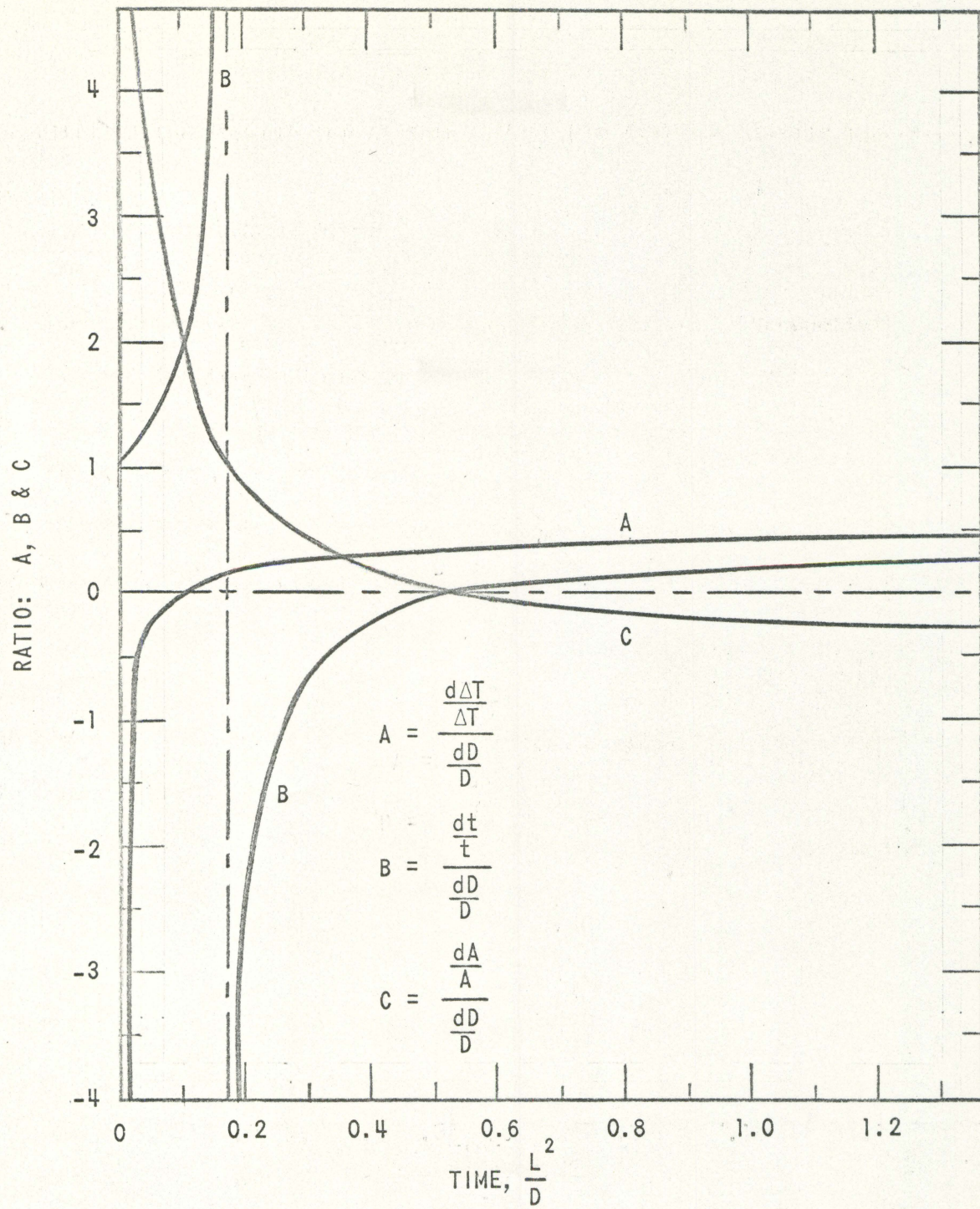


Fig. 3 Influence of $\frac{d\Delta T}{\Delta T}$, $\frac{dt}{t}$, $\frac{dA}{A}$ upon $\frac{dD}{D}$ vs
time (in units of $\frac{kL^2}{D}$) where $0 \leq k < 1.8$

$t=K(L^2/D)$, K equals a constant. The plotted curves illustrate the absolute influence of the errors in ΔT , A , and t upon dD/D .

As can be seen from Fig. 3 $\frac{d\Delta T/\Delta T}{dD/D}$ approaches ∞ at $t=0$, $\frac{dA/A}{dD/D}$ approaches ∞ at $t=0$, and $\frac{dt/t}{dD/D}$ approaches ∞ at $t=L^2/6D$.

From Fig. 3 it can, therefore, be concluded that the points of least influence (x) of $d\Delta T/\Delta T$, dA/A , and dt/t upon dD/D are either in or near the range $0 < x < L^2/6D$.

E. Times of Minimum Error Influence

The second factor involved in solving the given problem is finding the time of least error in measuring the values of t , ΔT , and slope, A , from which D is calculated.

1. To obtain the $\partial A/\partial t = f_1(t)$ differentiate the equation

$$\left(\frac{\partial \Delta T}{\partial t} \right)_L = \frac{1}{\sqrt{\pi}} \left(\frac{T_{01} - T_{02}}{t} \right) \frac{L}{2\sqrt{Dt}} e^{-\frac{L^2}{4Dt}},$$

once with respect to time yielding,

$$\frac{\partial A}{\partial t} = f_1(t).$$

Let

$$A = \left(\frac{\partial \Delta T}{\partial t} \right)_L$$

$$A = -\frac{1}{\sqrt{\pi}} \left(\frac{T_{01} - T_{02}}{2} \right) \frac{L}{t^{3/2} D^{1/2}} e^{-\frac{L^2}{4Dt}}$$

Differentiating once with respect to time, t ,

$$\frac{\partial A}{\partial t} = \left(\frac{L(T_{01} - T_{02})}{4\sqrt{\pi} D t^{1/2}} \right) e^{-\frac{L^2}{4Dt}} \left(\frac{L^2 - 6Dt}{2Dt} \right)$$

The change in the slope of the trace per change in time is equal to the error involved in measuring the slope A,

$$\frac{\partial A}{\partial t} = \frac{dA}{A}$$

$$\therefore \frac{dA}{A} = - \left(\frac{L(T_{01} - T_{02})}{4\sqrt{\pi} D t^{1/2}} \right) e^{-\frac{L^2}{4Dt}} \left(\frac{L^2 - 6Dt}{2Dt} \right)$$

2. The $dt/t = f_5(t)$ is given by

$$\frac{dt}{t} = \frac{C_t}{t}$$

in any time measurement device, there exists a given error of some magnitude. This error is of constant value throughout the period of time measurement; however, the error involved in such measurement decreases by the above formula as t increases.

3. The $dAT/AT = f_6(t)$ is given by

$$\frac{dAT}{AT} = C_{AT}$$

The error that exists in measuring AT is of the human type. Each person to physically measure the temperature difference from the data trace will do so in a different way. Since this cause of error is intangible and varying, it is said to be of constant value, C_{AT} , depending on the person involved.

Since the values of C_t and C_{AT} depend upon either the timing device used or the person analyzing the data, the values of C_t and C_{AT} were both

taken to equal 1 in this report. Any other value of C_t and C_{AT} will merely raise or lower the plotted curves involving C_t or C_{AT} . The points of least influence will not change.

Previously, the equations giving the influence of dAT/AT , dA/A , and dt/t upon dD/D and the formula yielding the values of dAT/AT , dA/A , and dt/t have been derived.

Let the equations

$$\frac{dD}{D} = \left(\frac{6Dt - L^2}{2Dt - L^2} \right) \frac{dt}{t}$$

$$\frac{dD}{D} = \left(\frac{4Dt}{L^2 - 2Dt} \right) \frac{dA}{A}$$

$$\frac{dD}{D} = -\sqrt{\pi} \left(\frac{2\sqrt{Dt}}{L} \right) e^{-\frac{L^2}{4Dt}} \operatorname{erf} \left(\frac{L}{2Dt} \right) \frac{dAT}{AT}$$

be known as the influence of the stated errors upon dD/D .

Let the formulae

$$\frac{dt}{t} = \frac{C_t}{t}$$

$$\frac{dA}{A} = - \left(\frac{L(T_{01} - T_{02})}{4\sqrt{\pi} D^{1/2} t^{5/2}} \right) e^{-\frac{L^2}{4Dt}} \left(\frac{L^2 - 6Dt}{2Dt} \right)$$

$$\frac{dAT}{AT} = C_{AT}$$

be known as the ability of measuring the stated quantity.

The point in time where the most accurate measurement of either t , A , or AT may be made is at that point where the minimum value of the error involved has the least influence on dD/D . By multiplying the influence equations by the respective ability equation; relationships yielding this

point as a $f(t)$ will be resolved. Thus for a measurement of time, t

$$\frac{dD}{D} = \left(\frac{6Dt - L^2}{2Dt - L^2} \right) \frac{C_t}{t},$$

for a measurement of the slope, A

$$\frac{dD}{D} = - \left(\frac{\frac{L^2 - 6Dt}{L^2 - 2Dt}}{e} \right) - \frac{L^2}{4Dt} \left(\frac{L(T_{01} - T_{02})}{2\sqrt{\pi} D^{1/2} t^{5/2}} \right)$$

and for a measurement of the temperature difference, ΔT ,

$$\frac{dD}{D} = - \sqrt{\pi} \left(\frac{2\sqrt{Dt}}{L} \right) e^{-\frac{L^2}{4Dt}} \left(C_{\Delta T} \right) \operatorname{erf} \left(\frac{L}{2\sqrt{Dt}} \right)$$

Figs. 4, 5, and 6 show the plots of the three above relationships. At any point where graphs 4, 5, and 6 approach ∞ , the influence upon dD/D becomes indeterminant and cannot be measured.

Fig. 4 illustrates the error involved in measuring ΔT as a function of time. At $t=0$, $dA/A \rightarrow \infty$ when $t \rightarrow \infty$, $dA/A \rightarrow 0$, therefore, the ideal time to measure ΔT is at $t=\infty$. Since this is impossible, it is recommended that any $t > \sim .35 L^2/D$ be used.

Fig. 5 shows the error involved in measuring A as a function of time. The influence of dA/A upon dD/D is indeterminant at $t=0$ and when $t \rightarrow .5 L^2/D$. The point of least influence at a measurable time is when $t=L^2/6D$.

Fig. 6 is the graph of the error involved in measuring t as a function of time. Again the influence of dt/t upon dD/D is indeterminant at $t=0$ and when $t=.5 L^2/D$. There is no influence of dt/t upon dD/D at $t=L^2/6D$.

Now that the relationships of

$$\frac{dD}{D} = f \left(\frac{dt}{t}, \frac{d\Delta T}{\Delta T}, \frac{dA}{A} \right)$$

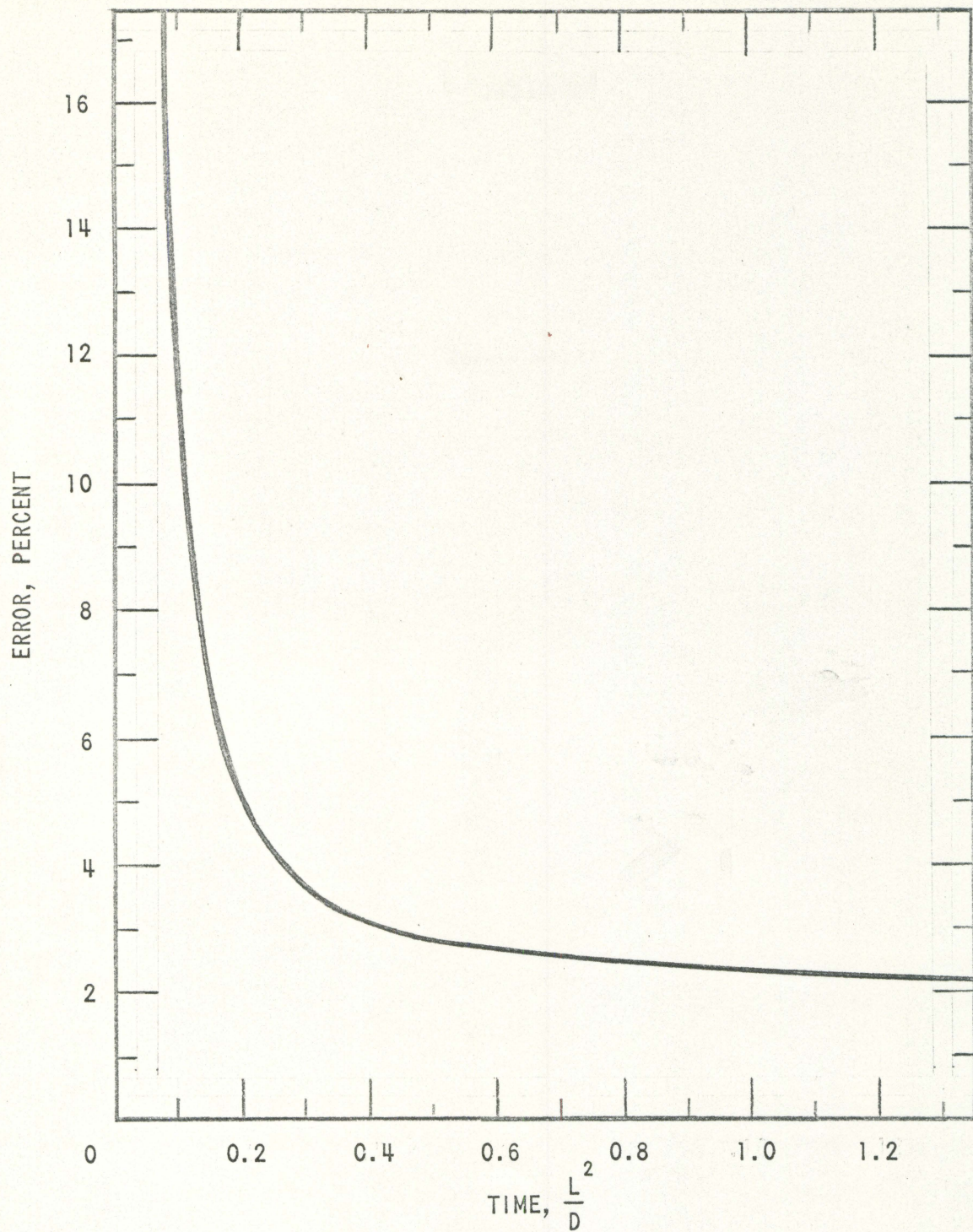


Fig. 4 Error in the temperature difference, $\frac{d\Delta T}{\Delta T}$,
vs time (in units of $\frac{kL^2}{D}$) where $0 \leq k < 1.8$

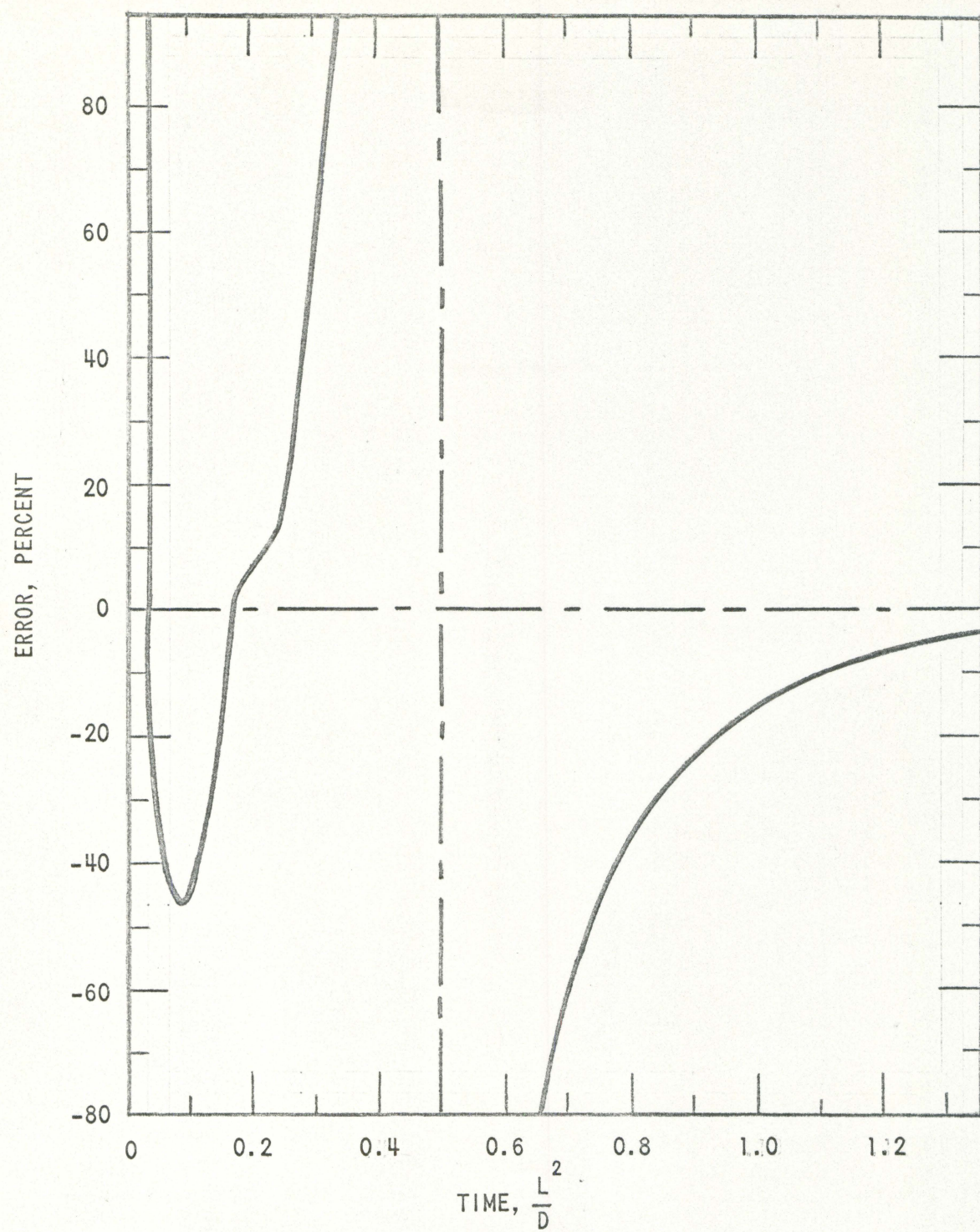


Fig. 5 Error in the slope, $\frac{dA}{A}$, vs time (in units

of $\frac{kL^2}{D}$) where $0 \leq k < 1.8$

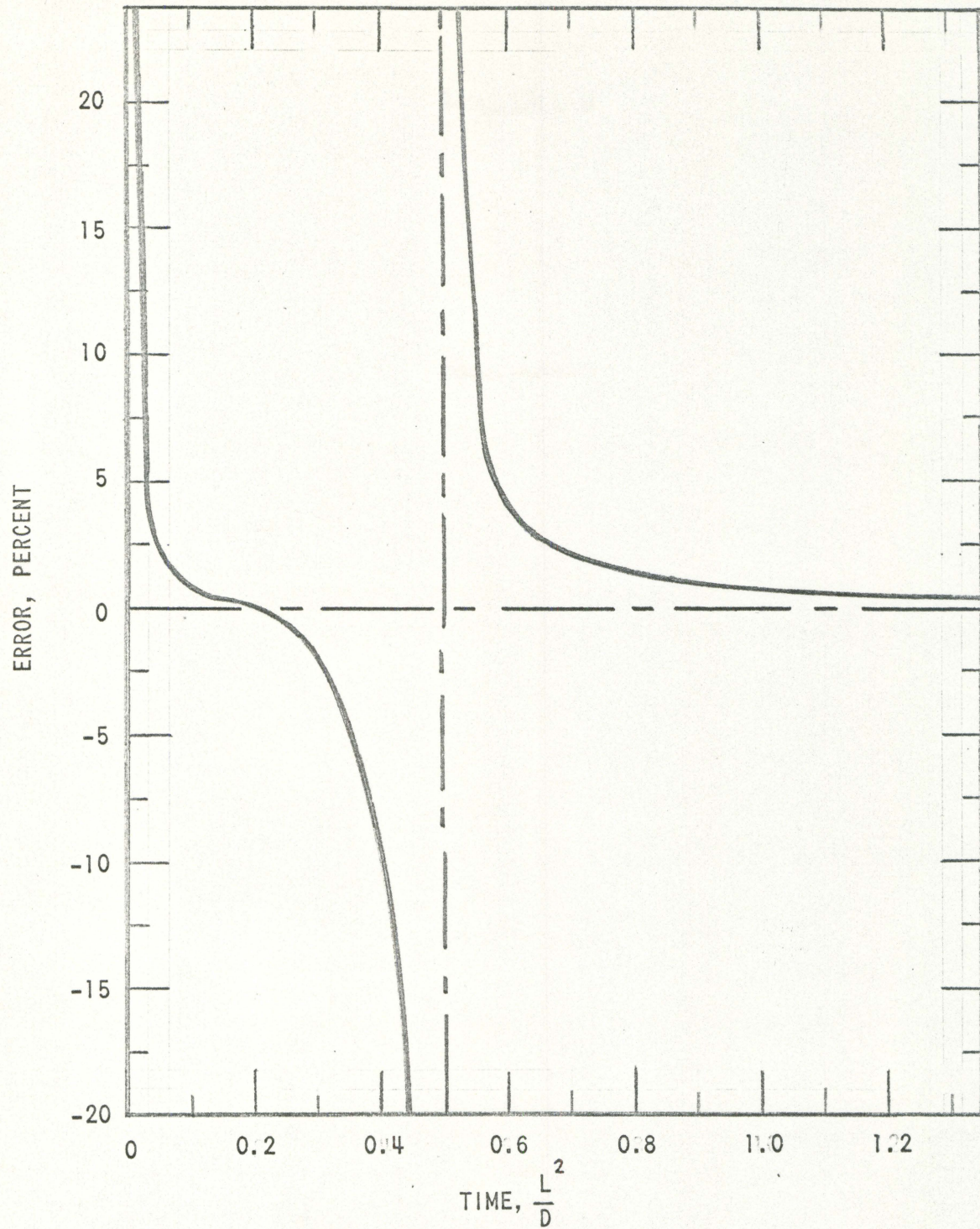


Fig. 6 Error in the time, $\frac{dt}{t}$, vs time (in

units of $\frac{kL^2}{D}$) where $0 \leq k < 1.8$

have been derived, it is possible to find the total effect of measuring D by means of either AT or A. Since both AT and A=f(t), the total error involved in each measurement to compute D will be the product of the dAT/AT and dt/t ; and dA/A and dt/t . Thus,

$$\frac{dD}{D} \text{ total by the slope measurement}$$

$$\frac{dD}{D} \text{ total } A = \frac{dA}{A} + \frac{dt}{t} + \frac{dA}{A} \left(\frac{dt}{t} \right)$$

and dD/D total by the temperature difference measurement.

$$\frac{dD}{D} \text{ total } AT = \frac{dAT}{AT} + \frac{dt}{t} + \frac{dAT}{AT} \left(\frac{dt}{t} \right)$$

Figs. 7 and 8 are the graphs of the total errors involved when measuring D, by means of the measurement of A or the measurement of AT, respectively.

F. Results and Conclusions

Fig. 7, combined error in slope and time, shows that the points of least error when measuring A is when $t=.02 L^2/D$, $.167 L^2/D$, $.26 L^2/D$ or when $t \rightarrow \infty$. The time $t=.02 L^2/D$ is undesirable due to the fact that any error in locating the point of time will result in a large error in the value of A. It is therefore, recommended that the measurement of A be made at $.15 L^2/D$ to $< .26 L^2/D$ ideally at $t=.167 L^2/D$. The maximum error in the range $.15 L^2/D < t < .26 L^2/D$ is 5%.

Fig. 8, combined error in temperature difference and time, gives the points of least error at $t=.235 L^2/D$ and as $t \rightarrow \infty$. The error in dD/D is indeterminant at $t=0$ and $t=.5 L^2/D$. The desirable range for measuring AT is when $.185 L^2/D < t < .35 L^2/D$, ideally at $t=.255 L^2/D$. The maximum error in the range $.185 L^2/D < t < .35 L^2/D$ is also 5%.

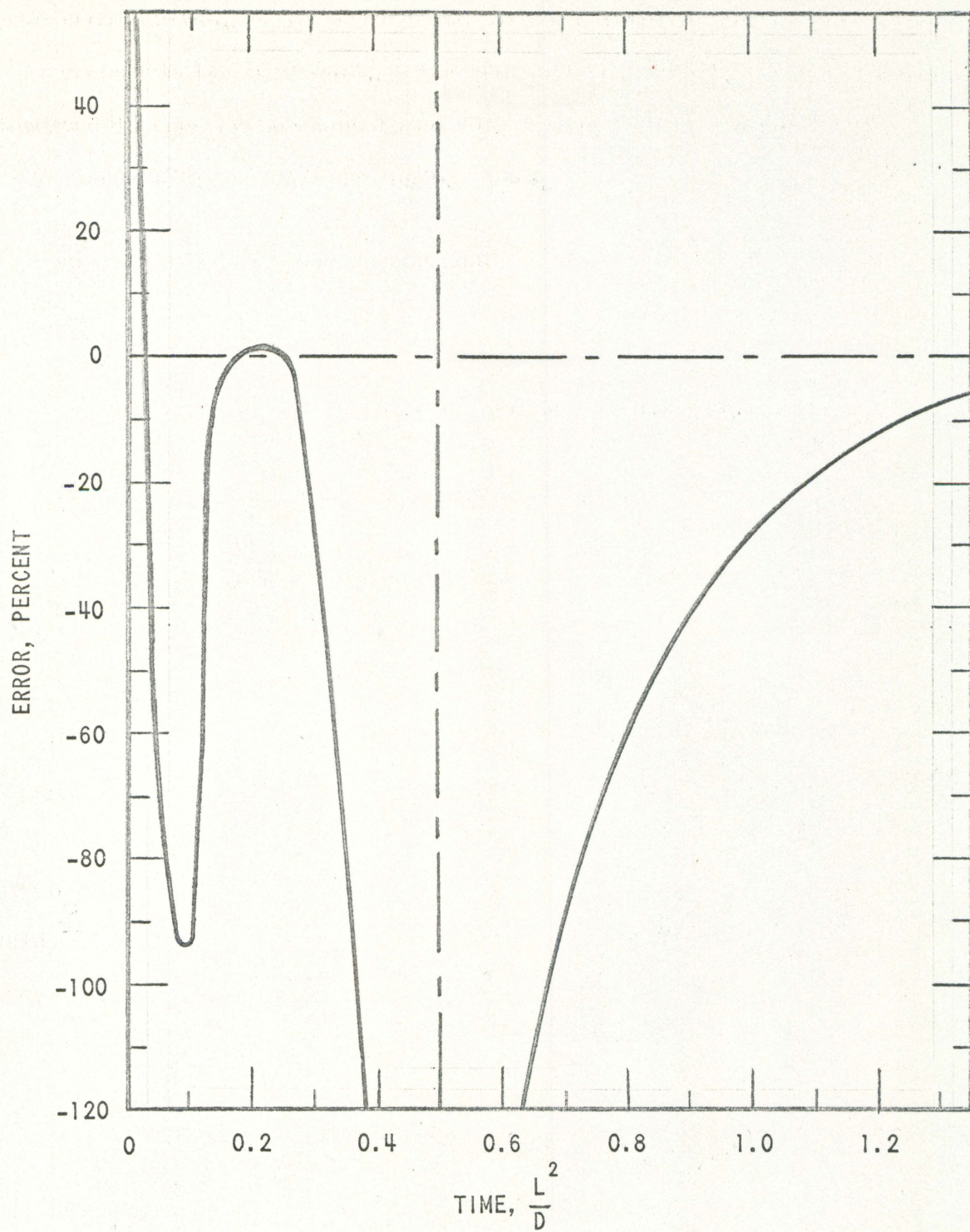


Fig. 7 Combined error in slope and time,
 $(d\Delta T/\Delta T + dt/t + d\Delta T/\Delta T + dt/t)$ vs
time (in units of kL^2/D) where $0 \leq k < 1.8$

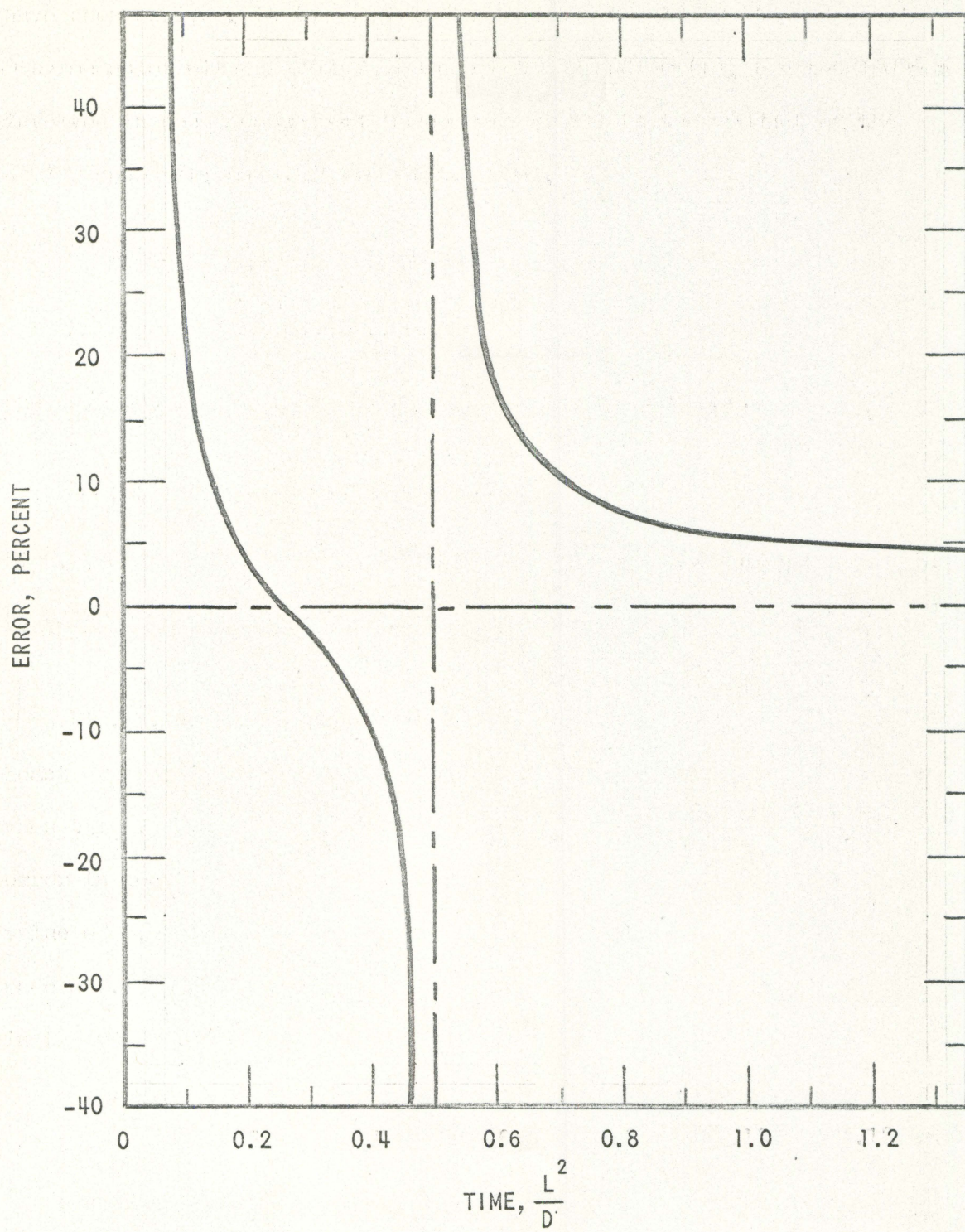


Fig. 8 Combined error in temperature difference and time ($d\Delta T/\Delta T + dt/t + d\Delta T/\Delta T + dt/t$) vs time (in units of kL^2/D) where $0 \leq k < 1.8$

(in units of kL^2/D) where $0 \leq k < 1.8$

From the above results, it was concluded that either method of computing D may be used with equal accuracy within the aforementioned ranges of t.

V. DESCRIPTION OF EXPERIMENTAL APPARATUS

A uranium dioxide sample was fabricated by Joseph Handwerk, Argonne National Laboratory, with two enrichments of U²³⁵. The sample consisted of two nominally half-inch diameter cylinders of eleven and ten weight percent enrichments fused together into a single cylinder, having two separate enrichments with an interface. The fusing was accomplished by firing the green unfired extrusions of individual enrichments while they were held in intimate contact.

A 0.125 cm hole was drilled in the fired sample from each end, along its centerline leaving 0.3125 cm of material between the bottom of each hole and the interface. These holes were to allow the insertion of sheathed thermocouples within the sample to measure the axial heat flow. Fig. 9 is a schematic diagram of the sample showing the relative position of the holes to the interface.

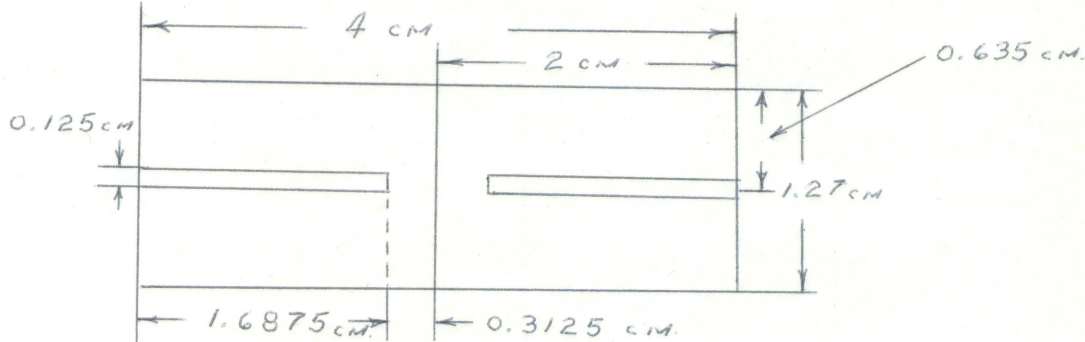


Fig. 9 Schematic diagram of sample.

The miniature, high-temperature thermocouples were tantalum sheathed, thoria insulated, tungsten 5% rhenium vs tungsten 26% rhenium. This type of thermocouple is capable of response times in the order of .1 seconds and can withstand temperatures in excess of 2300°C.

The experimental sample was supported within a refractory metal framework, Fig. 10, by spring loading the sheathed thermocouples into the axial holes. This mounting served the dual purpose of maintaining thermocouple contact during the transient and providing secondary shock mounting to the sample for shipment from Argonne National Laboratory to the TREAT facility at the National Reactor Testing Site in Idaho.

The sample, mounted in the refractory frame, was housed in a "transparent capsule", Fig. 11, (16), which provided a heat sink and particulate shield, and shipped to Idaho where it was sealed within the "transparent slot liner", Fig. 12, (16), which in turn was inserted in the TREAT reactor, Fig. 13, (25). The slot liner is a gas-tight encapsulation providing monitoring of released gaseous and airborne products while allowing motion picture studies of the sample during a reactor transient.

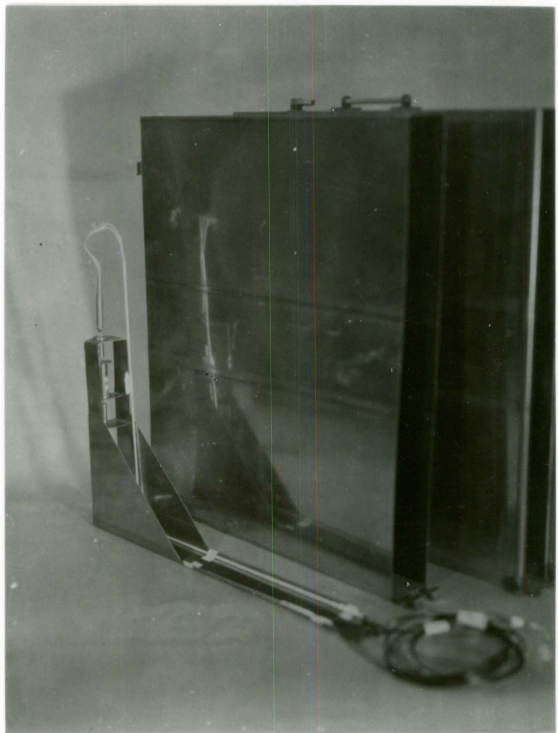
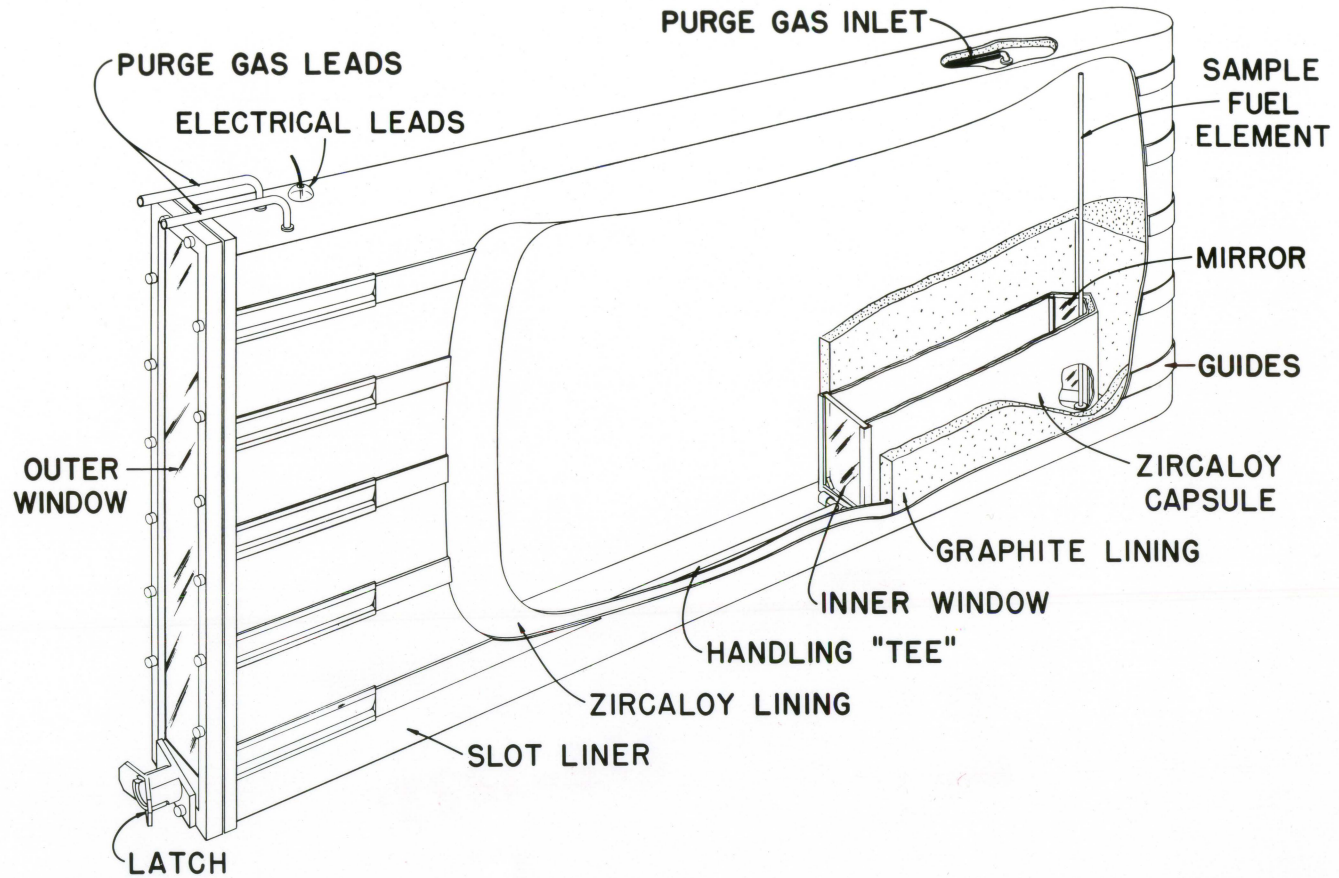


Fig. 10 Experimental "L" frame support
to be inserted in the transparent
slot liner within TREAT.



42

Fig. 11 Transparent meltdown facility



Fig. 12 Inner and outer capsule
subassemblies

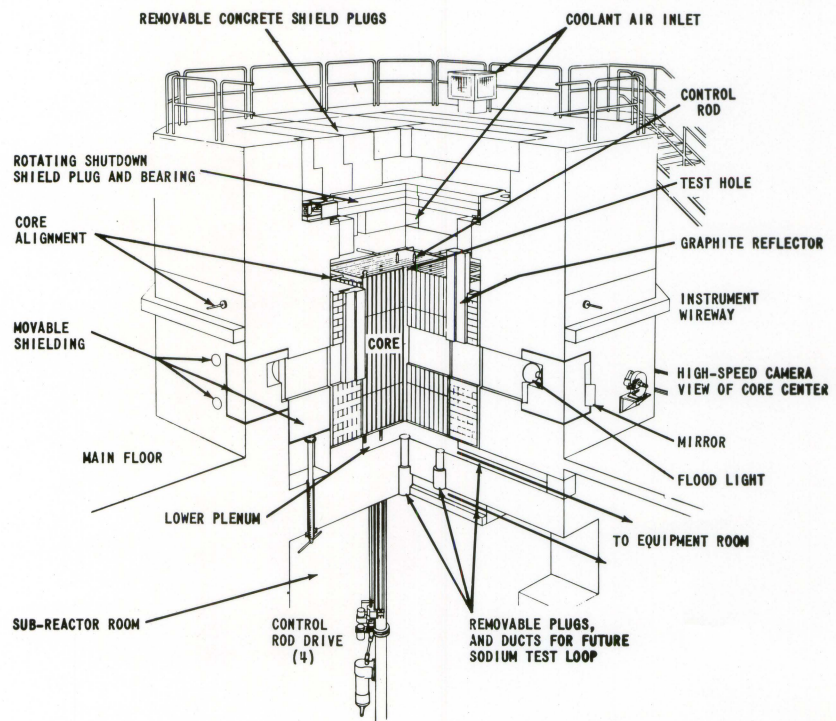


Fig. 13 Cutaway isometric of
TREAT reactor

VI. EXPERIMENTAL PROGRAM

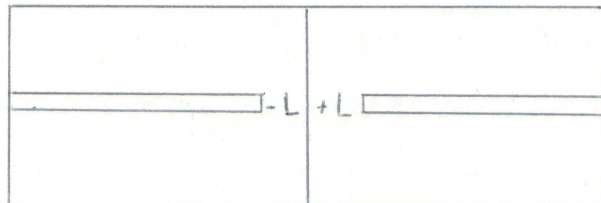
A. Sample Analysis

1. Thermocouple position

It is desired to determine the longitudinal and radial thermocouple position to be used in the experiment to determine the thermal diffusivity of UO_2 .

To facilitate calculations, one may consider the determination of each position as a separate problem. The geometry and method used in determining each position will be explained separately.

a. Longitudinal position By means of two thermocouples connected in series ΔT may be measured as a function of time, t . Let $\pm L$ be the axial distance from the bond to each thermocouple:



When determining the value L, three limiting positions will exist:

(1) Too small a value of L will yield a large decrease of ΔT per unit time. This fact leads to a graph similar to Fig. 14, in which it is difficult to accurately measure the slope, $\partial \Delta T / \partial t$, which is necessary for the calculation of D.

(2) Too large a value of L will yield a small decrease of ΔT per unit time. This fact leads to a graph similar to Fig. 16, in which it is difficult to resolve the various traces, caused by different values of D, at small values of t.

(3) The third factor which must be considered when positioning the thermocouple is the various heat losses involved in the experiment. Three types of heat loss or transfer exist in this experiment. They are:

(a) Longitudinal heat transfer across the bond, ΔT , which is necessary in order to determine D.

(b) Radial heat loss from the sample to its environment. This type of heat loss is explained and accounted for in the "Radial thermocouple position" discussion of this section.

(c) Axial heat loss from the ends of the sample to its environment.

Axial heat loss from the ends of the sample will directly affect the longitudinal thermocouple positions. If the thermocouples are placed too near the ends of the sample, end heat loss will introduce a major error into ΔT as a function of time. Therefore, it is necessary to have a value of L much less than the length of the rod. The ratio of $\pm L$ to sample length necessary to make the effect of end heat loss negligible will be determined and further elucidated in section VI, A-2.

A desirable value of L is one that will compromise the three limitations.

To show how the variance of L affects the calculation of D, it was necessary to employ a reversal of the given procedure. By graphing ΔT as a function of time for given values of D, holding L constant, it is possible to show the effect of L.

From Fig. 2 of the article "Thermal Conductivity of UO_2 Improves at High Temperature", (2), the three values of D used in this report were obtained. At

$$\sim 1900^\circ K, \quad k \sim = .03 \text{ watts/cm}^{-2}\text{K}$$

$$\sim 2200^\circ K, \quad k \sim = .045 \text{ watts/cm}^{-2}\text{K}$$

$$\sim 2700^\circ K, \quad k \sim = .0725 \text{ watts/cm}^{-2}\text{K}$$

From the above values of k, thermal conductivity, K, D was calculated to be $.00769 \text{ cm}^2/\text{sec}$, $.01154 \text{ cm}^2/\text{sec}$, and $.01791 \text{ cm}^2/\text{sec}$, respectively, using:

$$D = \frac{k}{\rho C_p}$$

where:

D = coefficient of diffusion

k = thermal conductivity

ρ = density

C_p = specific heat

The values of ΔT at various times were calculated using the equation:

$$\Delta T = \left(T_{01} - T_{02} \right) \operatorname{erf} \left(\frac{L}{Dt} \right)$$

where:

$$\left(T_{01} - T_{02} \right) = \text{maximum temperature difference}$$

t = time

L = thermocouple position, (previously defined)

The value of $T_{01} - T_{02}$ was chosen arbitrarily at 700°K. The values of L were chosen at .25 cm, .35 cm and .50 cm. Using the three values given for D , ΔT , as a function of time, was plotted for each of the above values of L .

To make the graphs obtained from this calculation independent of the value chose for $(T_{01} - T_{02})$, $\Delta T / (T_{01} - T_{02})$ was plotted vs time or:

$$\frac{\Delta T}{(T_{01} - T_{02})} = \operatorname{erf} \frac{L}{2\sqrt{Dt}}$$

Results and conclusions: Fig. 14 shows that $L=.25$ cm is an example of the first extreme. From Fig. 16 it appears that $L > .50$ cm is an example of the second extreme, difficult resolution of various values of D .

It is, therefore, concluded that a value of $.25 \text{ cm} < L < .50 \text{ cm}$ and $\sim .35 \text{ cm}$ would be the necessary compromise position of L . This conclusion is substantiated by Fig. 15.

b. Radial position When determining the radial thermocouple position, one is met by two types of heat transfer within the sample:

- (1) Longitudinal heat transfer,
- (2) Radial heat transfer, heat lost to the exterior environment of the sample.

Longitudinal heat transfer is the necessary ΔT , from which the value of D is computed. Radial heat loss, leads to an error in the measurement of ΔT , and therefore, must be kept to a minimum.

The ideal radial thermocouple position would be at the exact center of the sample. Since such an exacting thermocouple position is very

difficult to obtain, it becomes necessary to determine the tolerance of positioning error which will still yield an accurate measurement of AT.

To find this tolerance, a series of calculations, heat loss at various times, were made by C. Sayles using the RE-147, CYCLOPS, computer code (18). The temperature ranges for the properties of the material were chosen as 0°C to 800°C, 800°C to 1600°C, 1600°C to 2400°C, and 2400°C and up. The values used for thermal conductivity (2) are listed below.

<u>Temperature Range</u>	<u>K = watts/cm.⁻²K</u>
0-800	.01684
800-1600	.025
1600-2400	.045
2400-2500	.075

The values of specific heat of UO₂ are those given by Kelly (21).

These are presented in the form of the equation below.

$$C_p = 19.20 + 1.62 \times 10^{-3}T - \frac{3.96 \times 10^5}{T^2} \text{ cal/mole}$$

where:

T = temperature of material

The molecular weight of UO₂ is 270 gm/mole and an average value of the density is 10.6 gm/cm³. The values of volumetric specific heat are listed below.

Temperature Range, °C	C_p cal/mole-°C	C_p cal/gm-°C	C_p cal/cm³-°C
0-600	19.4157	.07643	.81015
600-1600	21.4038	.08426	.893
1600-2400	22.8056	.08978	.952
2400-2500	23.5578	.09274	.983

The value of the heat transfer coefficient is dependent on the environment, and the heat transfer coefficients for several different environments were examined. In all cases the pin was considered to be in the center of a two-inch diameter hollow cylinder.

In the first environment, the walls of the cylinder were considered to be graphite and the intervening space between the wall and pin was a vacuum. The second environment was the same as the first except that helium gas at a pressure of one atmosphere filled the space between the pin and cylinder wall. The third environment was the same as the first except the walls of the cylinder were aluminum. The purpose of the second environment was to observe the effect of convection on the heat transfer coefficients.

The heat transfer coefficient is composed of two parts, that due to radiation and that due to convection. At the temperature of interest, heat transfer due to radiation is the main course.

The equations for radiant heat transfer are given by Brown (5):

$$h = \frac{q}{A\Delta T} = \frac{q}{\Delta T} F_{1,2} \left(T_1^4 - T_2^4 \right)$$

where:

$$F_{1,2} = \frac{1}{1 + \left(\frac{1}{\epsilon_1} - 1 \right) + \frac{A_1}{A_2} \left(\frac{1}{\epsilon_2} - 1 \right)}$$

A_1 = area of pin

A_2 = area of wall

ϵ_1 = emissivity of UO_2 = 0.416

ϵ_2 = emissivity of wall - graphite = 0.95

alummel = 0.30

σ = Boltzman constant $.67785 \times 10^{-11}$ cal/cm² sec K⁴

T_1 = temperature of pin

T_2 = temperature of surroundings

$\Delta T = T_1 - T_2$

The equation for convective heat transfer is (27),

$$\frac{hD}{k_f} = \frac{1}{a} (Gr)^n (Pr)^m$$

where:

Gr = Grashaf number

Pr = Prandlt number

a, n, m = constants 2.6, .27, and .25 respectively

D = diameter of pin

k_f = thermal conductivity of gas (.000339 cal-cm/cm²-°C-sec)

Based on the equations, the following heat transfer coefficients at 2500°C were obtained.

Graphite - vacuum .06676 cal/cm² sec °C

Graphite - helium .06843 cal/cm² sec °C

Aluminum - vacuum .04545 cal/cm² sec °C

Since it is desired that as little heat be lost by the sample as possible, the worst cases are those with graphite. The effect of helium gas is seen to be very small. The values of the heat transfer coefficient used were

those of graphite and a vacuum.

Of the two coolant options with RE-147 (flowing coolant and stagnant coolant) only the flowing coolant option makes use of the heat transfer coefficient. Therefore, these problems were treated as flowing coolant and coolant velocity of zero.

The results of these calculations are presented in Fig. 17.

Results and conclusions: As can be seen from Fig. 17, negligible radial heat loss is experience between the center of the sample and sodium .127 cm even for periods of time up to six seconds. It is felt that the opportune time for measuring AT is well within this six-second duration. An approximate time for measurement of AT is when $t=L^2/6D$ or ~ 1.74 seconds.

It is therefore concluded that a radial thermocouple position of the center $\pm 10\%$ of the sample's radius will yield an accurate measurement of AT from which the value of D can be calculated.

2. Length of sample

As mentioned earlier, if the position of either of the thermocouples is close to the end of the sample, end heat loss will produce a large degree of error in the measurement of AT.

Presently, it is desired to determine the necessary length of the sample beyond a thermocouple which will make the effect of end heat loss negligible on AT.

Using the equation, describing the conduction of heat in the unsteady state during the condition of a sudden change of the surface temperature of a thick plane wall (19) it is to obtain the desired length, x.

The formula used is:

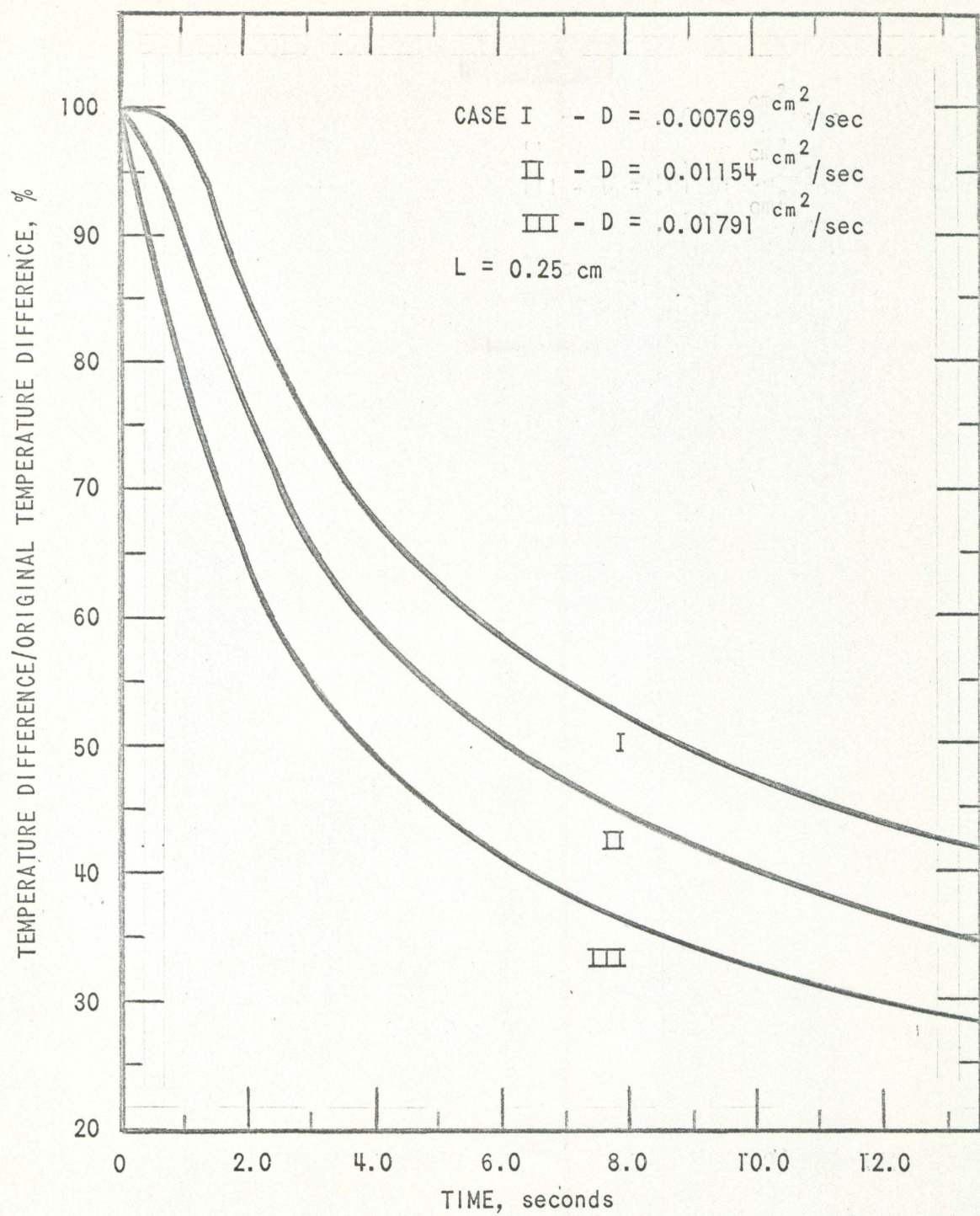


Fig. 14 Temperature difference (%)
vs time of UO_2

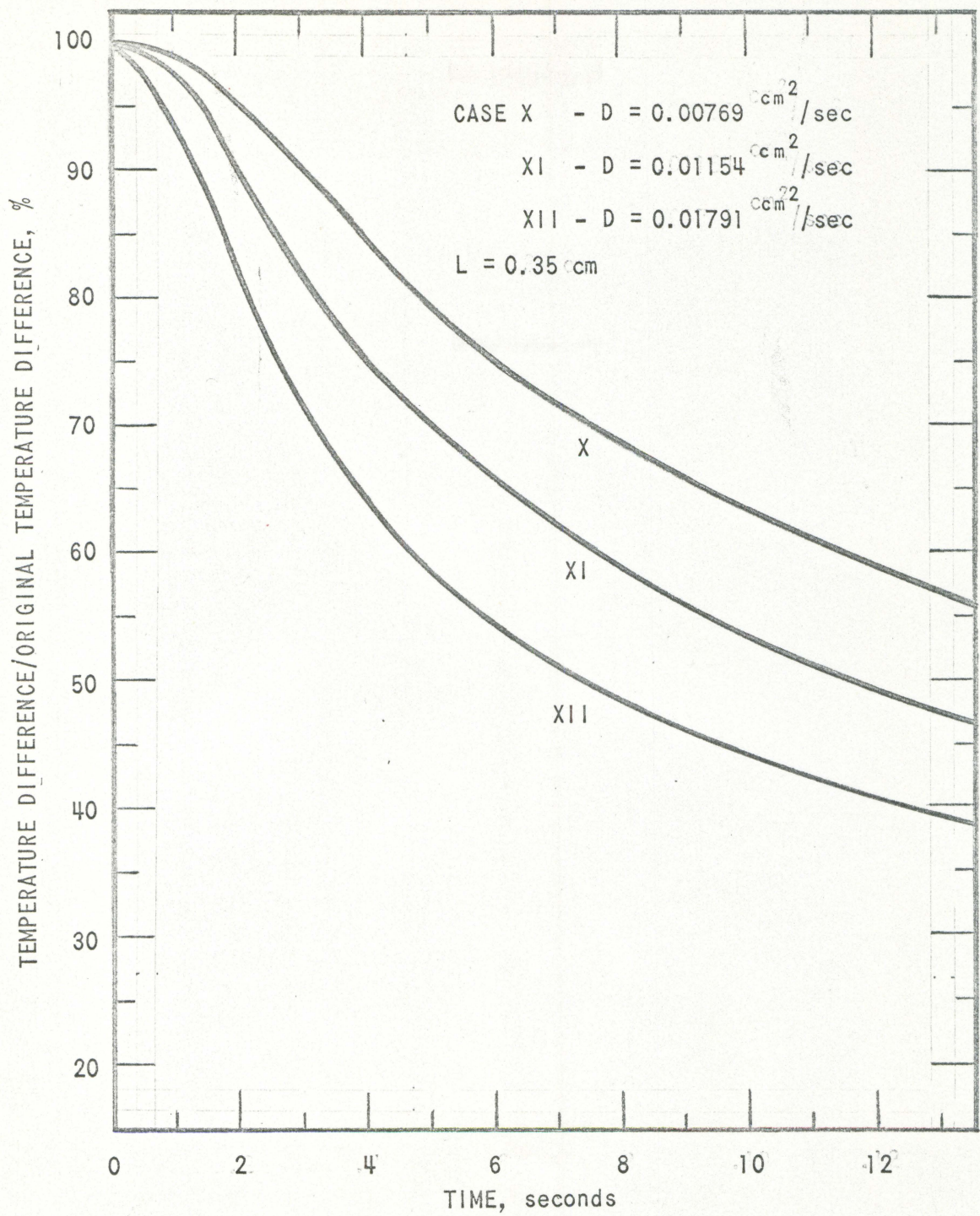


Fig. 15 Temperature difference (%)
vs time of UO_2

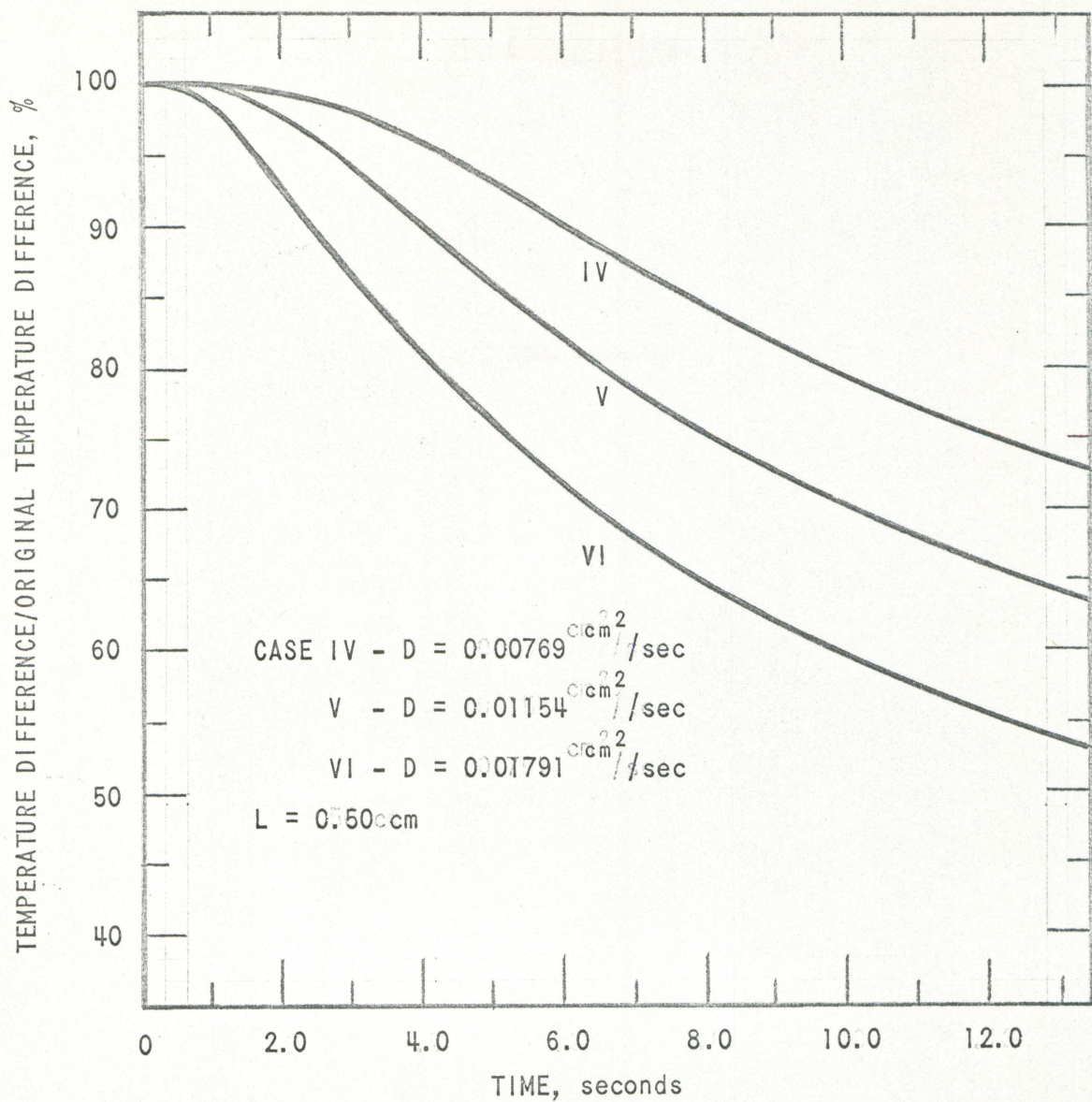


Fig. 16 Temperature difference (%)
vs time of UO_2

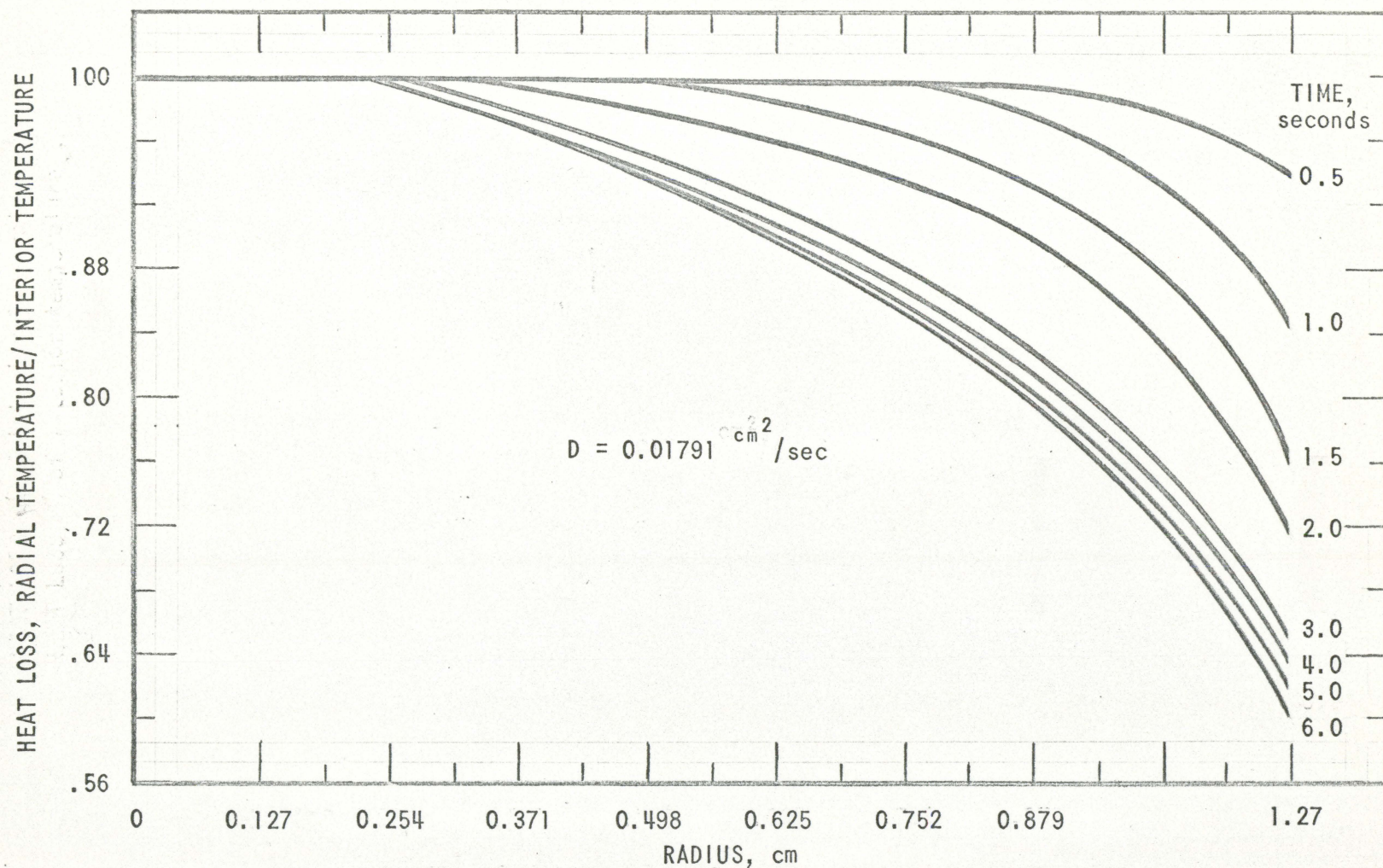


Fig. 1717 Radial temperature distribution within UO_2 rod

$$t = t_s + (t_i - t_s) \operatorname{erf} \left(\frac{x}{2\sqrt{\alpha\tau}} \right)$$

where:

t_i = initial temperature of sample

t_s = surface temperature instilled upon sample

α = thermal diffusivity of sample

x = previously defined

τ = time duration

t = temperature at position x at time τ

If the maximum conditions under which the given experiment can be conducted are substituted into the above equation, the maximum value of x needed to multiply the effect of end heat loss may be calculated.

The values used when calculating x are:

$t_i = 3000^\circ\text{C}$ (well above the melting point of UO_2)

$t_s = 30^\circ\text{C}$ (room temperature)

$t = (t_i - 1^\circ)$ (maximum heat loss allowed)

$\alpha = .01791 \text{ cm}^2/\text{sec}$ (maximum α investigated)

$\tau = 6 \text{ sec}$ (the time of measuring τT is 1.75 sec)

Substituting yields,

$$2999^\circ\text{C} = 30^\circ\text{C} + 2970^\circ\text{C} f \left(\frac{x \text{ cm}}{2\sqrt{.01791 \text{ cm}^2/\text{sec} (6 \text{ sec})}} \right)$$

$$f \left(\frac{x}{2\sqrt{.10746}} \right) = .9996633$$

$$\frac{x}{2\sqrt{.10746}} = 2.535$$

$$x = 2.535 (2) (.30626)$$

$$x = 1.55274 \text{ cm}$$

Results and conclusions: A length of 1.553 cm beyond L is needed to nullify all possible effect of end heat loss.

Summary: (1) The desired longitudinal thermocouple position, $\pm L$, is $\sim .35$ cm.

(2) The desired radial thermocouple position is the center $\pm 10\%$ of the sample's radius.

(3) If each half of the sample is at least 2 cm in length, the effect of end heat loss is negligible.

3. Enrichments

Due to the usage of the transparent meltdown capsule the value of the $K_{(0)}^{(0)}$ ex must be kept below 1.5%. A higher $K_{(0)}^{(0)}$ ex may result in damage to the test capsule.

To prevent error in the measurement of the shape or AT, the half width of the instantaneous power curve must be kept small in comparison to the desired time of measurement. A large value of the instantaneous power half-width will produce heat generation during the period of thermal diffusion between the portions of the sample. This will result in a distortion of the temperature difference vs time data trace, thus producing errors in the given values. A good first-order approximation of the error in time, dt/t , introduced by the instantaneous power half-width is: $dt/t = L/t$
where,

$$L = \frac{\text{half-width}}{2}$$

In order to get an approximate value of the enrichments necessary to attain the desired temperatures within the sample, calculations were made using the reactor specifications from Transient 41, Series SVII. Transient 41 was performed with a $K_{(0)}^{(0)}$ ex of 1.4%. Clipping the integrated power at

92.5 MWS will yield an integrated power of 150 MWS with a half-width of .24 sec. For this value of the instantaneous power half-width, $dt/t = \Sigma/t = .12/1.74 = 7\%$, which is within the permissible limits.

Therefore 150 MWS will be the specified reactor integrated power.

In order to raise the low enrichment portion of the sample to 2100°C:

$$H = \frac{C \Delta T}{P} = \frac{\left(2.31867 \times 10 \frac{\text{cal}}{\text{mole}} - ^\circ\text{C}\right) \left(2.1 \times 10^3 ^\circ\text{C}\right)}{(2.7007 \times 10^2) \text{ gm/mole}}$$

$$H = 1.80294 \text{ cal/gm}$$

will be needed.

Due to the usage of the transparent meltdown capsule there is 13% more reduction in the effective reactor integrated power than in the opaque capsule. The effective integrated power is 87% of 150 MWS or 130.5 MWS. To find the necessary calibration factor between heat generation and integrated power, the value of H was divided by the effective integrated power yielding $1.38156 \frac{\text{cal/gm}}{\text{MWS}}$.

Using the proper calibration factors for TREAT, $1.38156 \frac{\text{cal/gm}}{\text{MWS}}$ was found to be equivalent to $4.565 \times 10^{-12} \frac{\text{MWS}}{\text{fission/gm}}$. Comparing this value to $3.16 \times 10^{-11} \frac{\text{MWS}}{\text{fission/gm}}$ of the natural enriched EBR-II fuel pin, and taking into consideration the ratio of enrichments and absorptivities, the enrichment necessary to raise the low enrichment portions temperature to 2100°C was found to be 17.185%. The maximum permissible AT between the sample portions before fragmentation has been estimated to be 400°C.

Given a constant integrated power of 150 MWS it is necessary to determine an enrichment that will raise the second portion of the sample to 2500°C. The rate of the temperature increase in a reactor transient is:

$$\frac{dT}{dt} = \frac{P}{C}$$

where,

P = reactor power

C = heat capacity

$$P = \frac{\Sigma_f V}{C} \int_0^t nv dt$$

also,

$$\Sigma_f = N \bar{\sigma}_f$$

Σ_f = macroscopic fission cross section

σ_f = microscopic fission cross section

V = volume of sample

$$P = \frac{N \sigma_f}{C} \int_0^t nv dt$$

and C , heat capacity, = $\int_{T_1}^{T_2} \frac{PC}{P} V dT$

or $\frac{dT}{dt} = \frac{\frac{N \sigma_f}{C} nv V}{\frac{PC}{P} V}$

The number of U^{235} atoms/unit volume equals

$$N = \frac{\int_{T_1}^{T_2} \frac{PC}{P} dT}{\frac{\sigma_f}{C} \int_0^t nv dt}$$

For the same reactor power, but different enrichments, and temperatures,

$$P = \frac{\int_{T_1}^{T_2} P_1 C_1 \rho_1 dT}{N_1}$$

$$P = \frac{\int_{T_{01}}^{T_{02}} P_2 C_{p2} dT}{N_2}$$

or equating,

$$\frac{\int_{T_1}^{T_2} P_1 C_{p1} dT}{N_1} = \frac{\int_{T_{01}}^{T_{02}} P_2 C_{p2} dT}{N_2}$$

Substituting the given core in the above equation, the enrichment necessary to raise the second portion of the sample to 2500°C was found to be 20.92%.

4. Temperature distributions

The radial temperature distribution within the sample was calculated using the IBM-704 computer code RE-147 (CYCLOPS). Necessary calculations for the input data for this code include:

- (a) The energy release in the sample as a function of time, $n(\tau)$, during the transient;
- (b) The heat transfer coefficient, h , for the sample surface;
- (c) The relative neutron flux function, $\mu(r)$, along the radius of the sample and $\xi(z)$, along the axis of the sample, depending upon the sample enrichment.

For a particular reactor power value, a corresponding energy release in the UO_2 sample can be calculated from the known sample power-reactor power relationships. The rate of energy release or heat generation at each point (r, z) , in the sample (cylindrical coordinates with the z -axis through the center of the sample) and at time, τ , is then taken by the code to be:
 $(Q_0 = \text{constant})$

$$q(r,z,t) = q_0 + \mu(r) + \xi(z) + n(t) \quad (10)$$

The total energy release in the sample per unit volume of fuel, E, is then the integral over the pin and time:

$$E = q_0^1 \cdot \int_{\text{pin}} \mu(r) + \xi(z) \cdot dv \int_{\text{time}} n(t) dt \quad (11)$$

where:

$$q_0^1 = Q_0 / \text{volume of sample}$$

= normalization coefficient

$$E \text{ is expressed as cal/cm}^3$$

The energy released in a sample at a given time is dependent upon the transient integrated reactor power; and the enrichment, diameter and volumetric energy release, E, of the sample. For each transient, the total integrated power, and the relative power in the sample as a function of time [n(t)] must be assumed. For the assumed power vs time curve and specified sample parameters the heat generated in the sample can be obtained as a function of time and location given by:

a. Power vs time For the calculations here the n(t) curve was taken to be that of Transient No. 141, Series SVII - Shot 3 - Pin 4. This power vs time curve is considered typical of that under which the given experiment might be conducted and is illustrated in Fig. 18.

In Fig. 19, the power is expressed in units where one unit is equivalent to a certain power value, i.e., 1 unit=1/a cal. Then:

$$\int n(t) dt (\text{cal-sec}) = n \cdot \int n(t) dt (\text{unit-sec})$$

Now in equation 10, if the integral over the sample is normalized, then:

$$q_0^1 = E \left/ \int_{\text{time}} n(t) dt \right. \left[\frac{\text{cal/cm}^3}{\text{cal-sec}} \right]$$

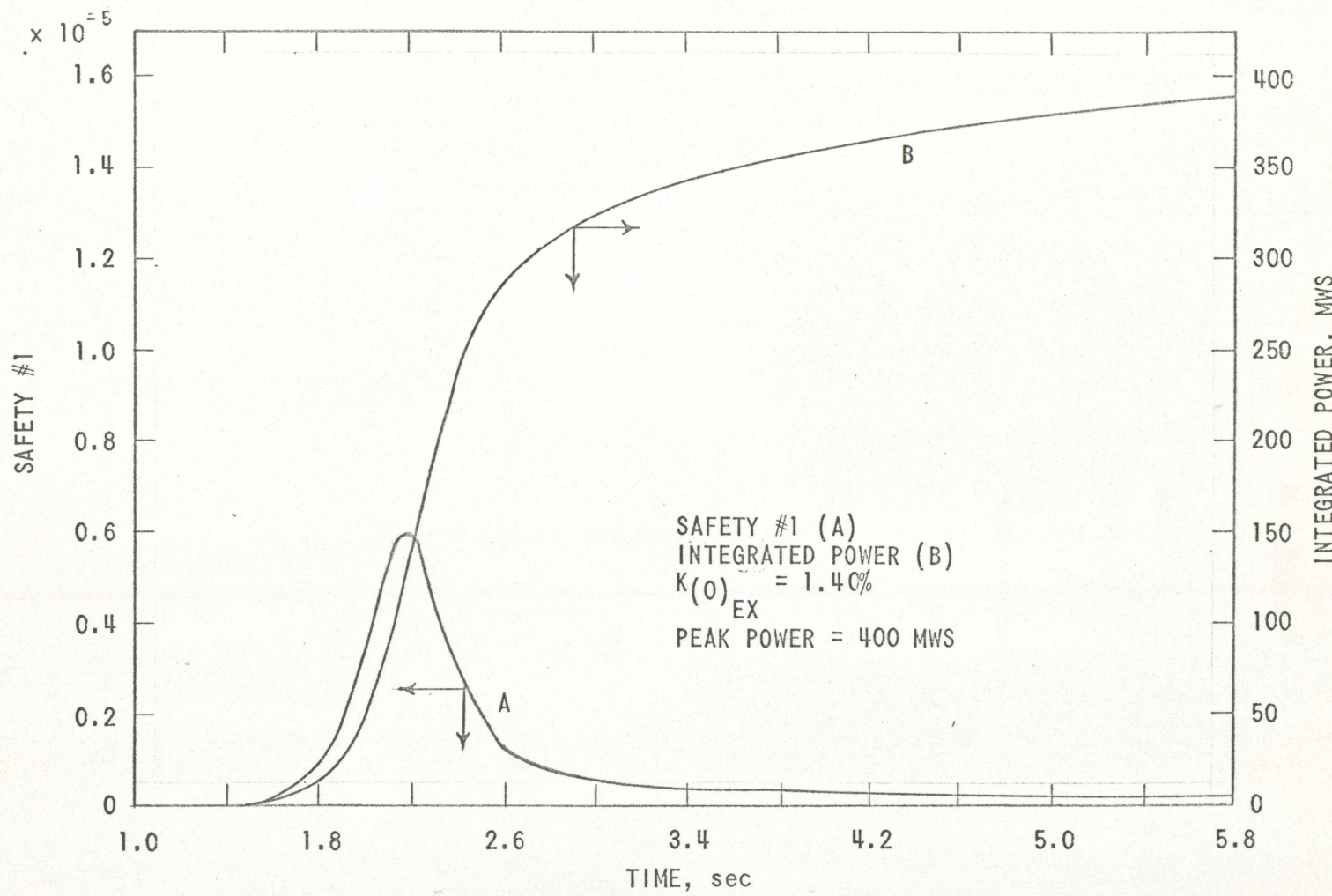


Fig. 18 Transient #141 series SVII - shot 3 - pin #4

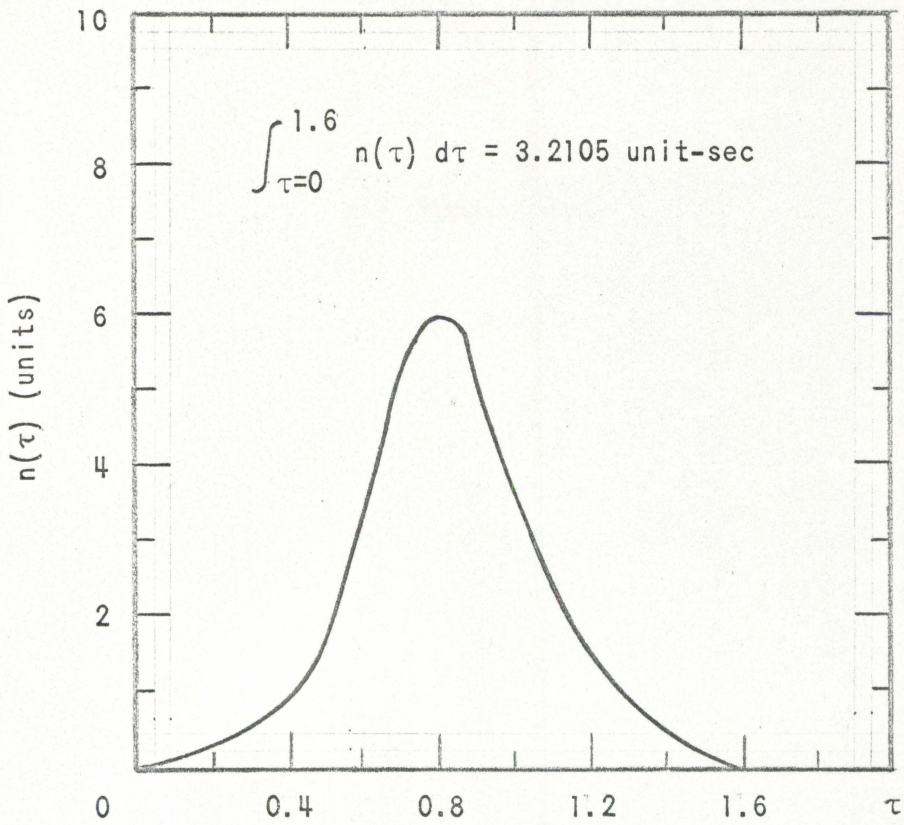


Fig. 19: Sample power as a function of time. Taken from transient #141, series #141 - shot 3 - pin #4

or

$$q_0 = q_0^1 \cdot a = E \int_{\text{time}} n(\tau) dt \left[\frac{\text{cal/cm}^3}{\text{unit-sec}} \right]$$

This value, q_0 , is the input parameter for the power that is given in the RE-147 code.

b. Heat transfer coefficient The heat transfer coefficient, h , enters into the RE-147 code equations (18) in the calculation of the rate of heat addition to the coolant, $q(z,t)$:

$$q(z,t) = hA_1 (T_1 - T_2) \quad (12)$$

where:

A_1 = surface area of sample

T_1 = temperature of sample surface ($^{\circ}\text{K}$)

T_2 = temperature of center of coolant ($^{\circ}\text{K}$)

Since the sample is an unclad slug of UO_2 the mode of heat transfer from the fuel is by direct radiation to its surroundings. The surroundings that will absorb the radiation consist of:

(1) helium gas which circulates through the test capsule at approximately 3 liters/min.

(2) the walls of the transparent capsule, which are coated with alumina paint.

The radiation absorbed by the flowing helium gas is negligible; amounting to 1-2% of the total heat lost from the sample. It can then be said that the coolant is the walls of the transparent capsule, intercepting the radiation. This condition can be approximated by a cylindrical wall containing the fuel and one inch in radius. The emissivity of this

wall was taken to be that of aluminum oxide.

The rate of radiation is given by McCabe and Smith (23):

$$q(t) = \sigma \cdot A_1 \cdot F_{1,2} \left(T_1^4 - T_2^4 \right) \quad (13)$$

where:

σ = Stefan-Boltzman constant,

$$1.3542 \times 10^{-12} \text{ cal/cm}^2\text{-sec-}^\circ\text{C}^4$$

T_1 = temperature of fuel surface ($^\circ\text{K}$)

T_2 = temperature of inside containment wall surface ($^\circ\text{K}$)

$$F_{1,2} = \left[\frac{1}{\epsilon_1} + \frac{A_1}{A_2} \frac{1}{\epsilon_2} - 1 \right]^{-1}$$

(for gray surfaces and assuming that all radiation from

A_1 falls upon A_2)

ϵ_1 and ϵ_2 = emissivity of fuel and containment wall, respectively

It can be assumed that the fuel surroundings have a sufficiently large heat capacity so that the temperature of the containment wall remains constant, therefore equations 12 and 13 can be combined giving:

$$h = \frac{\sigma \cdot A_1 \cdot F_{1,2} \left(T_1^4 - T_2^4 \right)}{A_1 \left(T_1 - T_2 \right)}$$

or

$$h = \sigma \cdot F_{1,2} \left(T_1^2 + T_2^2 \right) \left(T_1 + T_2 \right)$$

Since T_2 remains constant, h is a function of T_1 above. Using the values:

$$\epsilon_1 = .416 \text{ for } \text{UO}_2 \text{ (30)}$$

$$\epsilon_2 = .30 \text{ for alumina (27)}$$

$$T_2 = 300^\circ\text{K}$$

Thus:

$$F_{1,2} = .33367$$

for 1/2 inch diameter fuel.

In the RE-147 code, h , is dependent, upon the coolant temperature above. Since this temperature does not change, only one value of h can be chosen, corresponding to one certain fuel surface temperature. In the problems, a value of h was chosen corresponding to a T_1 about 200° below the maximum T_1 during the transient.

c. Flux depression The radial thermal neutron flux distribution for 1/2 inch diameter uranium dioxide fuel slugs of 5%, 10%, 15% and 20% enrichments have been calculated according to the empirical equation (34):

$$\mu(r,a) = A(a) \left[1 + .69713\left(\frac{r}{a}\right)^2 + .48598a^2\left(\frac{r}{a}\right)^4 + .33879a^3\left(\frac{r}{a}\right)^6 \right]$$

for $0 \leq r \leq a$, and $0 \leq a \leq 2$ where:

$$a = a \Sigma_{abs}^1 \text{ (geometric and absorption parameter)}$$

Σ_{abs}^1 = macroscopic absorption cross section of the material
in cm^{-1}

a = radius of the fuel in cm

$$A(a) = [1 + .69713a + .48598a^2 + .33879a^3]^{-1}$$

= axis-to-surface ratio of neutron density

$\mu(r,a)$ = radial distribution of neutrons, normalized to unity
at the surface

The results of the calculations are shown in Table 2 and Fig. 20.

The thermal neutron flux distributions for the same slugs in the TREAT reactor were calculated using the DSN one-dimensional neutron transport theory code. The results of these calculations agree

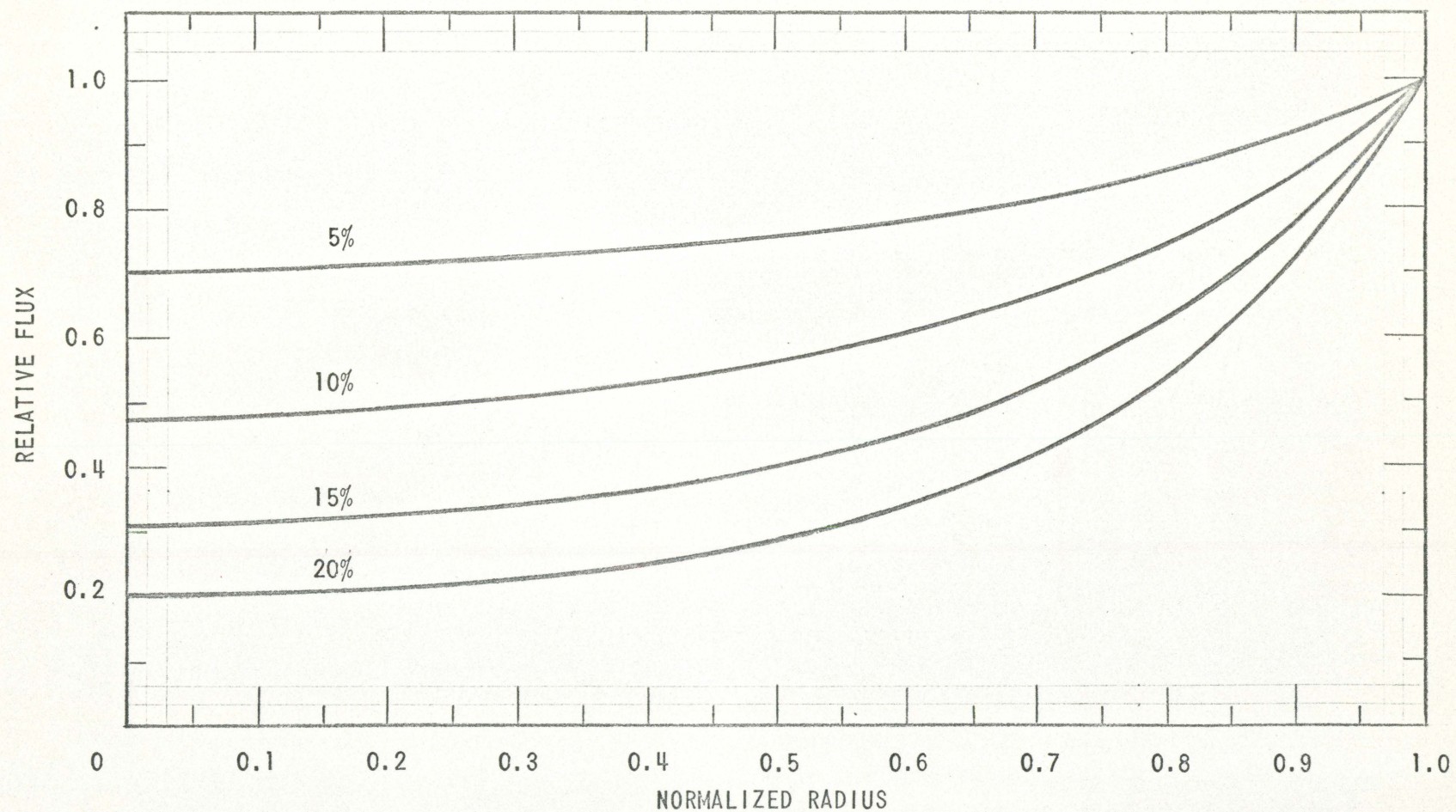


Fig. 20 Relative flux vs normalized radius of one half inch diameter UO_2 samples of designated enrichments

satisfactorily with those given in Fig. 20.

The axial flux distribution for all enrichments is assumed constant; i.e., $\zeta(z) \approx 1$ for all slugs. In giving the values of $\mu(r)$ and $\zeta(z)$ for the RE-147 code, it is necessary that each of these functions be normalized since

$$\int_{pin}^r \mu(r) \cdot \zeta(z) dV$$

must equal unity. For $\zeta(z) \approx 1$ for all z , it remains only to choose the unit interval of $\mu(r)$ so that according to (1),

$$\frac{2}{a^2} \int_{r=0}^a \mu(r) \cdot r \cdot dr = 1$$

This unit interval is known to be approximately the value of $\mu(r)$ at .8a. All values of $\mu(r)$ for each enrichment are thus given in the code input in respect to the value of $\mu(r)$ at eight-tenths of the fuel radius.

Table 2. Radial flux distribution

Enrichment	Σ_{abs}^1	a	$A(a)$	$\mu(r,a)$
For 1/2 inch diameter samples				
5%	.67888	.43109	.70522	Fig. 20
10%	1.3060	.82931	.47492	Fig. 20
20%	2.56012	1.626	.20514	Fig. 20

d. Input parameters The value of thermal conductivity, k , and the volumetric heat capacity, ρC_p , of the fuel used are:

$$k = .015 \text{ cal/sec-cm-}^\circ\text{C}$$

$$\rho C_p = .86 \text{ cal/cm}^3 \text{-}^\circ\text{C}$$

All material properties are considered constant over the entire temperature range.

The volumetric sample energy values, E , were chosen to attain sample temperatures of 2500°C and 2000°C. Then:

$$T_1^{\circ K} \quad E = \rho C_p (T_1 - 300) [\text{cal/cm}^3] \quad q_o = \frac{E}{3.2105} [\text{cal/cm}^3\text{-sec}]$$

$$\text{For } \rho C_p = .86$$

2773	2126.78	662.445
2273	1696.78	528.51

The adiabatic temperature rise assumption is a sufficiently close approximation of the corresponding energy parameter, q_o , to attain the desired maximum sample temperature.

An index to the problems run is given in Table 3.

Table 3. Radial temperature distribution

Enrichment	k	ρC_p	h	q_o	T(r)
5%	.015	.86	.0097	.665	Fig. 21
10%	.015	.86	.0097	.665	Fig. 22
5%	.025	.86	.0097	.665	Fig. 23
10%	.025	.86	.0097	.665	Fig. 24

where:

$T(r)$ = temperature as a function of radius

Under adiabatic conditions, the relation between sample energy and temperature is:

$$E = \rho C_p (T_1 - T_2) [\text{cal/cm}^3]$$

when the sample is raised from $T_2^{\circ K}$ to $T_1^{\circ K}$. The starting temperature for all calculations is 27°C or 300°K.

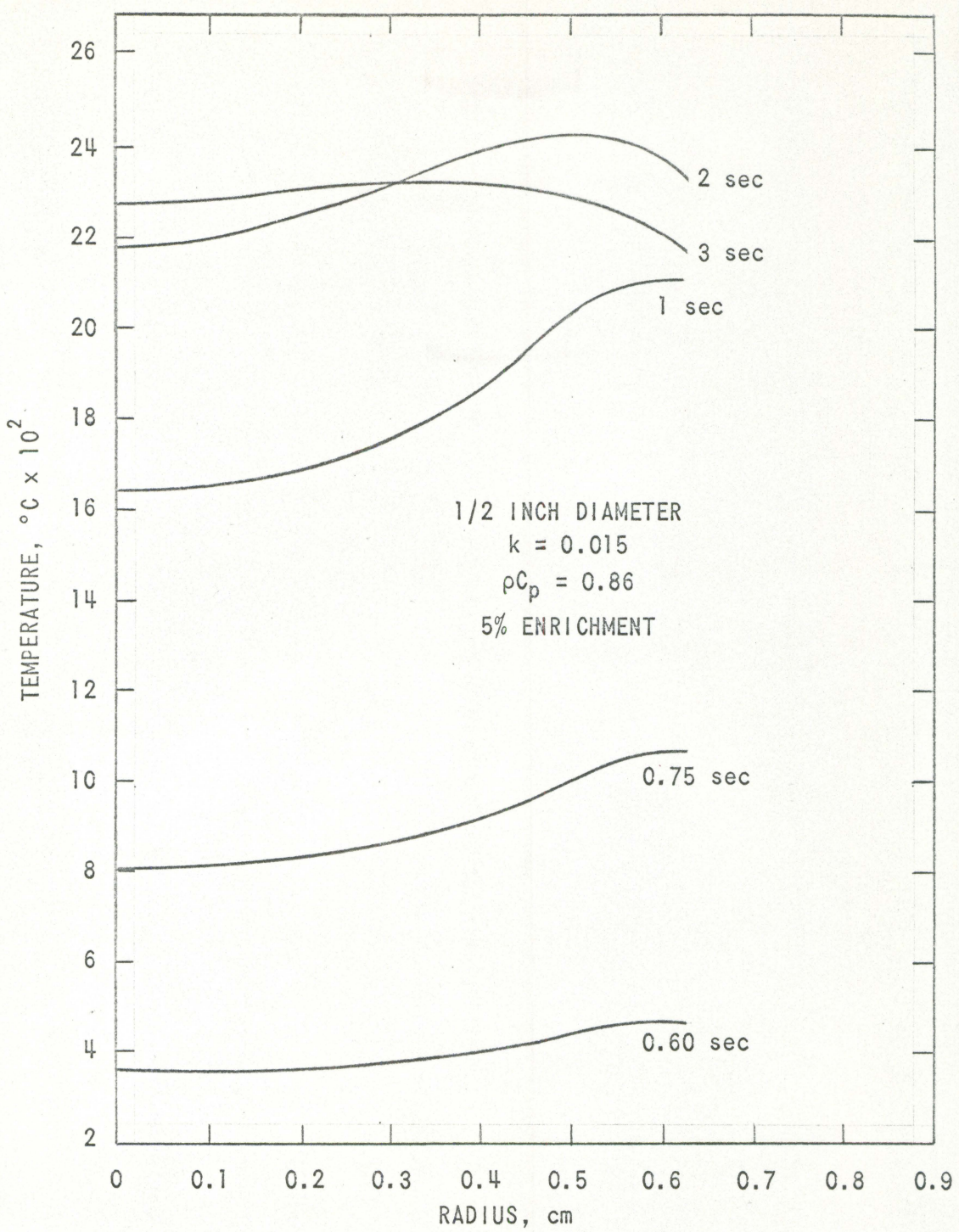


Fig. 21 Temperature of UO_2 sample as a function of radius at various times

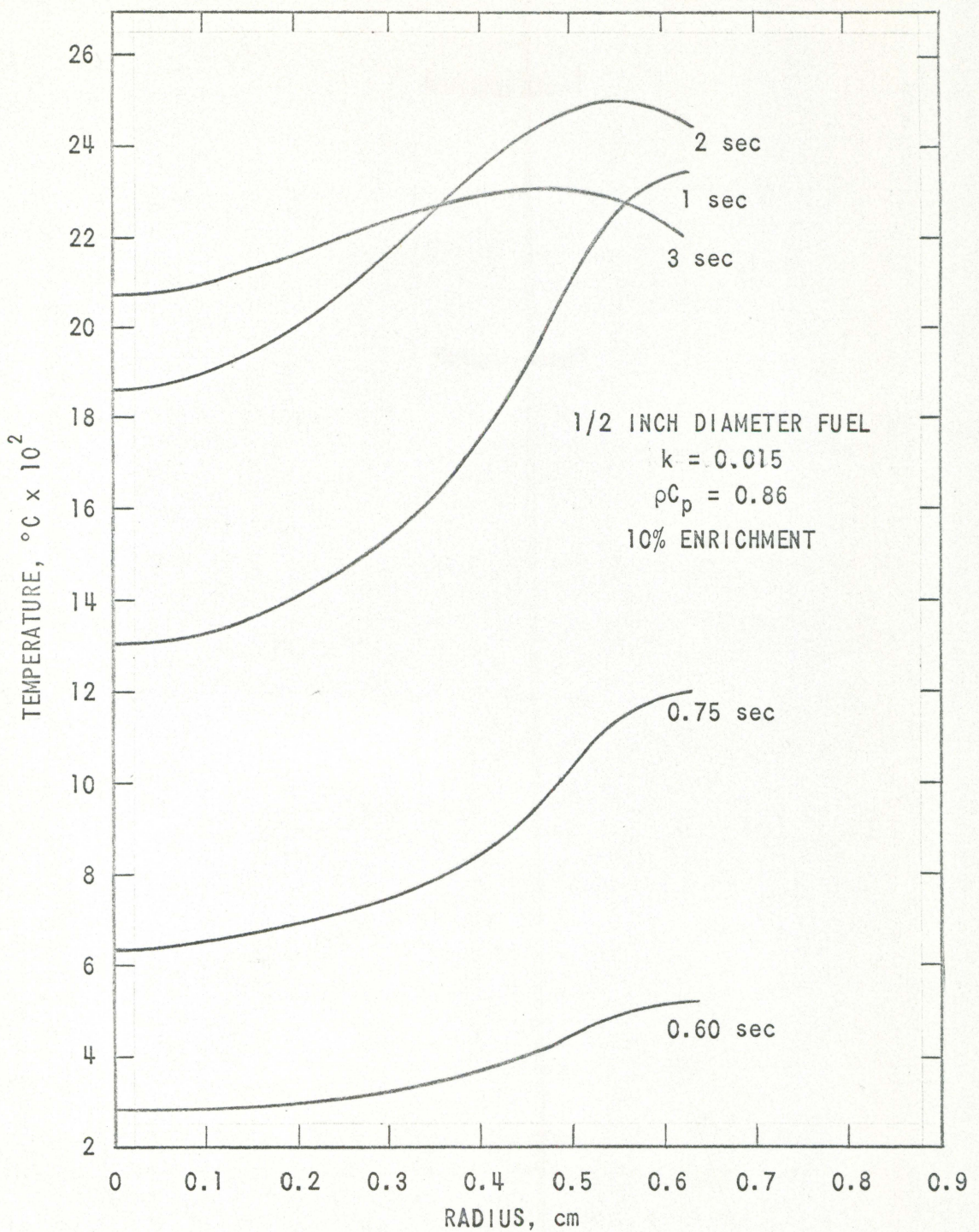


Fig. 22 Temperature of UO_2 sample as a function of radius at various times

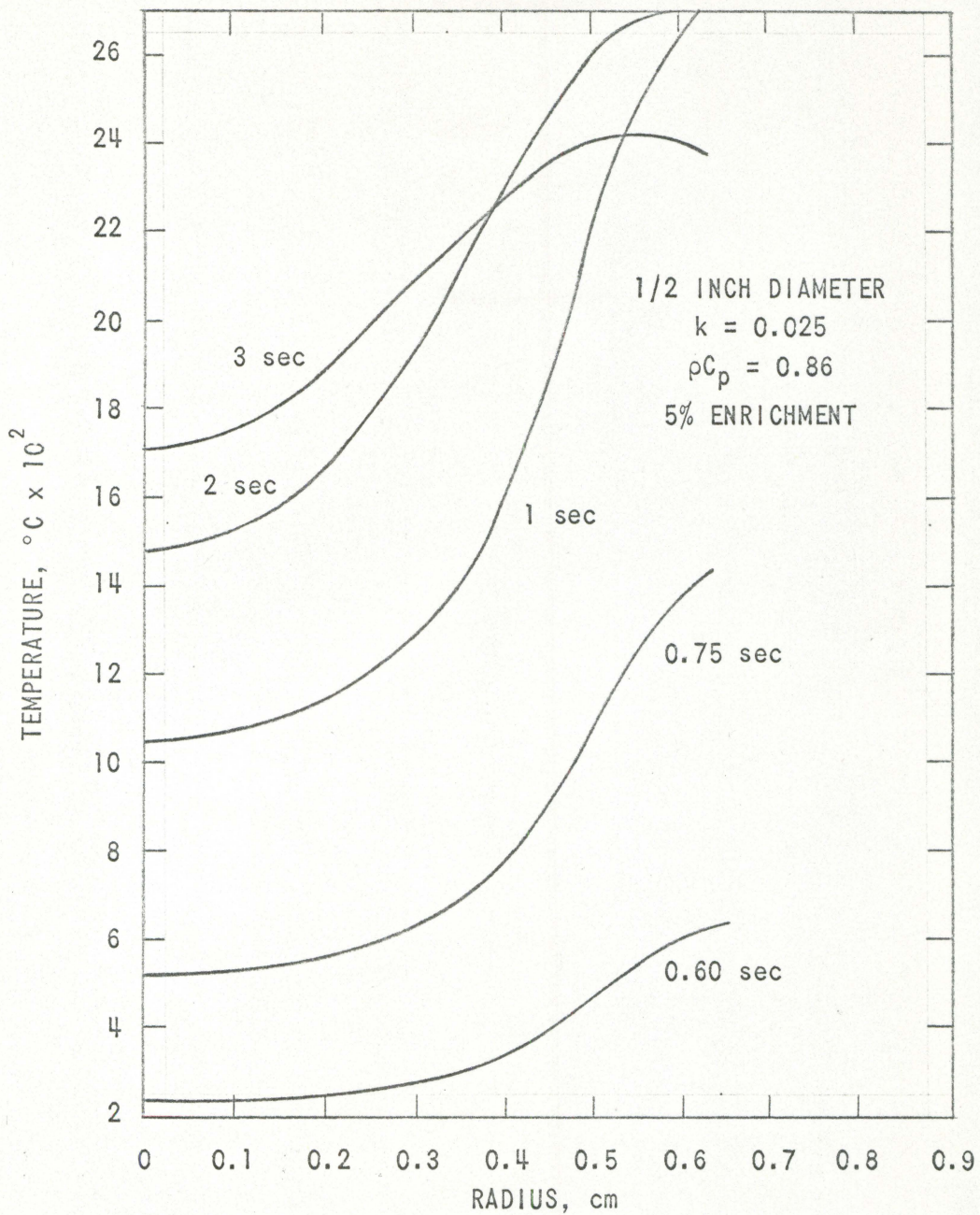


Fig. 23 Temperature of UO_2 sample as a function of radius at various times

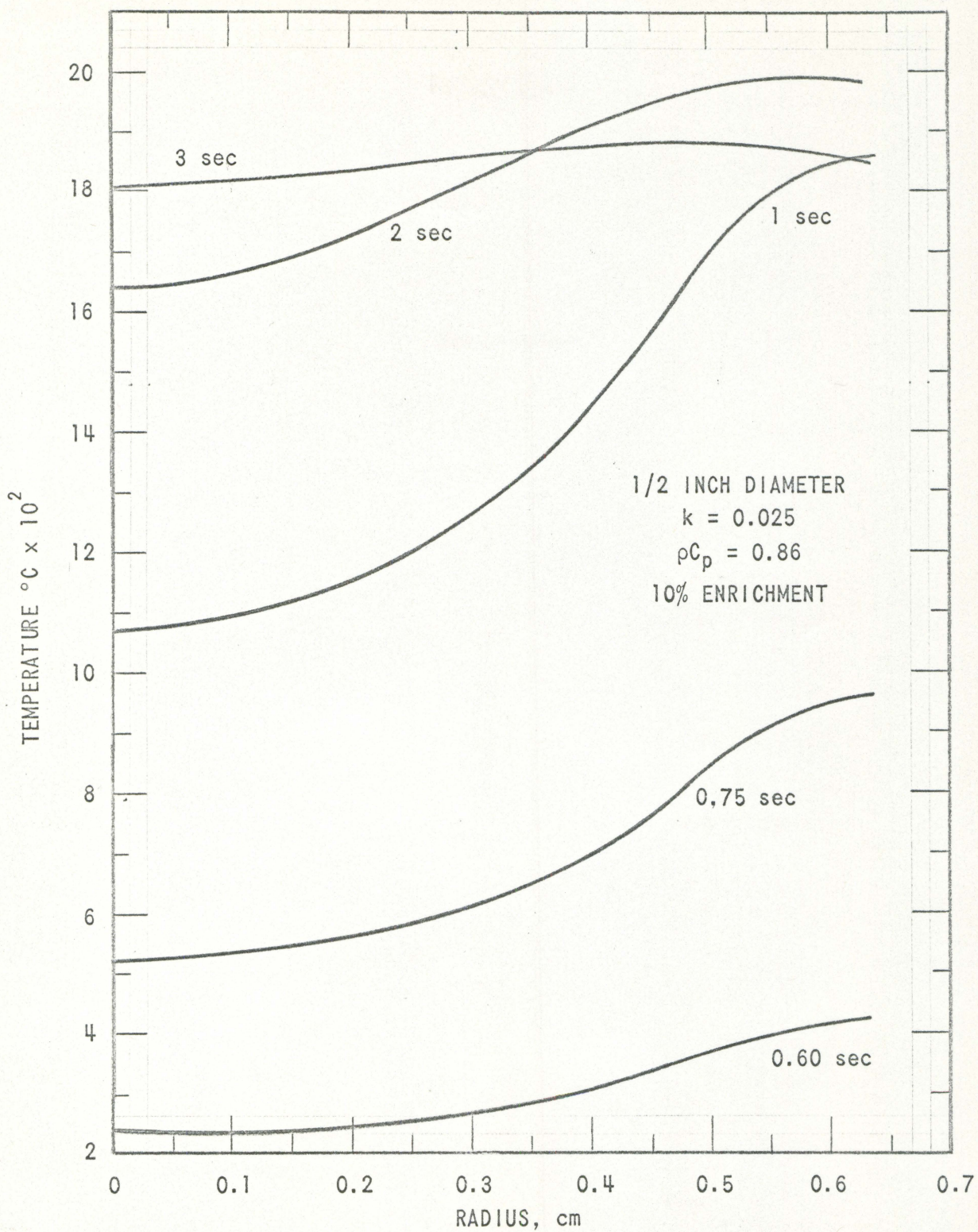


Fig. 24 Temperature of UO_2 sample as a function of radius at various times.

B. Stress Analysis

1. Axial maximum temperature differences

If the temperature rise, in the sample, is not uniform, each element will tend to expand by a different amount, that is, proportional to its own temperature rise. The resulting different-sized elements cannot, in general, fit together. Since the sample must remain continuous, each element must restrain the distortions of its neighbors, or, in other words, stress must arise.

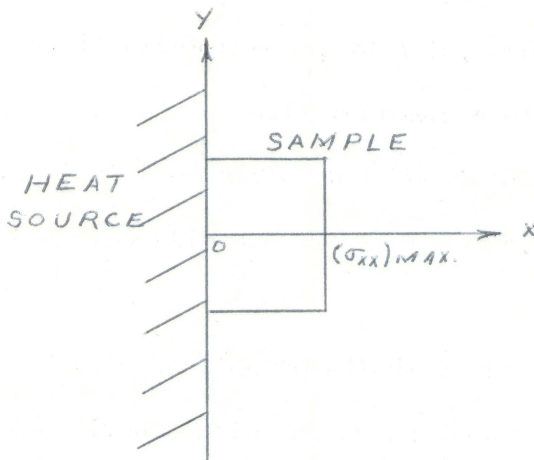
It is the purpose of this section to calculate the maximum initial temperature rise that the given sample may be subjected to without fracturing across the interface between the two portions of different enrichments.

To do this the following case was said to exist.

(a) The lower enrichment portion was considered as a plate, initially at room temperature throughout, exposed to a uniform heat input which varies with time, $q(t)$, and with the other face, the portion of higher enrichment, perfectly insulated.

(b) All edges were considered perfectly insulated and free of external tractions.

(c) A one-dimensional geometry was used giving the maximum stress in the x direction, $(\sigma_{xx})_{\max}$.



The thermal stress in the radial, y , direction under various conditions of temperature will be determined later.

The sample, initially at room temperature, is suddenly exposed to a uniform ambient temperature, T_a , through a boundary conductance. The maximum stress occurs at $t=0$ at the exposed surface and is given by Boley (4).

$$(\sigma_{xx})_{\text{MAX.}} = \frac{\alpha ET}{1 - \nu}$$

where:

α = linear coefficient of thermal expansion

E = Young's modulus

T_a = uniform ambient temperature rise to which the sample may be raised before fracturing

ν = Poisson's ratio $\frac{E}{2G} - 1$

E = Young's modulus

G = shear modulus

for UO_2

$$\alpha = 10.0 \times 10^{-6} \text{ } 1/\text{ }^{\circ}\text{C}$$

$$v = .302$$

$$E = 25 \times 10^6 \text{ psia}$$

$$(\sigma_{xx})_{\text{max}} = 1.5 \times 10^4 \text{ psia}$$

Therefore solving for

$$T_a = - \frac{(\sigma_{xx})_{\text{max}} (1 - v)}{6E}$$

$$= - 41.88^{\circ}\text{C}$$

This is the value of permissible temperature difference that may exist between the interface of the sample and one portion of enrichment, before the sample will rupture. This AT is one-half of the total temperature difference that will exist across the interface. Therefore the total permissible AT between the two portions $\approx 80^{\circ}$.

The calculated permissible value of AT is also assuming a perfectly uniform interface, such an assumption is not valid, due to the diffusion of the higher enriched UO_2 to the lower portion of the sample, and the converse, during fabrication of the sample. This non-uniform bond existing between the higher and lower enrichment portions of the sample will decrease the thermal discontinuity between the portions and thereby increase the permissible AT between the portions before fracturing will occur.

Since the calculated value of AT also yields a compressive stress it is felt that twice the 80° AT can be withstood before actual fragmentation

occurs, thus AT may be approximately 160°C.

It should be noted that while a small non-uniformity of diffusion bond between the portions of the sample is desired, too large a diffusion of the higher enriched UO_2 into the lower enriched portion will distort the AT data trace from the experiment and thereby introduce errors into the measured values of the thermal diffusivity obtained from the experiment.

A compromise diffusion width across the interface which will allow a large AT to exist between the sample portions and at the same time keep distortion of the data trace to a minimum value is desired.

2. Radial stress

One of the serious problems in the use of uranium dioxide is its tendency to crack under thermal stress. This tendency is the result of a combination of unfavorable physical properties. Most notable are its low ductility, its high coefficient of thermal expansion, and low ultimate strength.

A Fortran Code - 1560/RE - was written to calculate the thermal stresses existing within the sample as a result of a given radial temperature distribution. The radial, polar, and axial stresses were determined for the samples and conditions listed in Table 4 at times of .60, .75, 1, 2, 3 seconds following the time of maximum temperature difference within the sample.

The following equations (4) which are valid except near the ends of the sample cylinder, i.e., within one diameter of each end, are used:

$$\sigma_{rr} = \frac{\alpha E}{1-\nu} \left[\frac{1}{b^2} \int_0^b Tr dr - \frac{1}{r^2} \int_0^r Tr dr \right]$$

$$\sigma_{rr} = \frac{\alpha E}{1-\nu} \left[\frac{1}{b^2} \int_0^b Tr dr + \frac{1}{r^2} \int_0^r Tr dr - T \right]$$

$$\sigma_{zz} = \sigma_{rr} + \sigma_{\theta\theta} = \frac{2\alpha E}{(1-\nu)b^2} \int_0^b Tr dr - \frac{\alpha ET}{1-\nu}$$

where:

σ_{rr} = radial stress

$\sigma_{\theta\theta}$ = polar stress

σ_{zz} = axial stress

α = linear coefficient of thermal expansion

E = Young's modulus

ν = Poisson's ratio

b = outer radius of sample

r = radius

T = temperature

An index to the stress calculations made and the graphical results is given in Table 4.

Table 4. Radial and polar stress

Enrichment	k	ρC_p	h	q_o	Radial Stress	Polar Stress
5%	.015	.86	.0097	.665	Fig. 25	Fig. 26
10%	.015	.86	.0097	.665	Fig. 27	Fig. 28
5%	.025	.86	.0097	.665	Fig. 29	Fig. 30
10%	.025	.86	.0097	.665	Fig. 31	Fig. 32

From the figures illustrating the radial and polar stresses of 5 and 10% enriched samples it is possible to gain an insight into the magnitude of the stresses that may arise within the experimental sample.

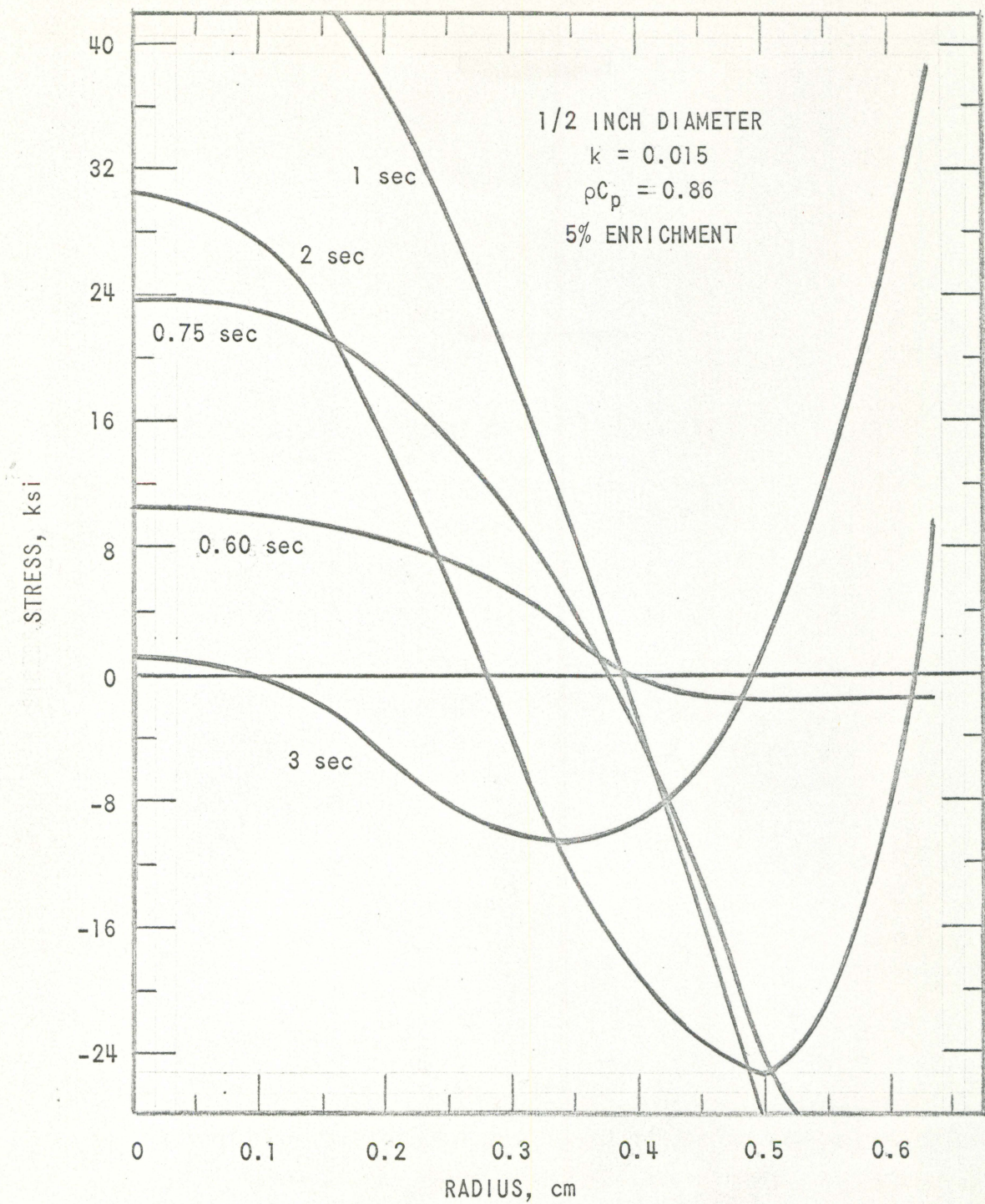


Fig. 25 Polar stress of UO_2 sample as a function of radius at various times

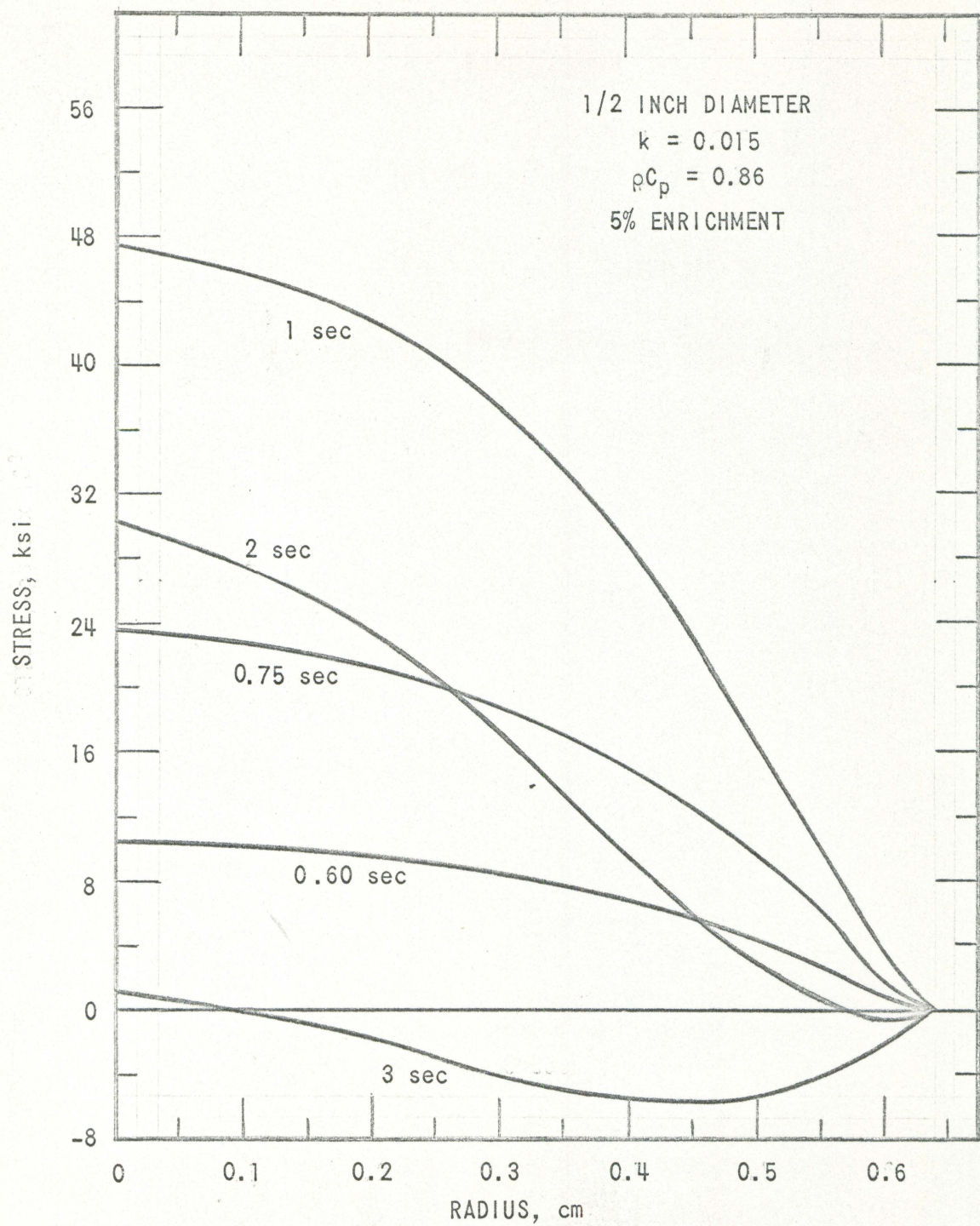


Fig. 26 Radial stress of UO_2 sample as a function of
of radius at various times

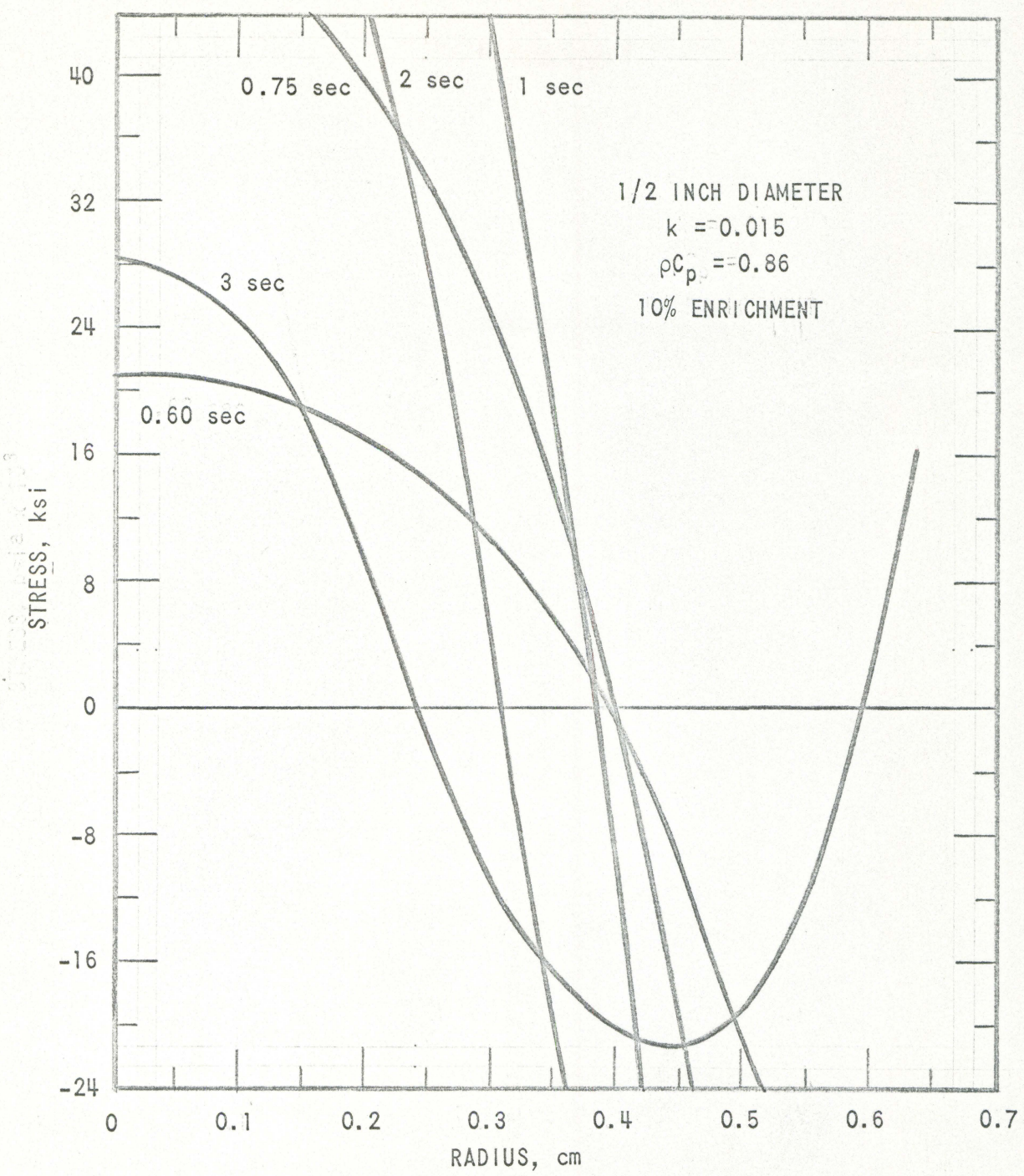


Fig. 27. Polar stress of UO_2 sample as a function of radius at various times

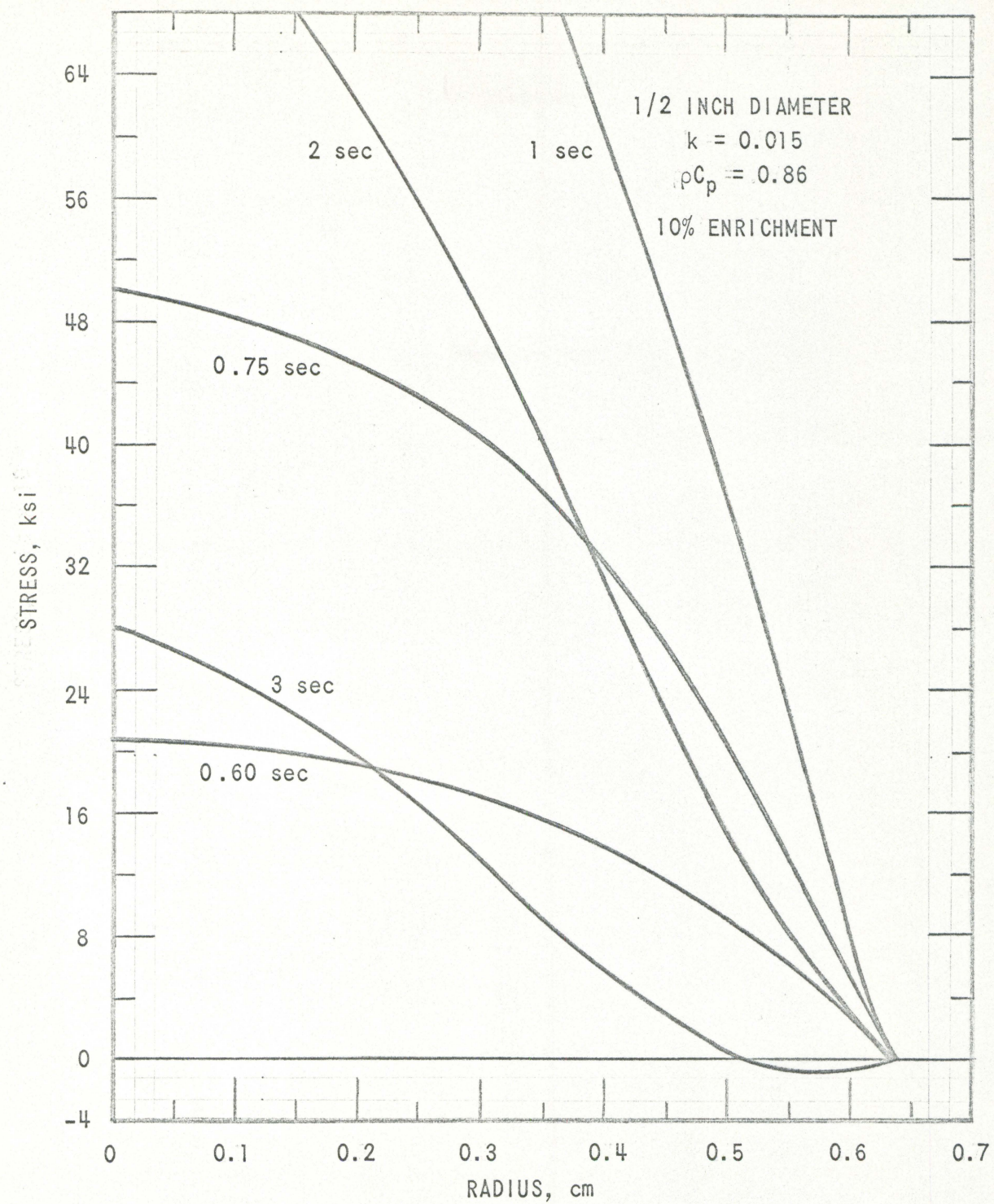


Fig. 28 Radial stress or UO_2 sample as a function of radius at various times

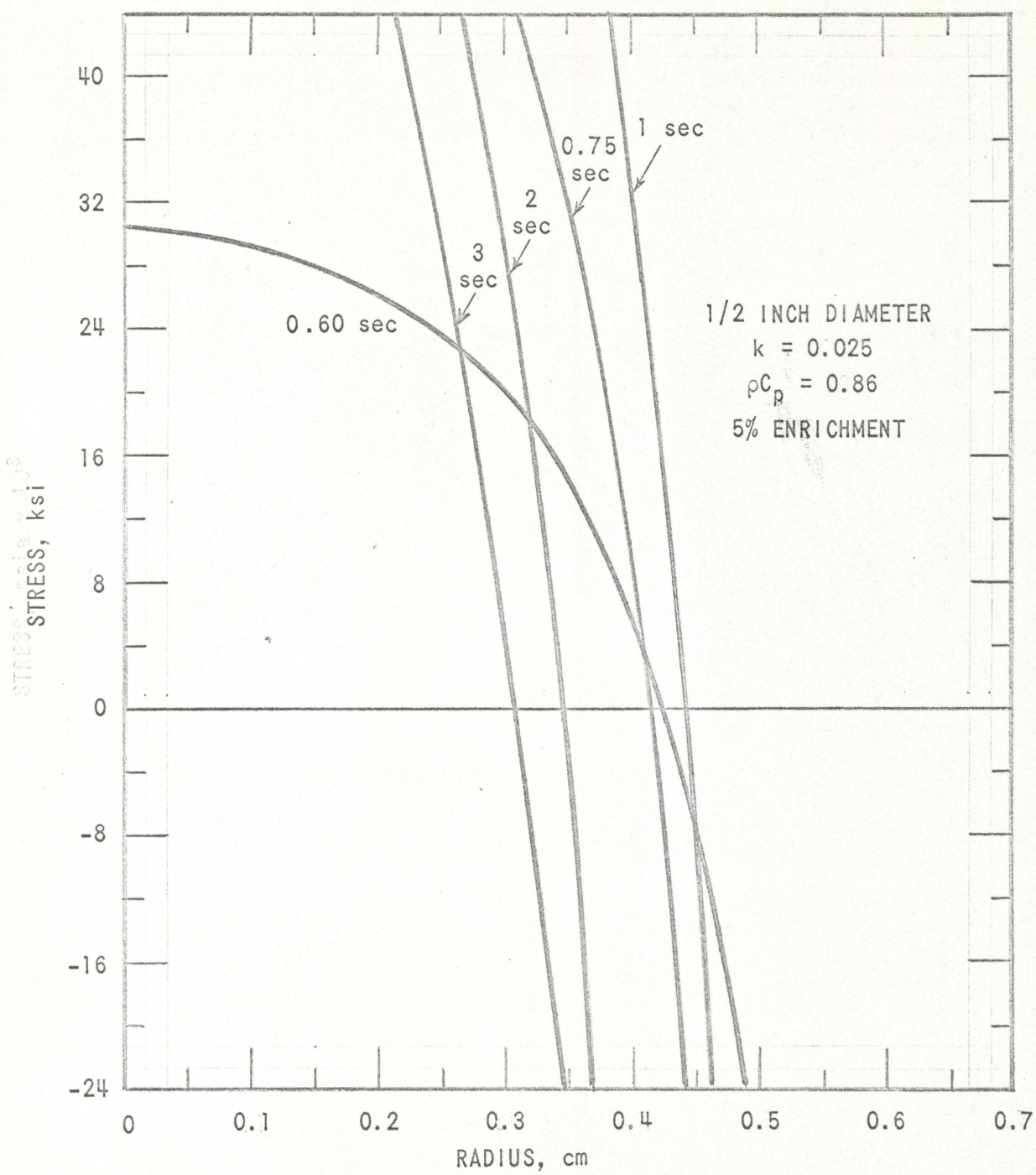


Fig. 29 Polar stress of UO_2 sample as a function of radius at various times

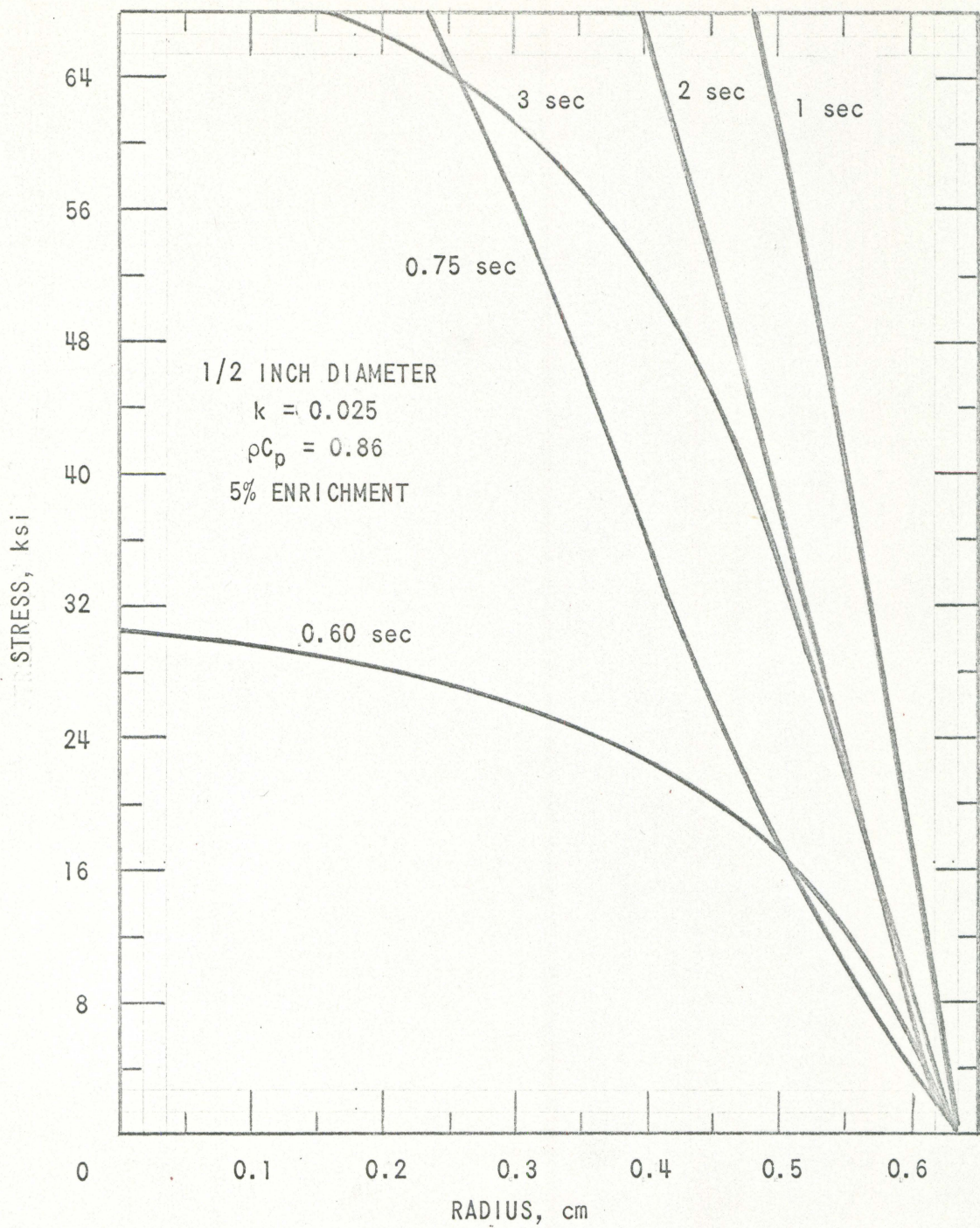


Fig. 30. Radial stress of UO_2 sample as a function of radius at various times

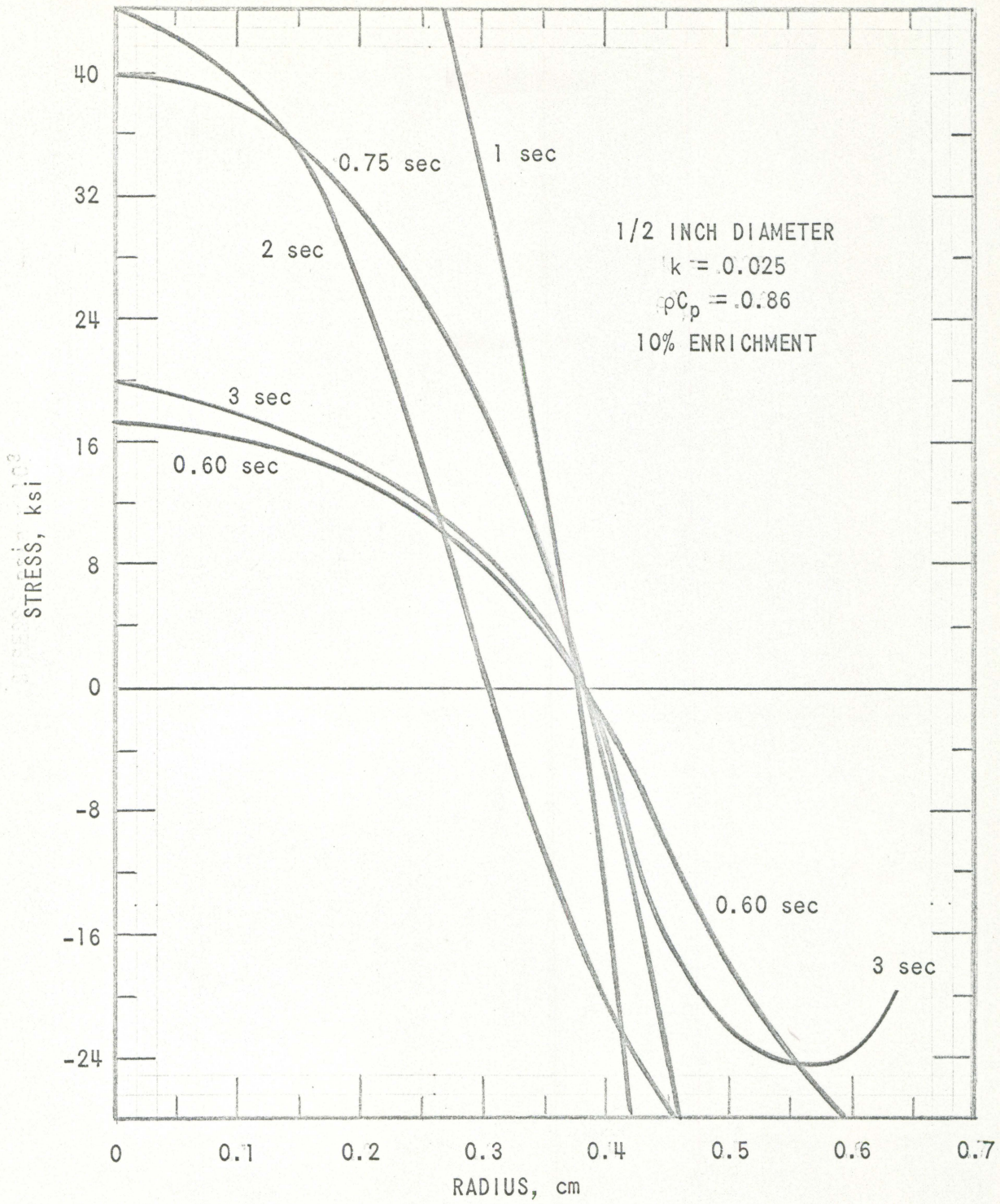


Fig. 31 Polar stress of UO_2 sample as a function
of radius at various times

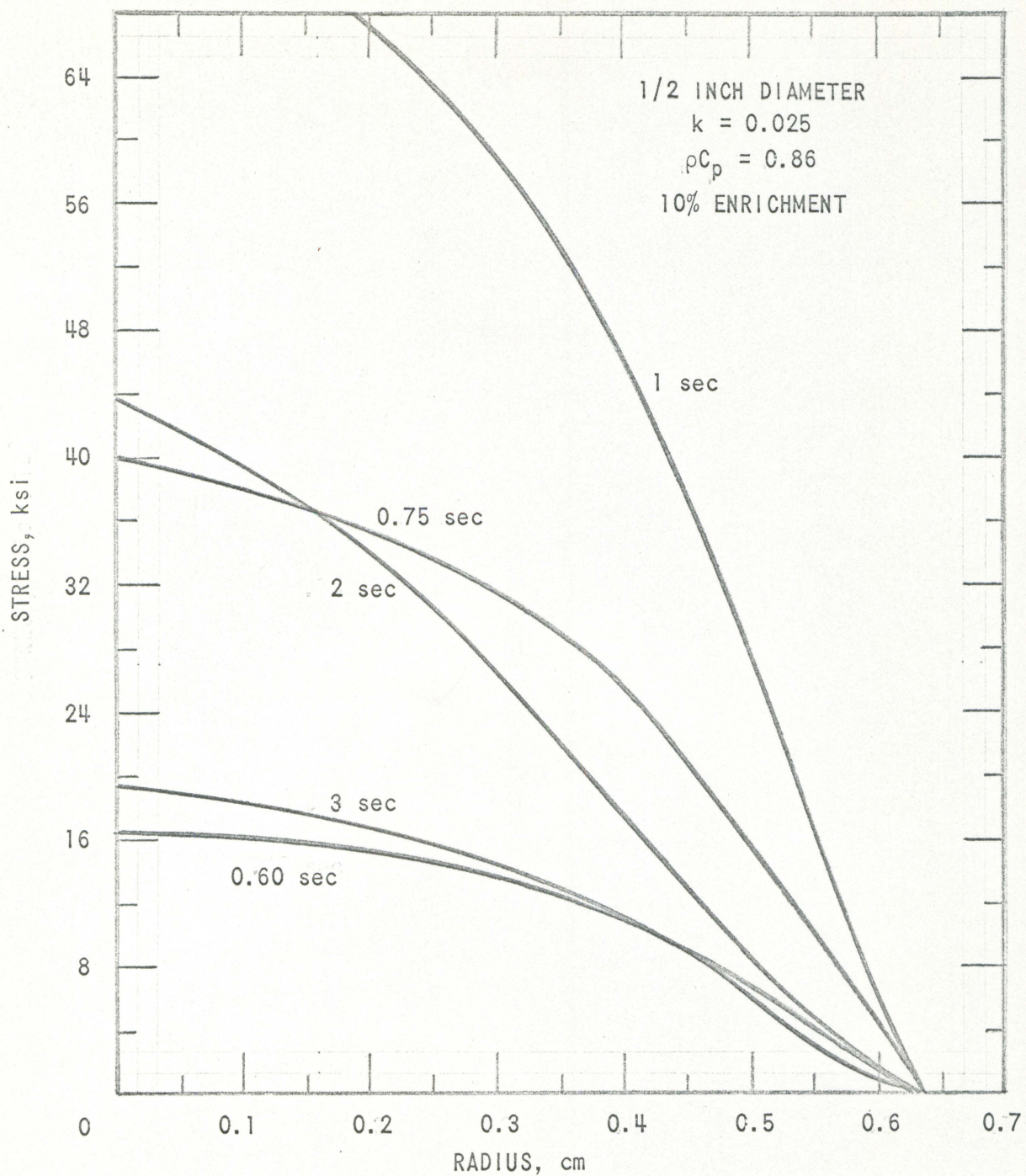


Fig. 32 Radial stress of UO_2 sample as a function of radius at various times

This investigation was conducted for qualitative reasons only. Experience may prove the actual thermal stresses within the sample much different than the calculated values. It is felt that the effects of plastic-deformation and axial heat flow will greatly reduce thermal stresses. Further limitations are placed upon the accuracy of the calculated values because they are based upon extrapolated temperature values taken from other computer problems.

Although the calculations are qualitative in nature it is possible to draw general conclusions from the given results.

Since polar stress is more severe than radial stress, the sample may crack in the form of planes perpendicular to the axis of the sample before cracking in the form of concentric cylinders parallel to the axis. Temperature gradients produced by end heat loss may produce cracking near the ends before fracturing occurs internally.

It will be necessary to perform a post-experimental examination of the sample before the exact nature or effect of thermal stresses can be determined.

VII. PREPARATION OF DATA FOR ANALYSIS

A. Graphing Experimental Data from Oscillograph Chart

The experimental data will return from the TREAT reactor in the form of a photographic oscillograph chart similar to the one shown in Fig. 2.

The course of the experimental transient is followed by recording power and temperature data on the direct-writing-type oscillograph with light beam galvanometers. These recorded traces are in units of current vs time which must be manually calibrated and graphed in units of temperature or reactor power vs time. The resulting graphs of sample temperature and reactor power vs time will be similar to those given in Figs. 33, 34, 35 and 36.

B. Determination of Thermal Diffusivity

The graphs of temperature and reactor power vs time are now used to determine the value of the thermal diffusivity of the sample by the following graphical approximation according to the formula:

$$\Delta T = (T_{01} - T_{02}) \operatorname{erf} \frac{L}{2\sqrt{Dt}}$$

by the following procedure:

- (1) Using the above equation plot,

$$\frac{\Delta T}{T_{01} - T_{02}} = \operatorname{erf} \frac{L}{2\sqrt{Dt}}$$

giving L the value of the L used in the given experiment, specifying several approximate values of D for the temperatures encountered in the given experiment, and varying time, t.

- (2) By inspecting the experimental ΔT vs t graphs, for each transient, choose some time that is within the range of maximum experimental temperature

difference. Call the theoretical value of $\Delta T / (T_{01} - T_{02})$ at this time $\Delta T_1 / (T_{01} - T_{02})$, plot the ratios of

$$\frac{\Delta T_1}{T_{01} - T_{02}} \\ \underline{\underline{\frac{\Delta T_n}{T_{01} - T_{02}}}}$$

for successive times of the curves obtained in part (1) for each transient. Such curves represent $\Delta T_1 / \Delta T_n$ for various values of D for the given value of L. These curves will be similar to traces A, B, C and D in Figs. 45, 46 and 47. By plotting the ratio, $\Delta T_1 / \Delta T_n$, the curves will be independent of the value of $T_{01} - T_{02}$.

(3) Normalize the experimental ΔT vs t curve for each transient to the same value of t chosen for that transient in part (2). Plot the experimental ratios of $\Delta T_{(t)} / \Delta T_{(n)}$ where:

$\Delta T_{(t)}$ = the value of ΔT at the time of normalization

$\Delta T_{(n)}$ = value of ΔT at successive times,

superimposed on the theoretical curves plotted in part (2).

(4) By comparing the experimental curves obtained in part (3) to the theoretical curves obtained in part (2) it is possible to approximate the value of D for a given transient, as is done in Figs. 45, 46 and 47.

VIII. RESULTS AND CONCLUSIONS

The experimental transients that have been analyzed are listed in Table 5.

Table 5. Experimental transients

Transient	L cm	Enrichments	Diameter in.	Maximum Temperature °C
539	0.3125	10 <u>vs</u> 11%	1/2	1450
535	0.3125	10 <u>vs</u> 11%	1/2	1650
536	0.3125	10 <u>vs</u> 11%	1/2	1850
537	0.3125	10 <u>vs</u> 11%	1/2	2050

The values of the maximum temperatures attained by the various transients given in Table 5 was taken as the average temperature registered by the sample's thermocouples.

Graphs of temperature and power input data as taken from the transient oscillograph charts, are given in

<u>Transient</u>	<u>Figure</u>
539	33
535	34
536	35
537	36

Zero time for these graphs was taken as the starting time of the TREAT control rod removal. The time for control rod removal will vary for each reactor transient. To give a uniform time basis of comparison the experimental zero time was taken as the time of peak power as indicated by the oscillograph chart safety value. The time correction was accomplished by

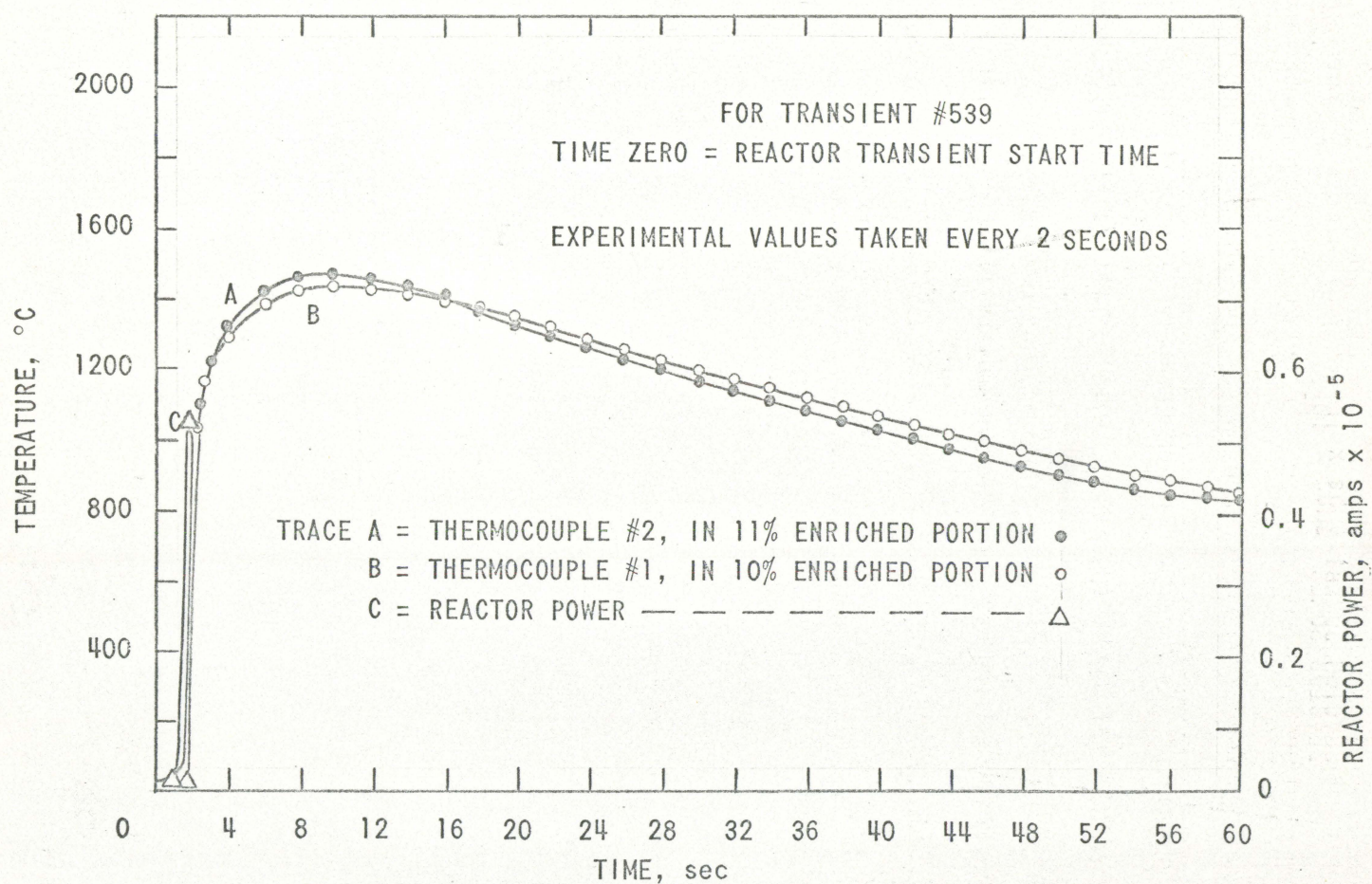


Fig. 33 Experimental temperature and power vs time

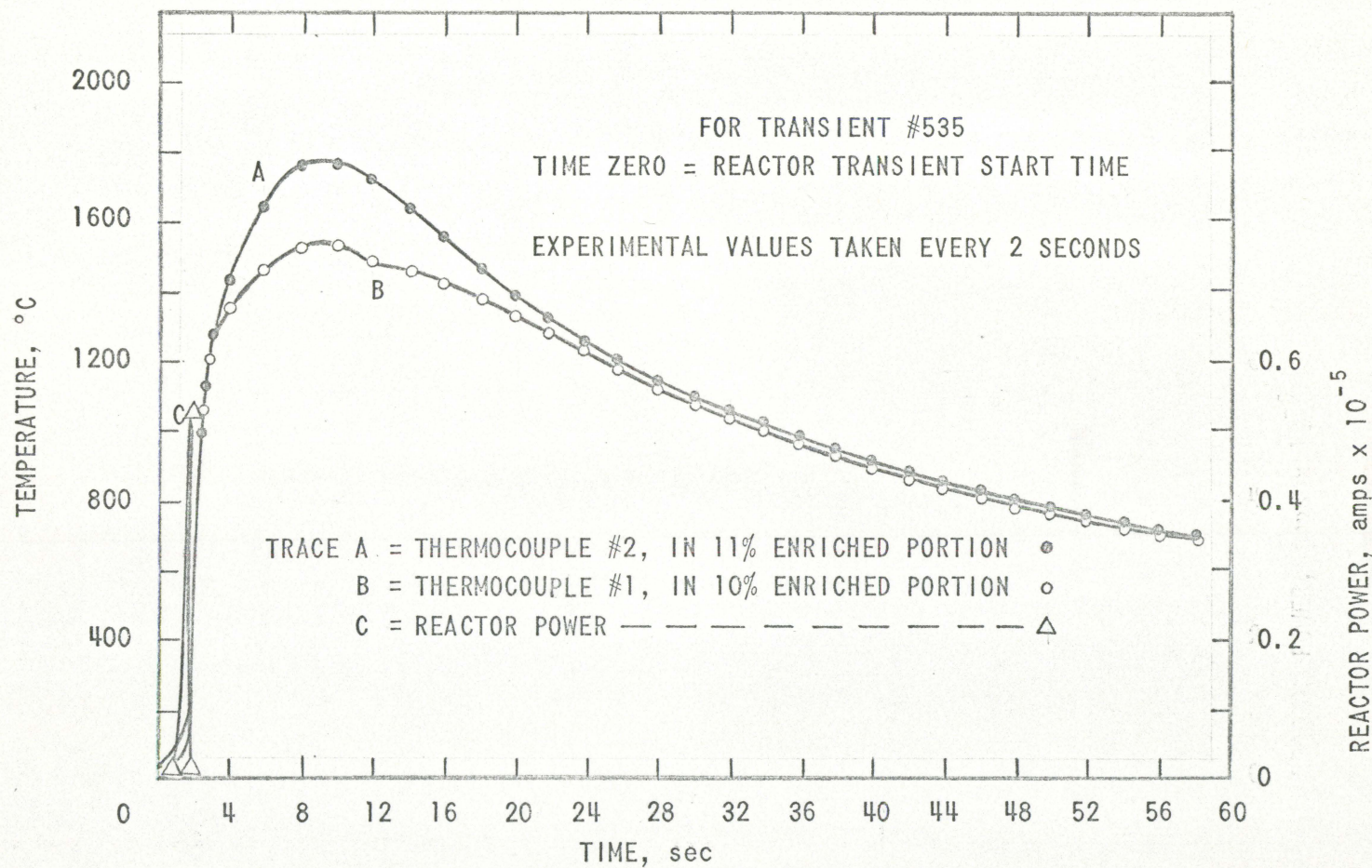


Fig. 34 Experimental temperature and power vs time

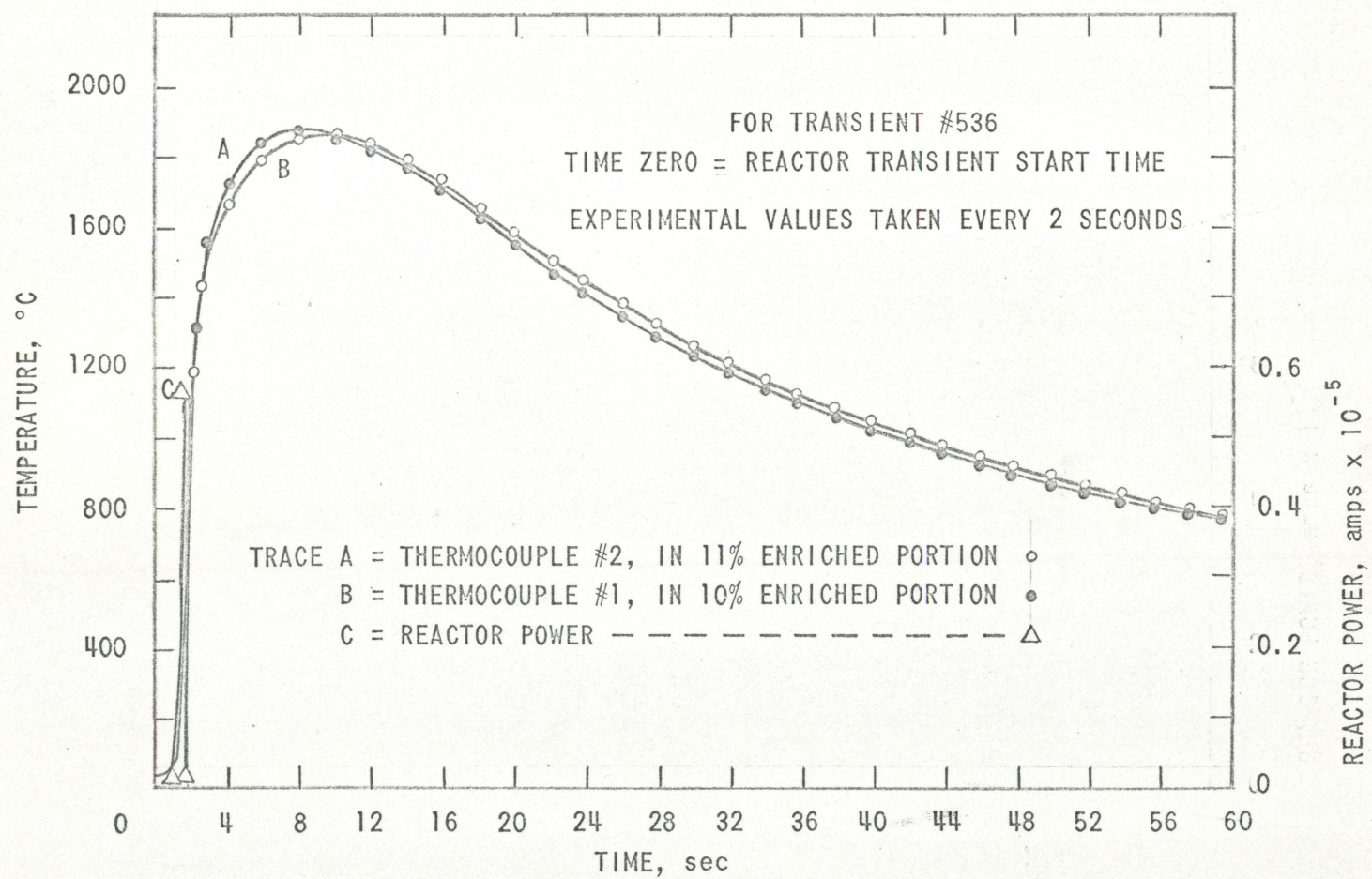


Fig. 35 Experimental temperature and power vs time

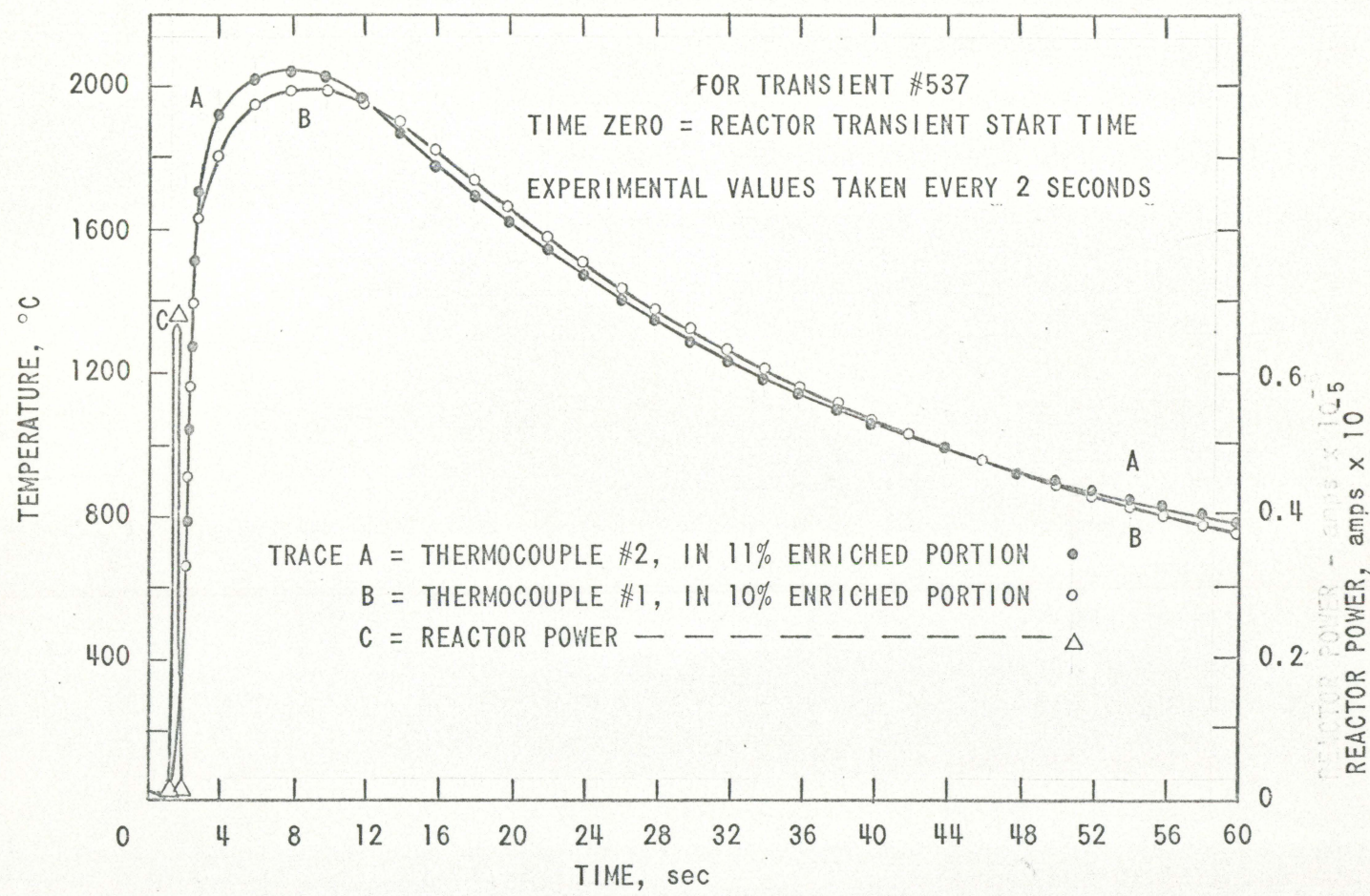


Fig. 36 Experimental temperature and power vs time

subtracting the period of time between the oscillograph zero time and the time of peak power from all experimental temperature data.

Graphs of the time-corrected transients are given in

<u>Transient</u>	<u>Figure</u>
539	37
535	38
536	39
537	40

For those transients in which the thermocouple traces cross, as in Figs. 37, 38 and 40, a temperature correction is necessary. This correction consists of adding the absolute measured temperature difference at $t \gg 0$, approximately 35 sec to the measured ΔT existing at smaller values of time, $0 < t \leq 20$ sec.

The values of corrected ΔT vs t for each transient are illustrated in

<u>Transient</u>	<u>Figure</u>
539	41
535	42
536	43
537	44

To facilitate comparison of experimental to theoretical data and to make the experimental data independent of $T_{01} - T_{02}$, the values of ΔT vs t for each transient are normalized. The time of normalization is arbitrary, but for ease of comparison, the time was chosen to be approximately the time of the maximum ΔT for each transient.

By comparing the experimental normalized curves to the theoretical, ΔT vs t , curves normalized to the same time, it is possible to approximate

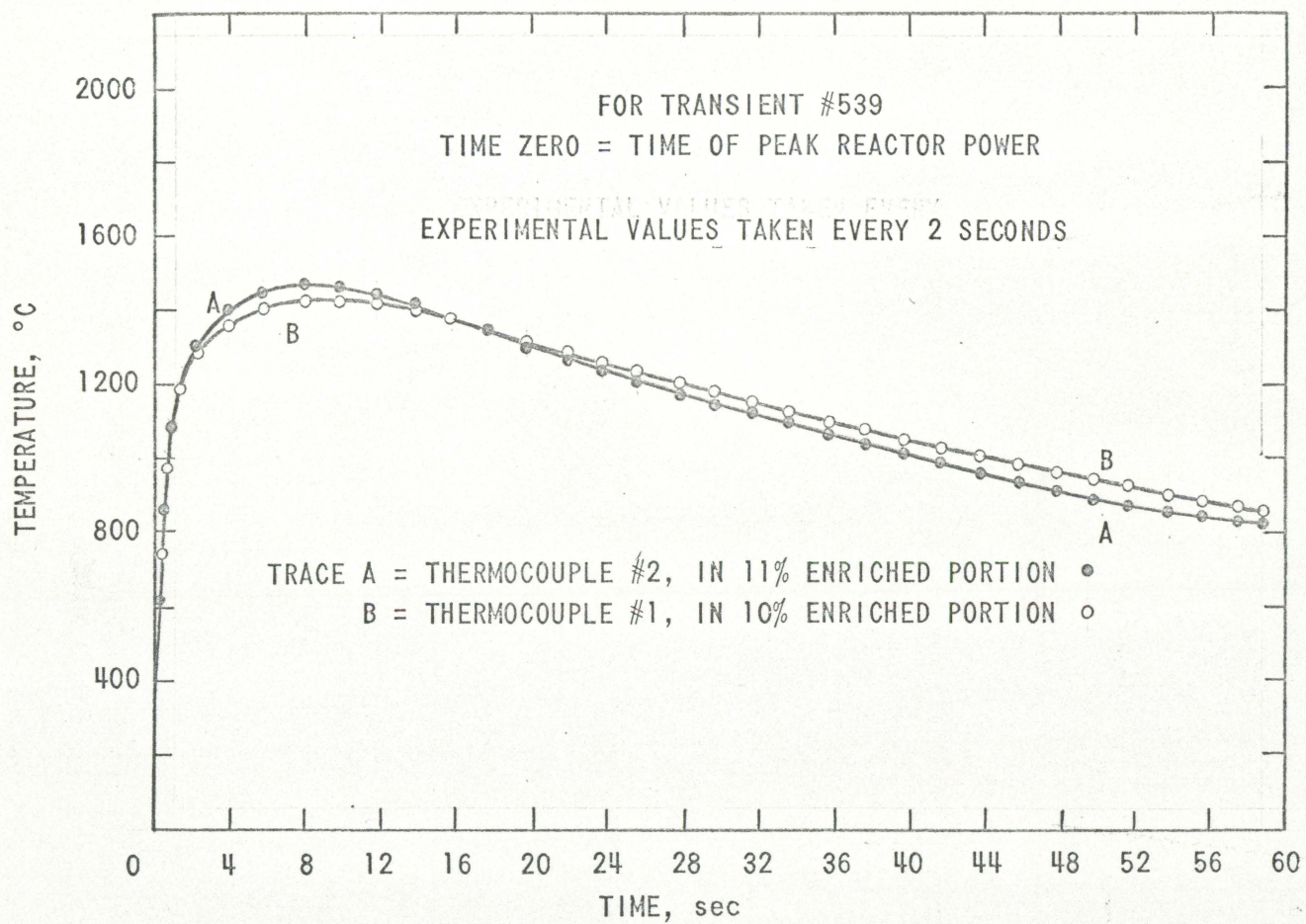


Fig. 37 Experimental temperature vs time

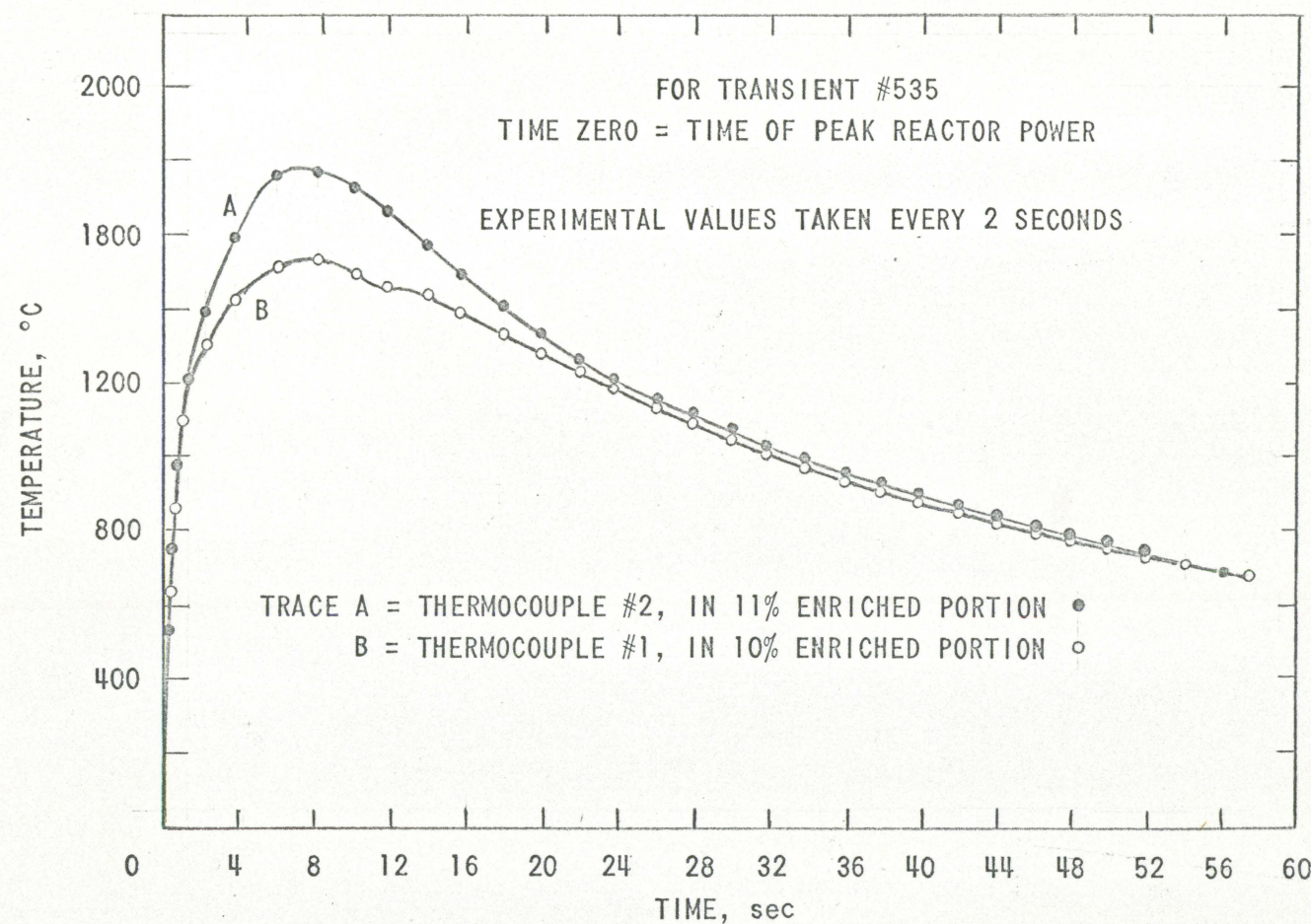


Fig. 38 Experimental temperature vs time

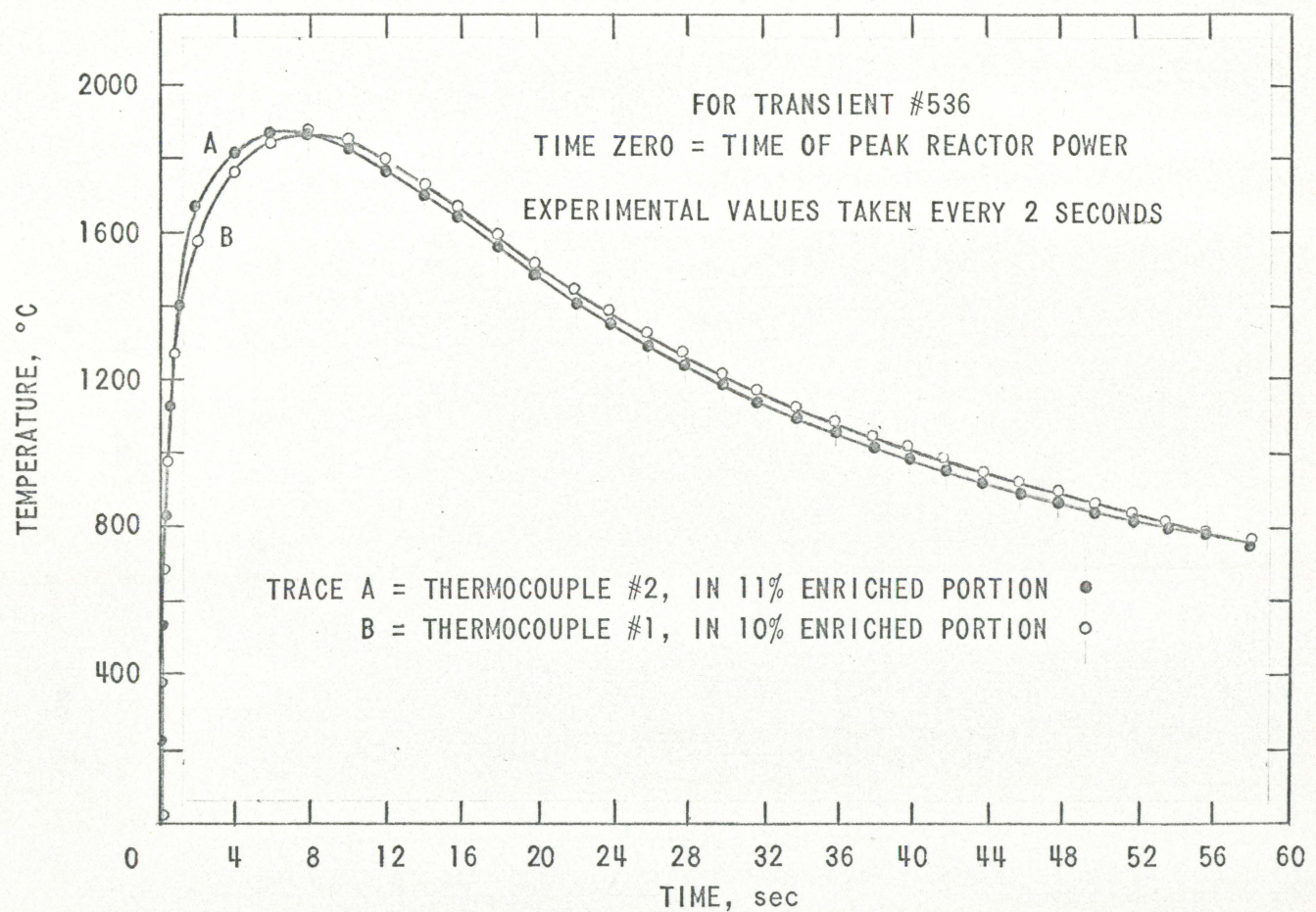


Fig. 39 Experimental temperature vs time

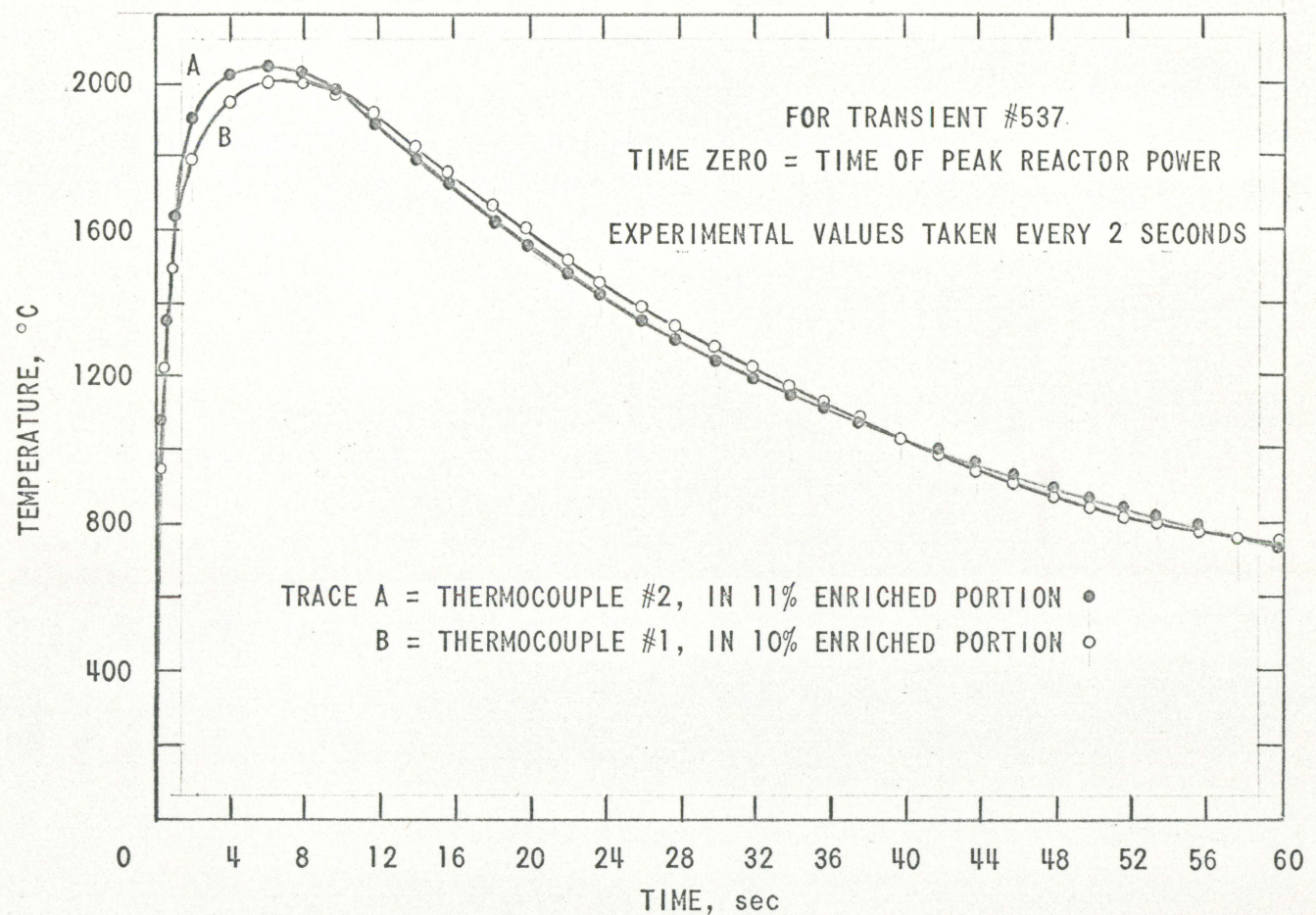


Fig. 40 Experimental temperature vs time

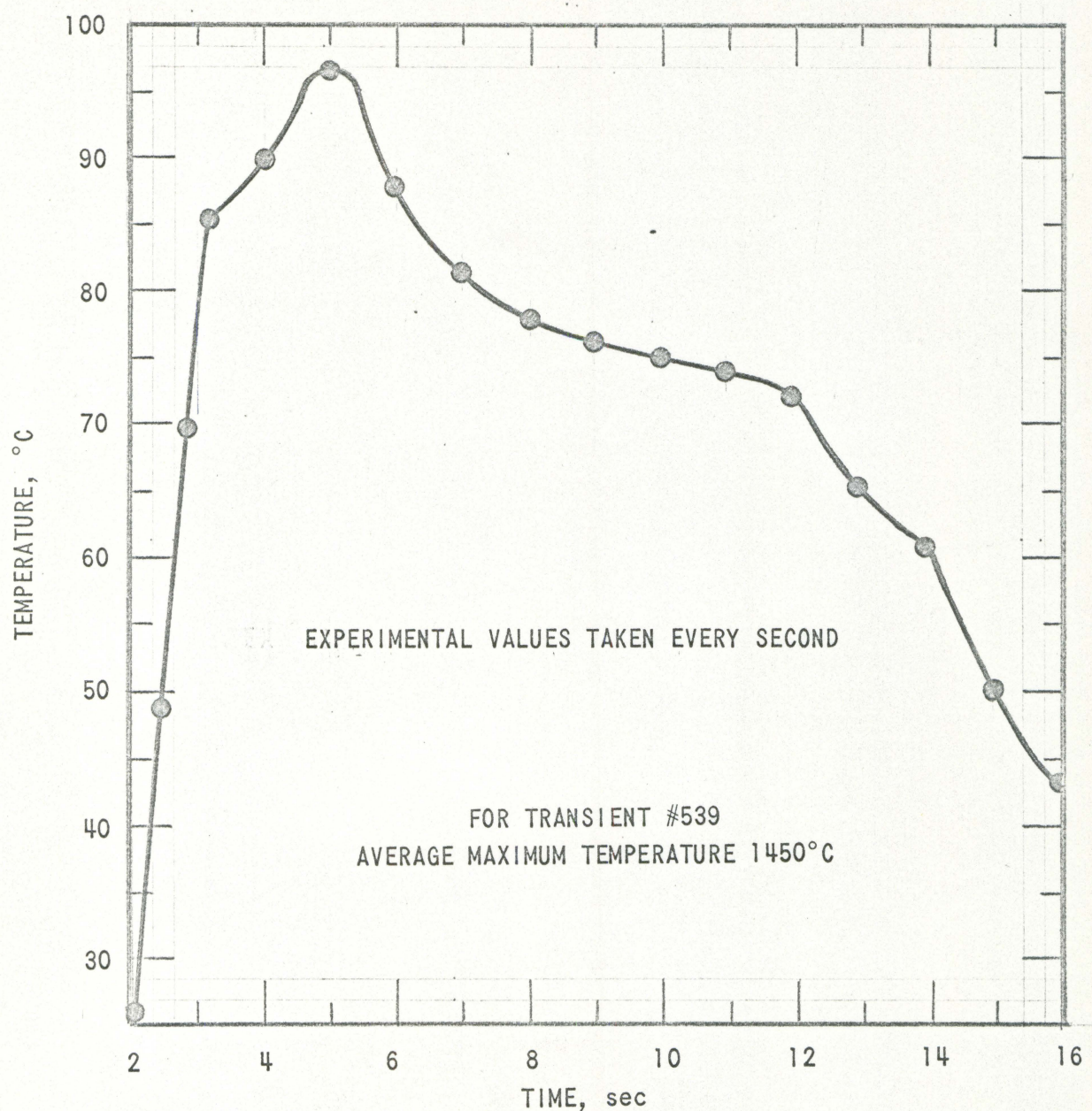


Fig. 41 Experimental temperature difference vs time

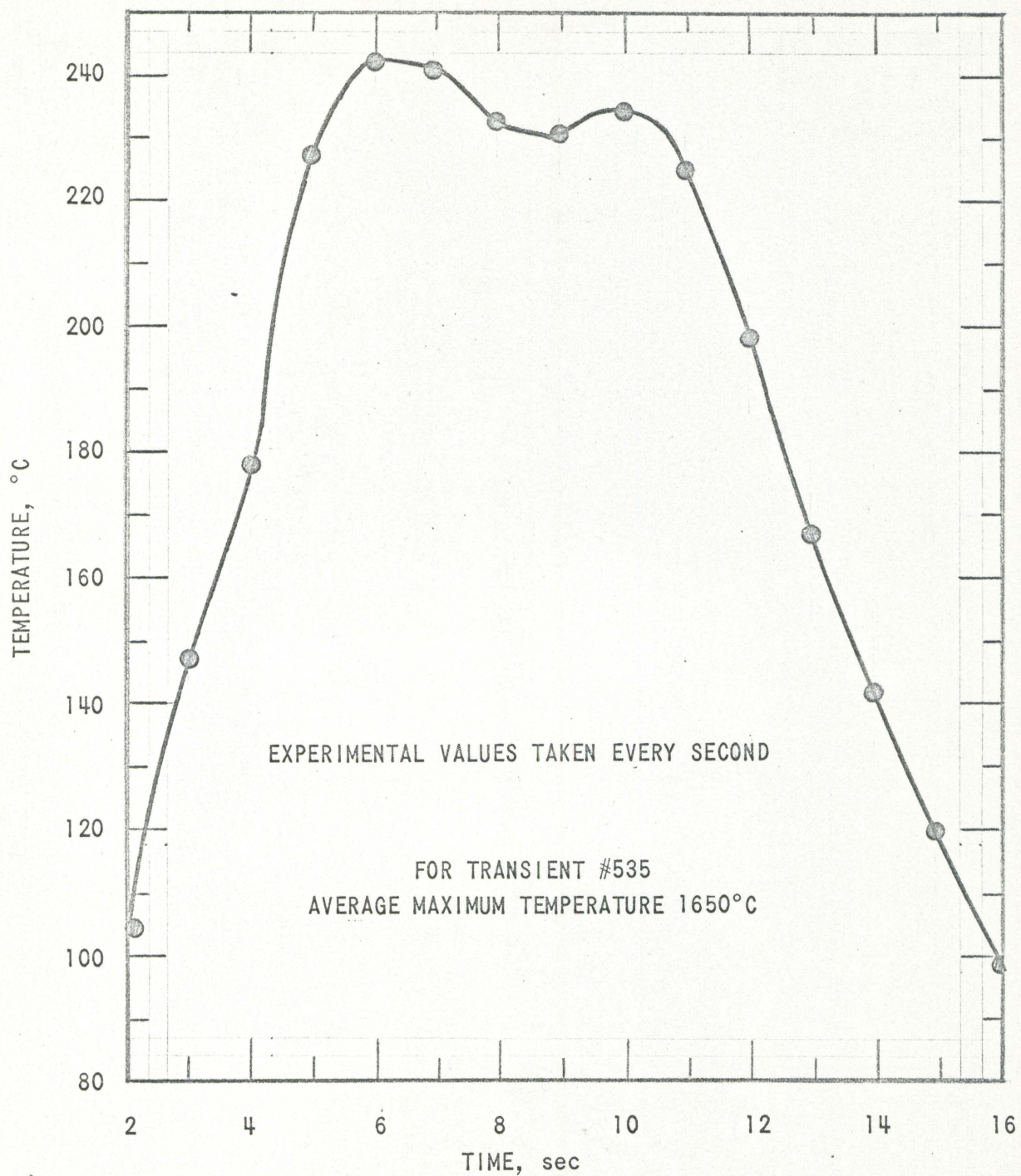


Fig. 42 Experimental temperature difference vs time

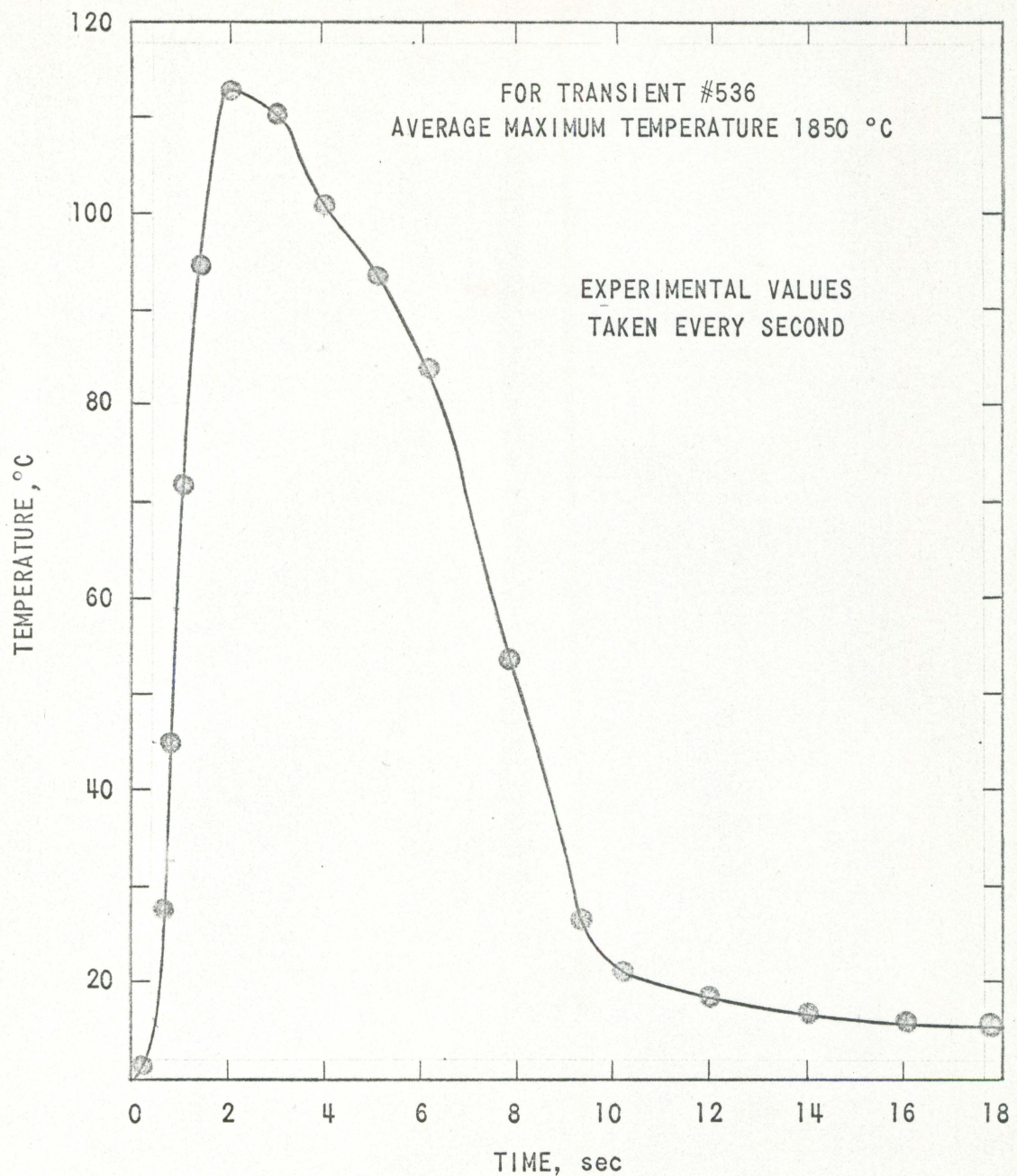


Fig. 43 Experimental temperature difference vs time

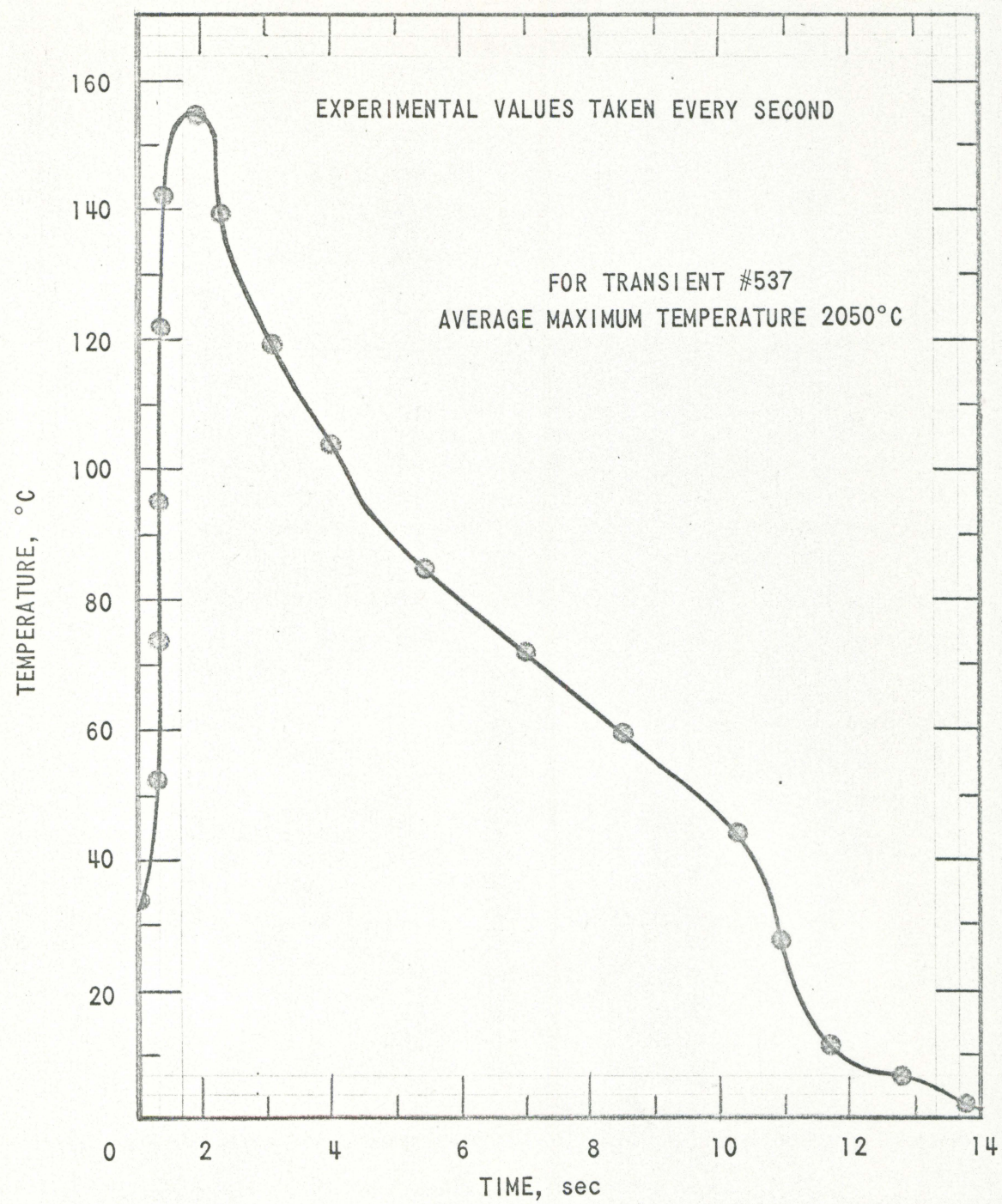


Fig. 44 Experimental temperature difference vs time

the value of D for the conditions of each transient. A tabulation of the comparison of experimental to theoretical data and the approximated values of D is given in Table 6.

Table 6. Approximate values of D

<u>Transient</u>	<u>Comparison Shown in</u>	<u>Approximated D</u>
539	Fig. 45	.007
535	Fig. 46	.010
536	Fig. 47	.025
537	Fig. 47	Indeterminate

Using the measured values of thermal diffusivity and the relationship $D=k/\rho C_p$, the thermal conductivity of UO_2 was calculated as a function of temperature. The volume of the sample was found to be 5.0443 cm^3 and weighed 47.141 gms which yielded a density of 9.345 gms/cm^3 . This density is 85.6% of the theoretical density of UO_2 .

The specific heat, C_p , of UO_2 varies with temperature according to the relationship:

$$C_p (\text{cal/mole-}^\circ\text{C}) = 18.45 + 2.431 \times 10^{-3}T - 2.272 \times 10^5 T^2$$

At the average maximum temperature in the transients analyzed the specific heat of UO_2 was found to be:

<u>Transient</u>	<u>Average Maximum Temperature</u>	<u>C_p cal/g-$^\circ\text{C}$</u>
539	1450	.0815
535	1650	.0830
536	1850	.0845

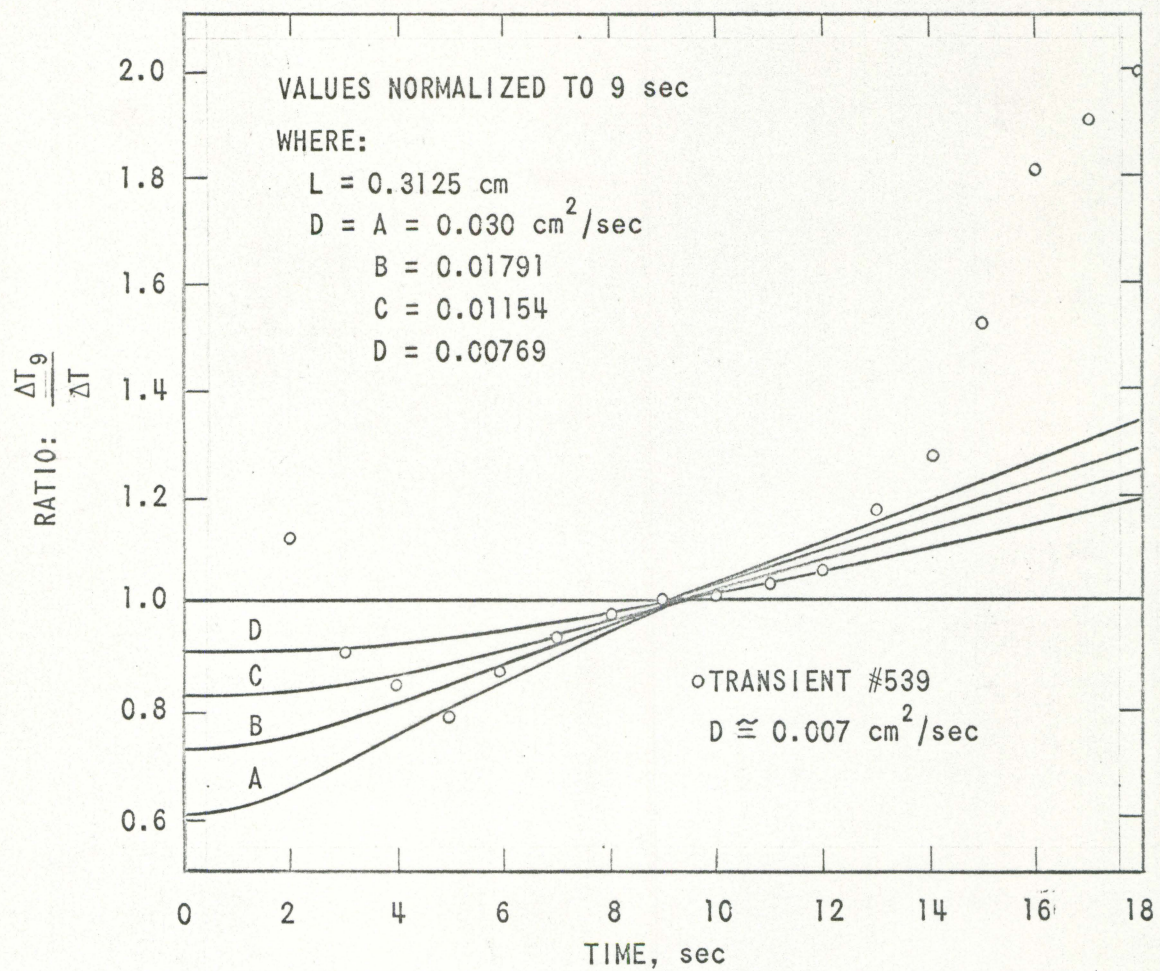


Fig. 45 Comparison of normalized experimental to normalized theoretical temperature difference vs time for various values of diffusivity, D

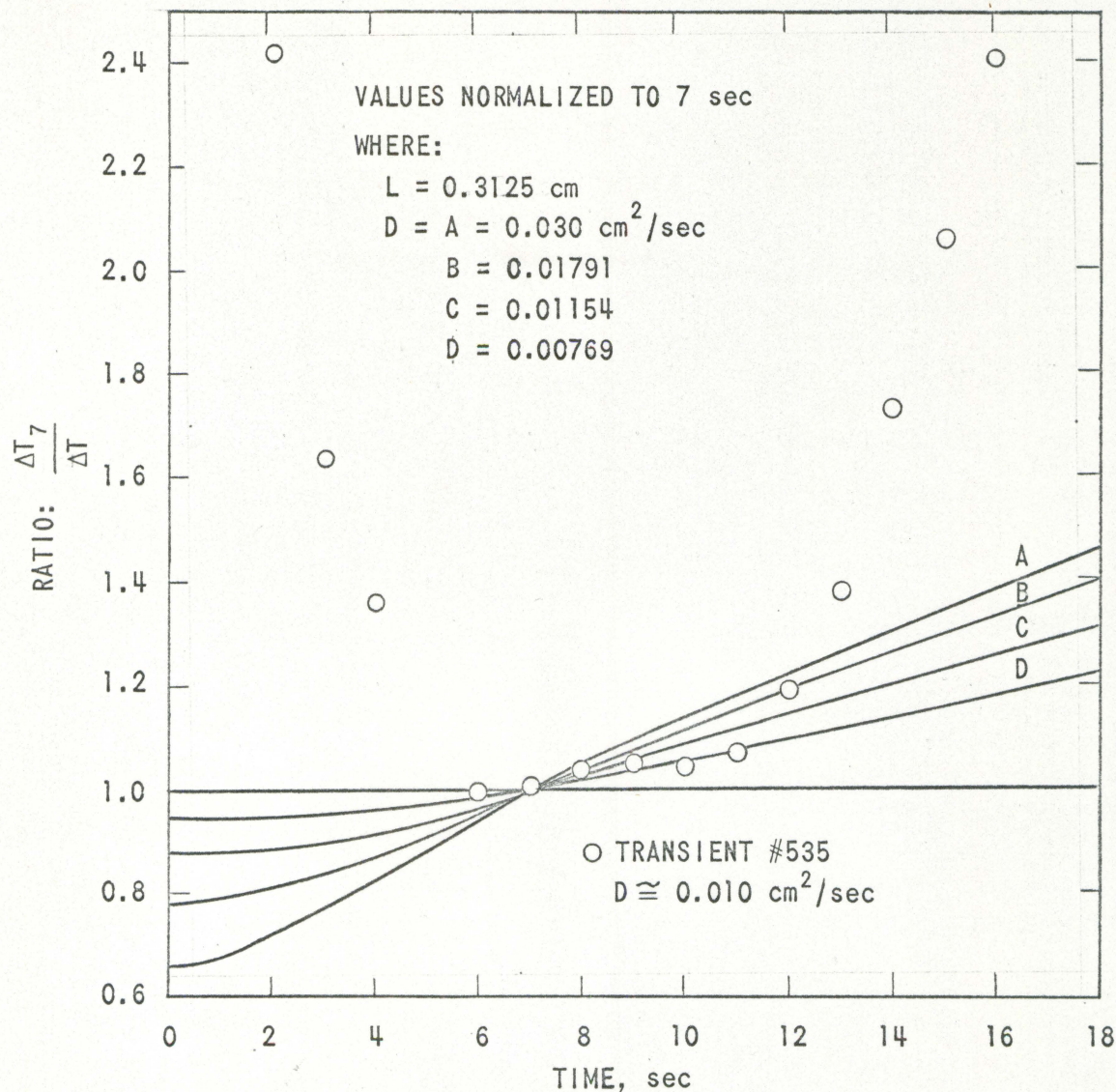


Fig. 46 Comparison of normalized experimental to normalized theoretical temperature difference vs time for various values of diffusivity, D

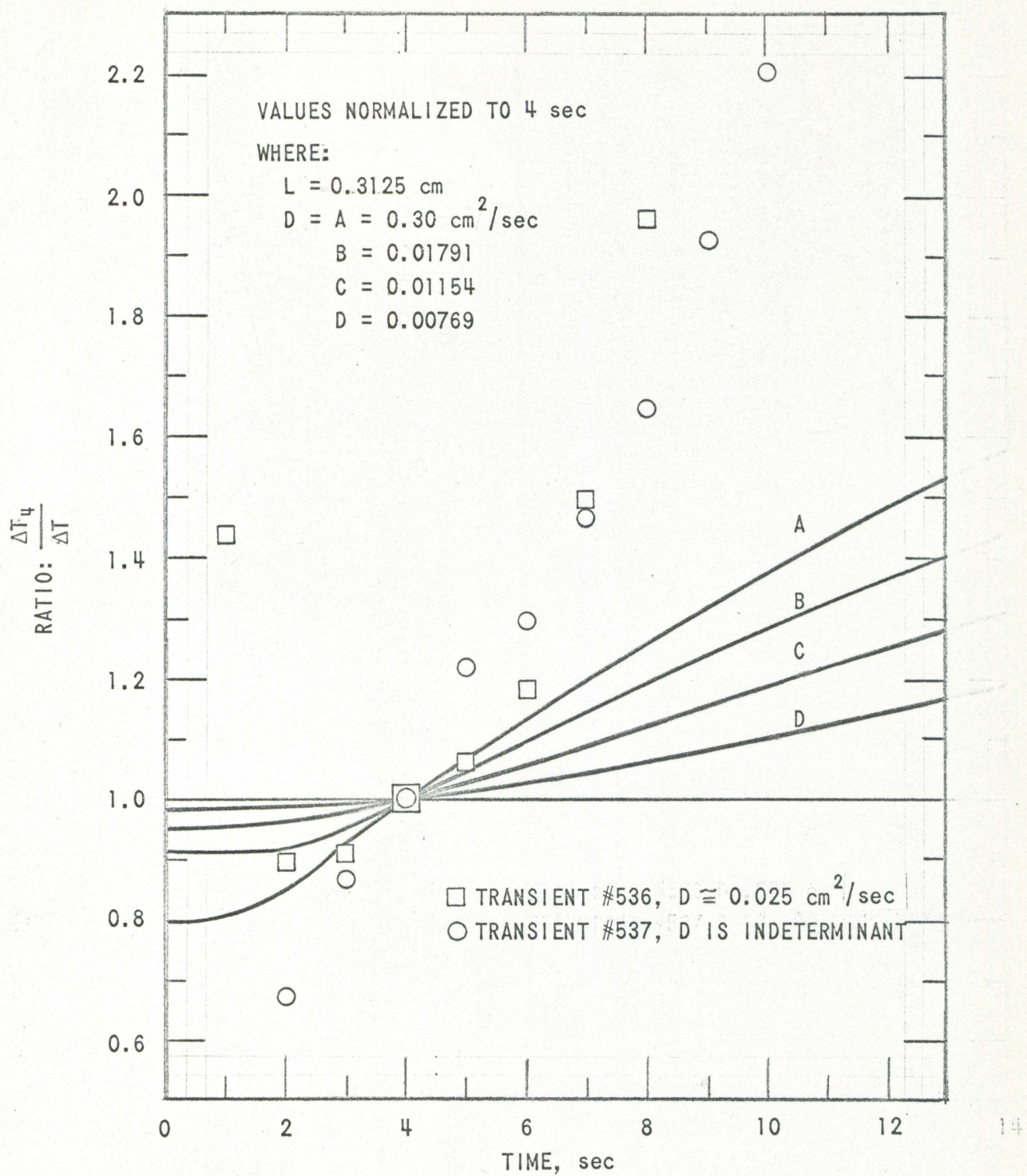


Fig. 47 Comparison of normalized experimental to normalized theoretical temperature difference vs time for various values of diffusivity, D

The calculated values of the thermal conductivity of UO_2 are shown and compared with existing measurements in Fig. 48. Since thermal conductivity is approximately proportional to density the calculated values were corrected to theoretical density and are given as the dashed line in Fig. 48.

The thermal diffusivity values obtained from transients 539 and 535 agree favorably with existing data, while the value obtained from transient 536 at 1850°C appears to be excessively high. The upward trend of thermal conductivity exhibited by the experimental data is in agreement with the prediction made by J. Lambert Bates (2) that the thermal conductivity of UO_2 increases appreciably at high temperatures.

As stated in section IV-F the optimum time for determining D by means of ΔT at various times is $.185 L^2/D$ to $.350 L^2/D$ with the ideal time at $.255 L^2/D$. Within this range the probable error in calculating the thermal diffusivity of the sample is 5% or less. At times other than those within the given range the probable error in the determination of D promptly increases to ∞ .

Outside the given range, the value of $\Delta T_t/\Delta T_{(n)}$ increases to infinity, indicating the influence of experimental errors. At small values of time the thermocouple "lag" and the finite time of power input are the major sources of error.

Even though the transients have been "time corrected" to the peak power input time, heat will continue to be generated for a short period of time. This upward "coasting" of temperature produces the rise to infinity at short periods of time.

At larger values of time radial heat loss from the sample is the

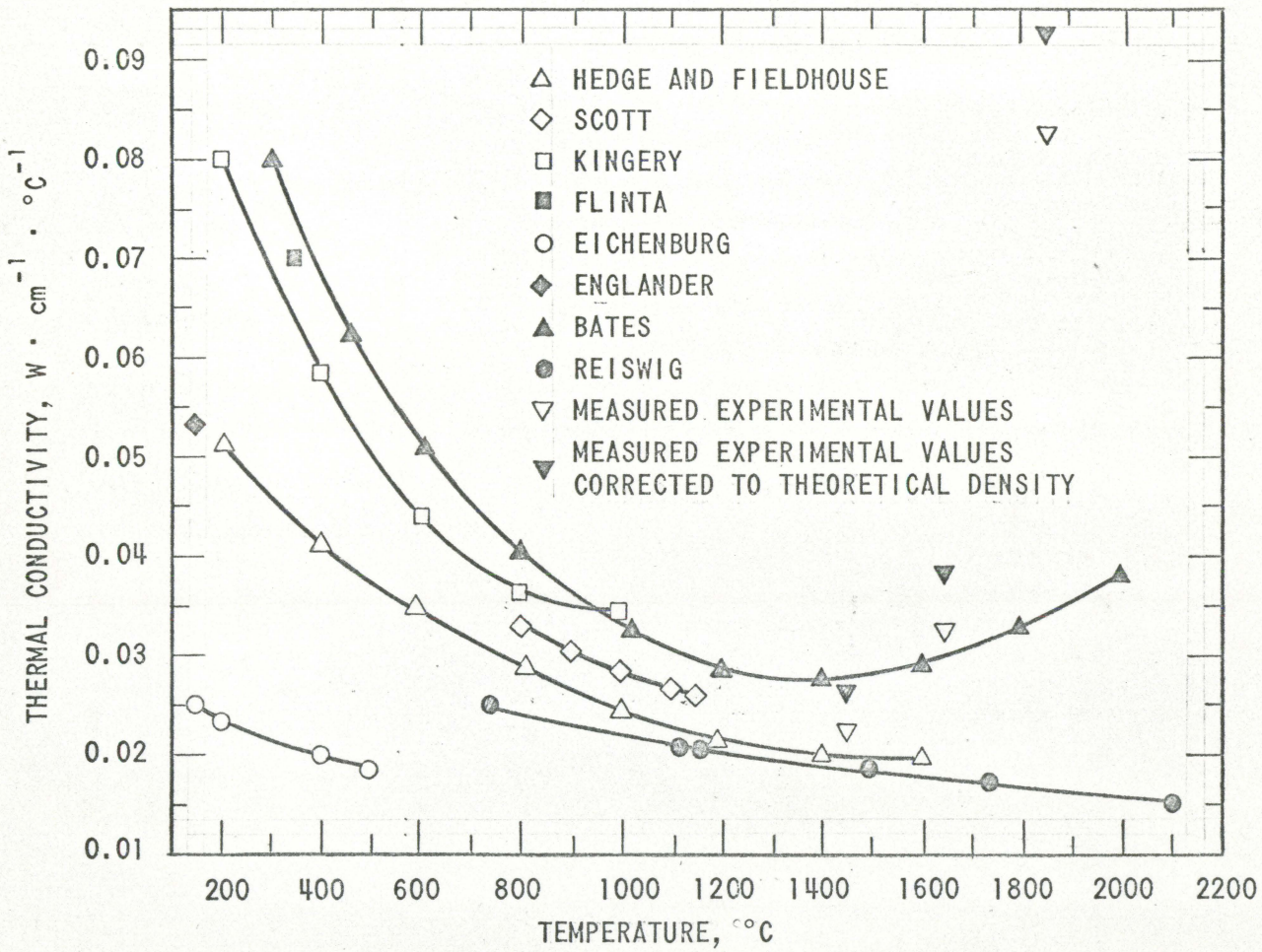


Fig. 48 Reported and experimental thermal conductivity values of uranium dioxide

main source of error. Since radiant heat loss is proportional to the fourth power of the sample temperature this error increases at elevated temperatures. This effect causes the normalized experimental ΔT vs t trace to increase to infinity at lower values of time as the transient maximum temperature is increased. Hence the optimum range for approximating thermal diffusivity values decreases until the normalized ΔT vs t trace becomes an acute parabola. This has occurred in the case of transient 537 making it impossible to approximate the value of the sample's thermal diffusivity at 2050°C.

Motion pictures of the sample transients show that cracking occurred near the end of transient 535. Prints of the motion pictures were made at the time of initial cracking and are given in Fig. 49. The cracks are visible as red lines near the bottom of the sample. It is felt that these cracks had little effect upon the thermocouple readings since they are well below the bottom thermocouple location.

Further cracking, as illustrated in Fig. 50 occurred near the end of transient 536. As can be seen these cracks are quite near the bottom thermocouple location.

Even though these cracks do not become visible until the end of transient 536, they no doubt occurred internally early enough during the transient to be responsible for the high value of D at 1850°C. The cracking became more severe near the end of transient 536 and is the cause for the lack of "effective" data in transient 537.

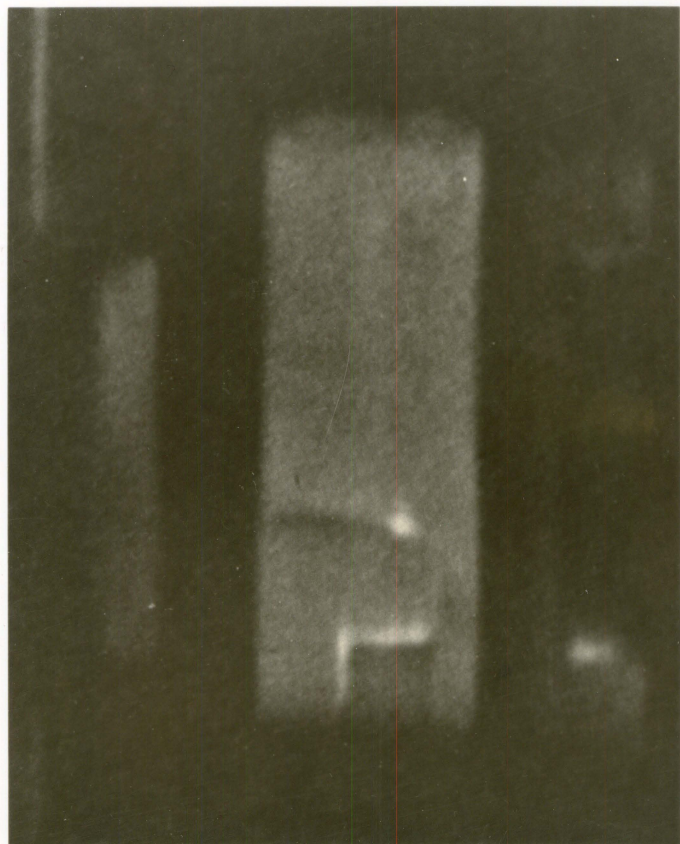


Fig. 49 Initial cracking of sample at
the end of transient #535

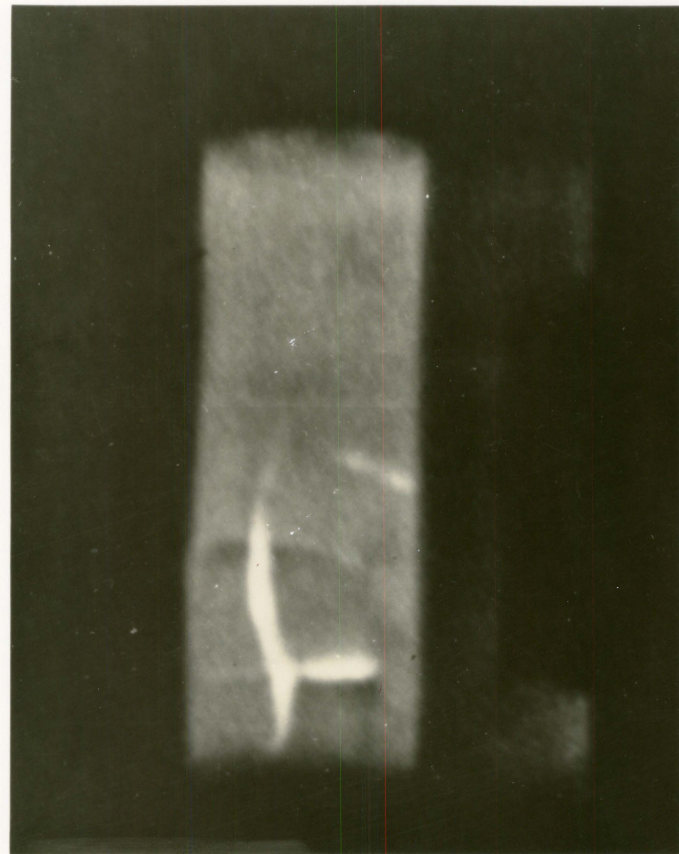


Fig. 50 Extensive cracking as occurred
during transient #536

IX. SUGGESTIONS FOR FURTHER EXPERIMENTATION

It is felt that the feasibility of this experiment has been demonstrated by the work presented herein. However it will be necessary to perform this experiment on other samples of UO_2 to obtain an accurate measurement of the thermal diffusivity of UO_2 over a wider range of temperatures. For this reason the following recommendations are made:

1. For values of D at lower temperatures perform the experiment using a sample of the same dimensions using lower enrichments but with a larger difference of enrichments, i.e., 3% vs 5%.
2. To obtain values of D at higher temperatures use the same experimental sample as used in this report with the addition of thermal shielding to decrease the effect of radial heat loss.

When the given experiment is applied to other ceramic materials it may be necessary to introduce refinements that will be dependent upon the properties of the material to be studied.

If the material to be studied possesses a large value of thermal diffusivity it may be desirable to increase the sample's radius and value of L. Since volume is proportional to r^2 while area is proportional to r, an increase in the sample's radius will result in less heat loss per unit volume. Hence there will be less radiation from the sample which will, in turn, decrease experimental errors. An increase in the sample's radius will also give greater leeway in the radial thermocouple position.

By increasing the value of L better "time resolution" of temperature measurements may be attained. It will take a longer period of time for temperature changes to be felt by the thermocouples which will, in turn, decrease the errors caused by the time "lag" of the thermocouples.

X. BIBLIOGRAPHY

1. Barsell, A. Transient temperatures of stagnant sodium experiments using EBR-II fuel elements in TREAT. Unpublished paper. Reactor Engineering Division, Argonne National Laboratory, Lemont, Ill. 1961.
2. Bates, J. Lambert. Thermal conductivity of uranium dioxide improves at high temperatures. Nucleonics 19, No. 6: 83-86. 1961.
3. Belle, J. and Lustmann, B. Properties of uranium dioxide. U. S. Atomic Energy Commission Report WAPD-184 [Westinghouse Electric Corp. Atomic Power Div., Pittsburgh]. 1957.
4. Boley, B. A. and Weiner, J. H. Theory of thermal stresses. New York, N. Y., John Wiley and Sons, Inc. 1960.
5. Brown, G. G., Foust, A. S., Brown, G. M., Katz, D. L., Brownell, L. E., Schneiderwind, R., Martin, J. J., White, R. R., Williams, C. B., Wood, W. P., Banchero, J. and York, J. L. Unit operations. New York, N. Y., John Wiley and Sons, Inc. 1950.
6. Chemical Rubber Company. Handbook of chemistry and physics. 35th ed. Cleveland, Ohio, Author. 1958.
7. Deem, H. W. and Wood, W. D. A flash thermal diffusivity measurement using a laser. Rev. Sci. Instr. 33: 10-14. 1962.
8. Eichenberg, J. D. An in-pile measurement of the effective thermal conductivity of uranium dioxide. U. S. Atomic Energy Commission Report WAPD-200 [Westinghouse Electric Corp. Atomic Power Div., Pittsburgh]. 1958.
9. Englander, M. Note on measurement of the thermal conductivity of sintered uranium dioxide. U. S. Atomic Energy Commission Report CEA-79 [France. Commissariat à l'Energie Atomique, Paris]. 1951.
10. Eberman, E. Uranium compounds for new high temperature fuels. Paris Fuel Elements Conference. Book 2. U. S. Atomic Energy Commission Report TID-7546 [Technical Information Service Extension, AEC.]. 1958.
11. Firman, E. C., Johnson, F. A. and Findley, J. R. A technique for the in-pile measurements of thermal diffusivity. U. S. Atomic Energy Commission Report AERE R/R-2395 [St. Brit. Atomic Energy Research Establishment, Harwell, Berks, England]. 1958.
12. Flinta, J. E. Thermal conductivity of uranium dioxide. Paris Fuel Elements Conference. Book 2. U. S. Atomic Energy Commission Report TID-7546 [Technical Information Service Extension, AEC.]. 1958.

13. Freund, G. A., Elias, P., MacFarlane, D. R., Greir, J. D. and Boland, J. F. Design summary report on the transient reactor test facility-TREAT. U. S. Atomic Energy Commission Report ANL-6034 [Argonne National Lab. Lemont, Ill.]. 1960.
14. Golden G. Thermal diffusivity of uranium dioxide. Unpublished paper. Reactor Engineering Division, Argonne National Laboratory, Lemont, Ill. 1961.
15. Golden, G. Kinetics of dissolution of zirconium in molten uranium. U. S. Atomic Energy Commission Report ANL-6167 [Argonne National Lab. Lemont, Ill.]. 1960.
16. Golden, G., Dickermann, C. H. and Robinson, L. E. Facility for photographic in-pile meltdown experiments in TREAT. U. S. Atomic Energy Commission Report ANL-6457 [Argonne National Lab. Lemont, Ill.]. 1959.
17. Hedge, J. C. and Fieldhouse, J. B. Measurement of thermal conductivity of uranium dioxide. U. S. Atomic Energy Commission Report AECU-3381 [Technical Information Service Extension, AEC.]. 1956.
18. Heestand, H. The calculation of transient temperature distributions in a solid cylindrical pin, cooled on the surface. U. S. Atomic Energy Commission Report ANL-6237 [Argonne National Laboratory, Lemont, Ill.]. 1960.
19. Jakob, M. and Hawkins, G. A. Elements of heat transfer and insulation. 2nd ed. New York, N. Y., John Wiley and Sons, Inc. 1950.
20. Kingery, W. D., Vasiles, F., Loeb, A. L., Norton, F. H., Franil, J. and Cable, R. L. The measurement of thermal conductivity of refractory materials. U. S. Atomic Energy Commission Report NYO-3647 [New York Operations Office, AEC.]. 1953.
21. Kelley, K. K. Contributions to the data on theoretical metallurgy. XIII. High temperature heat content, heat capacity, and entropy data for the elements and inorganic compounds. U. S. Bureau of Mines Bulletin 584. 1960.
22. Loeb, Arthur L. A theory of the envelope type of thermal conductivity tests. U. S. Atomic Energy Commission Report NYO-595 [New York Operations Office, AEC.]. 1950.
23. McCabe, W. L. and Smith, J. C. Unit operations of chemical engineering. New York, N. Y., McGraw-Hill. 1956.
24. Norton, F. H. and Kingery, W. D. The measurement of the thermal conductivity of refractory metals. U. S. Atomic Energy Commission Report NYO-3646 [New York Operations Office, AEC.]. 1953.

25. Okrent, D., Dickermann, C. E., Gasidlo, J., O'Shea, D. M. and Schoeberle, D. F. The reactor kinetics of the transient reactor test facility. U. S. Atomic Energy Commission Report ANL-6174 [Argonne National Lab. Lemont, Ill.]. 1960
26. Parker, W. J., Jenkins, R. J., Butler, C. P. and Abbot, G. L. A flash method of determining thermal conductivity, heat capacity, and thermal conductivity. U. S. Atomic Energy Commission Report USNRL-TR-424 [Naval Radiological Defense Lab. San Francisco] 1960.
27. Persey, J. H. Chemical engineering handbook. 3rd ed. New York, N. Y. McGraw-Hill. 1950.
28. Reiswig, R. D. Thermal conductivity of uranium dioxide to 2100°C. American Ceramic Society Journal. 36: 48-49. 1961.
29. Ross, A. M. The dependence of thermal conductivity of uranium dioxide on density, microstructure, stoichiometry, and thermal neutron irradiation. U. S. Atomic Energy Commission Report AECL-1096 [Atomic Energy of Canada, Ltd., Chalk River, Ont.]. 1960.
30. Schmitt, A. Literature survey of the properties of uranium dioxide. Unpublished paper. Reactor Engineering Division, Argonne National Laboratory, Lemont, Ill. 1960.
31. Scott, R. Thermal conductivity of uranium dioxide. U. S. Atomic Energy Commission Report AERE M/R-2526 [Gt. Brit. Atomic Energy Research Establishment, Harwell, Berks, England]. 1958.
32. Stokes, R. H. One-dimensional diffusion with the diffusion coefficient a linear function of concentration. Faraday Society Transactions 48: 887-891. 1952.
33. Taraba, F. R. and Paine, S. H. The longitudinal distribution of thermal neutron flux in cylindrical fuel specimens during irradiation. U. S. Atomic Energy Commission Report ANL-5945 [Argonne National Lab. Lemont, Ill.]. 1959.
34. Taraba, F. R. and Paine, S. H. Quarterly progress report for July, August, September, 1957, metallurgy division, U. S. Atomic Energy Commission Report ANL-5797 [Argonne National Lab. Lemont, Ill.]. 1957.

XI. ACKNOWLEDGMENTS

The author of this paper wishes to express his sincere thanks for the help and guidance given him by Dr. Glenn Murphy, Head of Nuclear Engineering Department, who is his major professor. Thanks also to Dr. Charles E. Dickerman, Mr. Lewis E. Robinson and the rest of the staff of the Reactor Engineering Division of Argonne National Laboratory, where this work was carried out.

XII. APPENDIX A

Heat Conduction with D a Linear Function of Temperature

Consider the solution of the heat equation:

$$\frac{\partial}{\partial X} [D \frac{\partial T}{\partial X}] = \frac{\partial T}{\partial t},$$

with the initial conditions:

$$T(X, t) = T_{01}, \quad X < 0, \quad t=0$$

$$T(X, t) = T_{02}, \quad X > 0, \quad t=0,$$

and boundary conditions:

$$\lim_{X \rightarrow -\infty} T(X, t) = T_{01}; \quad \lim_{X \rightarrow \infty} T(X, t) = T_{02}.$$

This problem is treated by Stokes (32) as follows:

Let:

$$Y = Xt - \frac{1}{2}.$$

With this substitution the heat equation becomes:

$$-\lambda \frac{\partial}{\partial Y} [D \frac{\partial T}{\partial Y}] = Y \frac{\partial T}{\partial Y},$$

with the transformed boundary conditions:

$$\lim_{Y \rightarrow -\infty} T(Y) = T_{01}; \quad \lim_{Y \rightarrow \infty} T(Y) = T_{02}.$$

Take the linear variation of D with T to be:

$$D = \bar{D} [1 - \frac{\alpha}{2} (T_{01} + T_{02}) + \alpha T],$$

where for:

$$T = \frac{T_{01} + T_{02}}{2}, \quad D = \bar{D}.$$

Let:

$$\sqrt{\frac{\left[1 - \frac{\alpha}{2} (T_{01} + T_{02}) + \alpha T\right]^2}{\left[1 - \frac{\alpha}{2} (T_{01} - T_{02})\right]}},$$

$$W = \left[1 - \frac{a}{2} (T_{01} - T_{02}) \right]^{-\frac{1}{2}} \cdot \frac{1}{2} \sqrt{\frac{D}{t}}$$

Then the heat equation transforms to:

$$\frac{d^2v}{dw^2} = - \frac{2w}{\sqrt{v}} \frac{dv}{dw},$$

with the boundary conditions:

$$w \rightarrow +\infty; v \rightarrow 1$$

$$w \rightarrow +\infty; v \rightarrow [1 + \frac{a}{2} (T_{01} - T_{02})]^2 / [1 - \frac{a}{2} (T_{01} - T_{02})]^2 \equiv \frac{1}{b^2}.$$

The results of numerical integration of the above second order differential equation appear in the literature; these are presented in terms of the independent variable:

$$Z = W \left(\frac{2}{1+b} \right)^{\frac{1}{2}} = \frac{X}{2 \sqrt{Dt}}$$

If the average value of the thermal diffusivity is kept constant, but the ratio of the diffusivities in the two regions at time zero is varied, the temperature does not vary greatly with $X/2 \sqrt{Dt}$. Due to this relative insensitivity, a TREAT experiment based upon the linear thermal diffusivity model does not appear to be warranted.

XIII. APPENDIX B

Analytical Solution of One-Dimensional Rectangular Constant-Diffusivity

Heat Equation for Rod of Finite Length

Consider the physical model below and its associated equations:

T_1	T_2
$X=-a$	$X=0$
$-a < X < 0$	$0 < X < a$
$\frac{\partial T_1}{\partial t} = D \frac{\partial^2 T_1}{\partial x^2}$	$\frac{\partial T_2}{\partial t} = D \frac{\partial^2 T_2}{\partial x^2}$
$T_1(X,0) = T_{01}$	$T_2(X,0) = T_{02}$
$\frac{\partial T_1(-a,t)}{\partial x} = 0$	$\frac{\partial T_2(a,t)}{\partial x} = 0$
$T_1(0,t) = T_2(0,t)$	
$\frac{\partial T_1(0,t)}{\partial x} = \frac{\partial T_2(0,t)}{\partial x}$	

This is a classical-type problem that is readily solved by means of the Laplace transform. Define:

$$L \left\{ T_n(X,t) \right\} = \int_0^\infty e^{-pt} T_n(X,t) dt = \theta_n(X,p) ; \quad n = 1, 2$$

Then:

$$p\theta_1 - T_{01} = D \frac{d^2 \theta_1}{dx^2} ;$$

$$\theta_1 = A_1 e^{-\sqrt{\frac{p}{D}} X} + B_1 e^{\sqrt{\frac{p}{D}} X} + \frac{T_{01}}{p} .$$

From the end-condition in this region:

$$A_1 = B_1 e^{-2\sqrt{\frac{P}{D}}a},$$

and:

$$\theta_1 = B_1 \left[e^{\sqrt{\frac{P}{D}}X} + e^{-\sqrt{\frac{P}{D}}(2a+X)} \right] + \frac{T_{01}}{P}$$

$$\frac{\partial \theta_1}{\partial X} = B_1 \sqrt{\frac{P}{D}} \left[e^{\sqrt{\frac{P}{D}}X} - e^{-\sqrt{\frac{P}{D}}(2a+X)} \right].$$

Similarly:

$$\theta_2 = A_2 \left[e^{-\sqrt{\frac{P}{D}}X} + e^{-\sqrt{\frac{P}{D}}(2a-X)} \right] + \frac{T_{02}}{P}$$

$$\frac{\partial \theta_2}{\partial X} = A_2 \sqrt{\frac{P}{D}} \left[-e^{-\sqrt{\frac{P}{D}}X} + e^{-\sqrt{\frac{P}{D}}(2a-X)} \right]$$

Employing the coupling conditions it is found that:

$$A_2 = -B_1 = \frac{1}{2} (T_{01} - T_{02}) \frac{1}{P} \sum_{n=0}^{\infty} (-1)^n e^{-2na} \sqrt{\frac{P}{D}}$$

Thus:

$$\theta_1 = \frac{T_{01}}{P} - \frac{1}{2} (T_{01} - T_{02}) \sum_{n=0}^{\infty} (-1)^n \left[\frac{1}{P} e^{-\sqrt{\frac{P}{D}}(2na-X)} + \frac{1}{P} e^{-\sqrt{\frac{P}{D}}[2a(n+1)+X]} \right]$$

and:

$$T_1 = T_{01} - \frac{1}{2}(T_{01} - T_{02}) \sum_{n=0}^{\infty} (-1)^n \left[\frac{\operatorname{erfc}(\frac{2na-X}{2\sqrt{Dt}}) + \operatorname{erfc}(\frac{2a(n+1)+X}{2\sqrt{Dt}})}{2\sqrt{Dt}} \right]$$

Similarly:

$$T_2 = \frac{T_{02}}{P} + \frac{1}{2}(T_{01}-T_{02}) \sum_{n=0}^{\infty} (-1)^n \left[\frac{1}{P} e^{-\sqrt{\frac{P}{D}}(2na+X)} + \frac{1}{P} e^{-\sqrt{\frac{P}{D}}[2a(n+1)-X]} \right]$$

and:

$$T_2 = T_{02} + \frac{1}{2}(T_{01}-T_{02}) \sum_{n=0}^{\infty} (-1)^n \left[\operatorname{erfc}\left(\frac{2na+X}{2\sqrt{Dt}}\right) + \operatorname{erfc}\left(\frac{2a(n+1)-X}{2\sqrt{Dt}}\right) \right]$$

Consider the expansion of T_1 :

$$T_1 = T_{01} - \frac{1}{2}(T_{01}-T_{02}) \left\{ \operatorname{erfc}\frac{|X|}{2\sqrt{Dt}} + \operatorname{erfc}\frac{2a-|X|}{2\sqrt{Dt}} - \operatorname{erfc}\frac{2a+|X|}{2\sqrt{Dt}} - \operatorname{erfc}\frac{4a-|X|}{2\sqrt{Dt}} + \dots \right\}$$

As a approaches infinity all terms in the brackets but the first go to zero;
i.e.:

$$T_1 = T_{01} - \frac{1}{2}(T_{01}-T_{02}) \operatorname{erfc} \frac{|X|}{2\sqrt{Dt}}$$

and similarly:

$$T_2 = T_{02} + \frac{1}{2}(T_{01}-T_{02}) \operatorname{erfc} \frac{|X|}{2\sqrt{Dt}}$$